Université Mohammed V
Faculté des Sciences
Rabat

CENTRE D'ETUDES DOCTORALES - SCIENCES ET TECHNOLOGIES

N° d'ordre : 3576

THÈSE

En vue de l'obtention du : ***DOCTORAT***

***Centre de Recherche** : Centre de Recherche en Énergie*
***Structure de Recherche** : Équipe de Mécanique et des Matériaux*
***Discipline** : Physique*
***Spécialité** : Géophysique et Génie Civil*

Présentée et soutenue le 25/12/2021 par :

Oussama ARAB

CONTRIBUTION USING CODA WAVE ATTENUATION AND SOIL LIQUEFACTION IN THE RIF REGION

JURY

Mohammed Ouadi BENSALAH	PES, Université Mohammed V, Faculté des Sciences - Rabat	Président
Mohammed Majid HIMMI	PES, Université Mohammed V, Faculté des Sciences - Rabat	Rapporteur / Examinateur
Younes EL FELLAH	PH, Institut Agronomique et Vétérinaire Hassan-II -Rabat	Rapporteur / Examinateur
Jamal MHAMDI	PES, Université Mohammed V, Ecole nationale supérieure d'arts et metiers- Rabat	Rapporteur / Examinateur
Mimoun CHOURAK	PES, Université Mohammed Premier, École nationale des sciences appliquées - OUJDA	Rapporteur / Examinateur
Mimoun HARNAFI	PES, Université Mohammed V, Institut Scientifique - Rabat	Invité
Mohammed Jamal Eddine SEBBANI	PES, Université Mohammed V, Faculté des Sciences - Rabat	Directeur de Thèse

Année Universitaire : 2021/2022

*Dear parents,

You were and you still the kind of parents who done perfectly there job. You need to know both that you are the source of my motivation, my energy, my balance and many of other beautiful things that keep me better than yesterday. You need also to know that this devoted section will never be enough neither to express nor to describe my feelings toward you. I may not be much expressive, but still, I love you. May god protect you.

To my dear sister,

I remember those days we were studying all night. We were the source of each other motivation. Far or near you are permanently in my mind, I mean I love you. May god enlighten your way.

To all my grandparents, may god have mercy upon your souls and bless the living. To all the big family, I dedicate this work to you.

To all my friends, that have been by my side in bad and good moments, thank you.

ACKNOWLEDGEMENT

This work was carried out at the Scientific Institute at the Department of Earth Sciences, Laboratory of Geophysics and Natural Hazards and with the collaboration with physics department at the faculty of science rabat.

In collaboration with international institutions and organizations, the Scientific Institute with the coordination of Professor HARNAFI Mimoun had managed to succeed a scientific research projects in seismology between 2009 and 2015. These projects consist of the installation of seismological broadband stations across the national territory:

1. TopoIberia Project, 19 stations, with the collaboration of Jaume Almera Institute of Earth Sciences of Barcelona, Spain

2. PICASSO Project, 40 stations, with University of Oregon, USA collaboration.

3. MoroccoArray project, 15 stations, with University of Münster, Germany collaboration.

4. Project with the University Of Bristol, UK, 6 stations.

The realization of these projects has resulted in the constitution of a very important database that spread of the vast majority of the national territory of Morocco.

We thank, through these institutions, the persons in charge of the above projects, who allowed us to constitute this invaluable database.

It is for me a pleasure as well as a duty to thank all the people who have contributed in any way to the establishment of this thesis project, who have helped me, supported me and made this work possible.

I would like to express my thanks to Pr. Mohammed Ouadi BENSALAH, President of the jury for the interest he has shown in my research work. He did me the honor to accept to chair this jury despite his many concerns.

Pr. Mohammed Majid HIMMI, did me the honor to read and to sit among the members of this jury; I thank him infinitely.

I wanted to thanks Pr. Younes EL FELLAH for having invested in this thesis, for all the exchanges that we had throughout the time of this work and for the interest for serving in this honorable committee as a reporter.

I would like to express my gratitude to Pr. Jamal MHAMDI who has been kind enough to examine my work, and to enhance the quality of this manuscript.

I express my warm thanks to Pr. Mimoun CHOURAK, for having accepted to judge my work and for the relevant remarks brought to this thesis.

I would like to express my deepest gratitude to my supervisor Pr. SEBBANI Mohammed Jamal Eddine and my co-supervisor Pr. Mimoun HARNAFI, for the advice they gave me, there judicious supervision and there assistance throughout my thesis. You are the persons who made me want to do seismology and continue to reach one of my aims.

I thanks also Pr. Abd el aziz Khairy Abd el-aal for his contribution to this work in a way that enhanced the quality of this work.

Thanks to Ms. Sara FERRI for editing and reviewing the linguistic aspects of this research.

Finally, I would like to thank all those who have contributed to the accomplishment of this work. I would like to express my warmest thanks to them.

This work was funded by PPR2 project which is a scientific collaboration between the scientific institute of rabat and the National Center for Scientific and Technical Research (CNRST), Rabat, Morocco.

ABSTRACT

The aim of this work is to estimate the seismic vulnerability in the RIF northern morocco using two different approaches. The first one is based mainly on the attenuation of seismic coda waves while the second one is the estimation of the liquefaction potential in the same region. The investigation using the attenuation of coda wave's technic has been accomplished relying on the back-scattering model. In this case of study we utilized Topo-Iberia network which consist of 15 broadband stations widespread in the whole surface area of the Rif zone. The quality factor of Coda Qc was computed under 5 lapse time windows 20, 30, 40, 50 and 60s at different central band frequencies from 1.5 to 18HZ. Moreover, the assumption of the dependency principle between the quality factor and the frequency and the lapse time windows has been proven. This statement lead the facts to substantiate the presence of heterogeneities under the crust and to reveal the intricacy of the geological/geophysical pattern. The quantification of the Qc has come to put the region of the Rif in a tectonic active region. On the other hand the estimation of the liquefaction potential was evaluated using the so-called HVSR Nakamura method `Horizontal-To-Vertical Spectral Ratio`. The purpose of the liquefaction inquest is to be capable to evaluate the seismic vulnerability in the Rif area by adding parameters other than the quality factor. We conducted this study by extracting the fundamental frequency F_0 and the amplification factor A_0 to calculate the vulnerability index Kg. In addition, the estimation of the liquefaction potential can lean on the value of the Kg index, the geological setting and the existence of aquifer nappes. Generally the Kg index has shown a low value on all the stations beside one station with a kg index around 11. All this outcomes refers to unsaturated ground granules due to a minor content. Therefore, the Rif area is not high risky toward the liquefaction.

Key words: Attenuation; Coda wave; Quality factor; Liquefaction; Micro-tremor measurement; Seismic vulnerability; Rif region.

Résumé

Le but de ce travail est d'estimer la vulnérabilité sismique, dans le RIF, région nord du Maroc, en utilisant deux approches différentes. La première est d'évaluer l'atténuation des ondes sismiques de la coda, tandis que la seconde est l'estimation du potentiel de liquéfaction dans la même région. L'investigation utilisant la technique d'atténuation des ondes coda a été réalisé en se basant sur le modèle de rétrodiffusion. Dans ce cas d'étude, nous avons utilisé le réseau Topo-Iberia qui comprend 15 stations à large bande réparties sur toute la surface de la zone du Rif. Le facteur de qualité de Coda Qc a été calculé dans 5 fenêtres de temps 20, 30, 40, 50 et 60s à différentes fréquences de la bande centrale de 1.5 à 18HZ. De plus, l'hypothèse du principe de dépendance entre le facteur de qualité et la fréquence et les fenêtres de temps a été prouvée. Cette affirmation a conduit les faits à étayer la présence d'hétérogénéités sous la croûte et à révéler la complexité du modèle géologique/géophysique. La quantification du Qc est venue placer la région du Rif dans une région tectonique active. D'autre part, l'estimation du potentiel de liquéfaction a été évaluée en utilisant la méthode dite HVSR de Nakamura `Horizontal-To-Vertical Spectral Ratio`. Le but de l'estimation du potentiel de liquéfaction est d'être capable d'évaluer la vulnérabilité sismique dans la région du Rif en ajoutant des paramètres autres que le facteur de qualité. Cette étude a été accomplie en extrayant la fréquence fondamentale F0 et le facteur d'amplification A0 pour calculer l'indice de vulnérabilité Kg. En outre, l'estimation du potentiel de liquéfaction peut s'appuyer sur la valeur de l'indice Kg, le contexte géologique et l'existence de nappes aquifères. En général, l'indice Kg a montré une faible valeur sur toutes les stations à l'exception d'une station avec un indice Kg autour de 11. Tous ces résultats se réfèrent à des granules de sol non saturés en raison d'un contenu mineur. Par conséquent, la région du Rif ne présente pas de risque élevé de liquéfaction.

Mots clés: Atténuation; l'onde de Coda; Facteur de qualité; Liquéfaction; Mesure de bruit de fond; Vulnérabilité sismique; Région du Rif.

ملخص

الهدف من هذا البحث هو تقييم الحساسية الزلزالية على مستوى منطقة الريف شمال المغرب باستخدام نهجين مختلفين. النهج الأول يعتمد بالأساس على معامل التوهين المنبثق من ذيل الموجات الزلزالية (الكودا) بينما الثاني هو تقدير جهد التميع أو التسييل. تم إنجاز هذا الاستقصاء باستخدام تقنية التوهين لموجة كودا بالاعتماد على نموذج التشتت الخلفي. علاوة على ذلك، تم حساب عامل الجودة Qc الذي يتناسب عكسياً مع التوهين الزلزالي لموجة الكودا تحت 5 نوافذ زمنية منها 20 , 30 , 40 , 50 و60 ثانية على ترددات نطاق مركزي مختلفة من 1.5 إلى 18 هرتز. بالإضافة، تم إثبات افتراض مبدأ التبعية بين عامل الجودة، التردد والنوافذ الزمنية بحيث تقودنا هذه الحقائق لإثبات وجود مبدأ عدم التجانس تحت القشرة السطحية للأرض والكشف عن تعقيد النمط الجيولوجي / الجيوفيزيائي بهذه المنطقة. وأخيرا وليس آخرا، إن تقدير معامل الجودة لذيل الموجة الزلزالية Qc قد وضع الريف في منطقة نشطة تكتونيا. من ناحية أخرى، تم حساب جهد التميع باستخدام ما يسمى بـ "النسبة الطيفية الأفقية إلى الرأسية" للباحث ناكامورا. الغرض من استقصاء التميع هو القدرة على تقييم الضعف الزلزالي في منطقة الريف عن طريق إضافة معاملات أخرى غير معامل الجودة. هذه الدراسة من خلال استخراج التردد الأساسي F0 وعامل التضخيم A0 لحساب مؤشر الضعف Kg. بالإضافة إلى ذلك، يمكن أن يعتمد تقدير إمكانات التميع على قيمة مؤشر Kg، الإعداد الجيولوجي ووجود الخزانات الجوفية. بشكل عام، أظهر مؤشر Kg قيمة منخفضة في جميع المحطات عكس محطة واحدة بمؤشر Kg يقارب 11. كل هذه النتائج تشير إلى وجود حبيبات أرضية غير مشبعة بسبب محتوى مائي ضئيل. ومنه يمكننا الاستنتاج أن منطقة الريف ليست عالية الخطورة تجاه التميع.

الكلمات المفاتيح: التوهين، موجة الكودا, معامل الجودة, التمييع, قياس الضوضاء الخلفية, الضعف الزلزالي, منطقة الريف

Table of Contents

LISTE OF ABBREVIATIONS

CPT : *Cone Penetration Test*

CRR : *Cyclic Resistance Ratio*

CSR : *Cyclic Stress Ratio*

EERC : *The Earthquak Engineering research Center*

HVSR : *Horizontal to Vertical Spectral Ratio*

IGN : *National Geographic Institute*

MSK : *Medvedev–Sponheuer–Karnik scale*

NT : *Nanometrics Trillium*

RPS : *Le Règlement de Construction Parasismique*

SCPT : *The Seismic Cone Penetration Test*

SPT : *Standard Penetration Test*

SSI : *Soil-structure Interaction*

LIST OF FIGURES

LIST OF TABLES

General introduction

An earthquake corresponds to a fracturing of rocks at the bottom of the earth along faults generally pre-existing. This rupture is accompanied by a sudden release of a large amount of energy which is translated on the surface by ground vibrations. Earthquakes are regarded as the most deadly and damaging natural hazard. With 484,553 deaths caused by natural disaster, earthquakes account for nearly 36% of the victims in the last 20 years. Tsunamis come second with 291,860 deaths (21.6% of the total) followed by cyclones and tropical storms which caused the death of 259,117 people (19.1% of the total) (CATNAT, 2021).

Contrary to the other geological hazards (volcano, land slide …), the force released during earthquakes, which are related generally to the movement of the blocs, can easily damage an entire city in a short time. During these crises, it became apparent that seismic risk reduction was becoming a priority in the policies of countries around the world. An earthquake will be less destructive in a country that has integrated earthquake-resistant construction into its construction standards. However, the poor comprehension of earthquake parameters that affect time, location and magnitude estimation make the prediction of an earthquake impossible. Nevertheless, the current evolution of earthquake engineering has allowed analysis methods development and calculation of the structures subjected to seismic loads, as well as more efficient process and designs to mitigate the destructive effects of large ground motions. Moreover, it is common to evaluate the seismic risk for a region in a probabilistic way which allows a long-term prediction of the seismic activity. With regard to this mathematical assessment, this method is based essentially on the analysis of historical earthquakes that have already occurred. To do so, it is necessary to determine their source parameters and their frequency in a period of time that is relatively short compared to the geological time.

To reach the increase in the development of risk analysis methods (Attenuation, liquefaction, tomography, probabilistic approach…) toward earthquakes, we first need to lean on a data base that gather all the information we seek. The seismic station is a required component and a raw material to initiate data collection. Thus, lunching the analysis process.

The interest of this thesis lies in the perspective of providing new interpretations based on techniques whose potential has been demonstrated in several studies all over the overlaps zones. Such a study was prescribed following the massive number of earthquakes, which was the first indicator to initiate this inquiry. This indicator is a direct manifestation of relative movements of tectonic blocks in this area of the southern west Mediterranean. The area is already known

by its seismic activity, but the risk on the population is little evaluated. We are not going to establish a seismic risk map of the area, but we will try to estimate the quality factor and liquefaction potential as a source parameters in order to bring a complementary explanation of the active tectonics in the studied zone.

Thesis organization

In the first chapter we will proceed to discuss the seismic history and the tectonic setting as a part to illustrate the reasons behind the high risk of earthquakes in the region. In the same chapter we will briefly mention the used seismic network and the data acquisition systems in order to clarify to the reader the data operation sequence and it importance for the study.

The main objectives of the second and third chapters are to overview the methods used whether in attenuation of coda waves to estimate the quality factor or in the seismic vulnerability to estimate the vulnerability to liquefaction. These chapters are essential to gain insight into both phenomena.

The fourth chapter will speak on a case study of an investigation using the attenuation of coda waves in the Rif, northern part of Morocco, exploring the network that has been already described in the previous chapter. Furthermore, we are intended to list all the results in figures and tables to interpret the outcomes.

The fifth chapter will also illustrate a case study of the liquefaction potential in the same region (Rif) with also the same stations that have been used to estimate coda attenuation. Moreover, the findings will be compared to geological and topographical classifications to judge the risk to liquefaction

STATE OF THE ART

1.1 Background and motivation:

The strongest earthquakes (M>6) take place essentially in the borders of the tectonic plates where the tectonic activity is associated to an extensive lithospheric faults location, where the deformation rate (Shrinking, stretching …) are the highest (**Figure 1-1_page 17**).

Near to borders of differing plate's interaction, high ground shaking can frequently occur while the most destructive earthquakes can be spotted exactly in the spots of convergent plates. It is the case of subduction zones (Chili (2010) : Mw 8.8 ; Japon (2011) : Mw 8.9 ; San Francisco (1906) :Mw 8.2...) et de collision (ChiChi, Taïwan (1999) : Mw 7.6 ; Sichuan (2008) : Mw 7.9 ; Himalaya (1950) : Mw 8.6...).

However, it has been shown that strong earthquakes are not limited to plate boundary regions but can occur also in the intracontinental domain, far from the plate boundaries, where deformation rates are low to moderate and where tectonic activity is often associated with a distribution of deformation on several fault segments, or slow fault systems (e.g. Champagnac et al., 2010; Ritz et al., 1995; Tuttle et al., 2002). In some cases, these large intracontinental earthquakes show temporal organization that allows us to speak of seismic swarms separated in time by long periods of quiescence. We can give as an example the case of Mongolia (Chéry et al., 2001; Rizza et al., 2011).

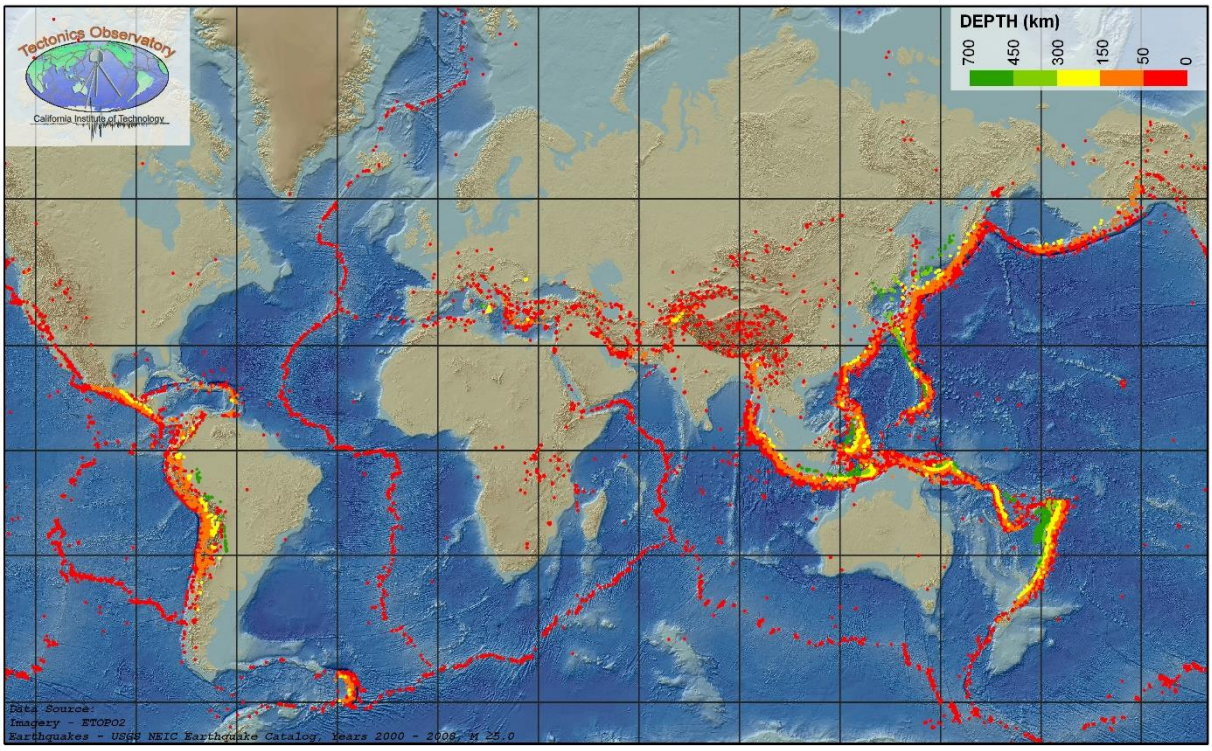

Figure 1-1: seismicity map of the earth from USGS earthquake catalogue between 2000 to 2008, with magnitude of 5.0 M and above . (https://www.nsf.gov/news/mmg/mmg_disp.jsp?med_id=64691)

1.2 Historical seismicity

Between 1994 and 2019 tree destructive earthquakes has been occurred in the northern morocco on which can be known as one the most violent earthquakes in the history of the Rif region. A region who incurred a brutal earthquake can be a spot of several series of earthquakes invoked as aftershocks that are occurred right after the main shock. Therefore, beside the historical earthquakes in this tectonic active area, which we will prove in the following manuscript, uncountable of moderate and small earthquakes occur each year. In addition, the spot with a brutal seismic antecedent can be also a provenance of another similar around earthquake in a long term. The similar earthquake recurrence interval probability of it instance can be statistically computed as per fault activity nature, seismic source, seismic movement and other parameters.

The region of Rif is an area which can be described as the front of the African plate that interplay with the Eurasian plate. This tectonic interference result in a huge amount of faults with a massive diversity in type and nature. Furthermore, faults in this area can be sorted out into different orientations relative to the earth, different mean velocity slip and different directions relative to the fault plane motion.

In this manuscripts we will use two different approaches that are way different to help in assessing risks from two different views.

The objective of this thesis is to evaluate seismic risk in the Rif mountain range (Morocco) located in a region of the world where the plate boundary is still debated (Bird, 2003; Gutscher, 2004; Klitgord and Schouten, 1986), such that Rif can be either north or south of the Eurasian-African boundary. The Alboran Sea is then, according to the plate boundary models, either part of Eurasia or Africa, or is directly on the boundary. Recent geodetic data obtained in the Alboran region (Koulali et al., 2011; Poujol, 2014; Tahayt, 2008; Vernant et al., 2010) show locally significant displacements in the Moroccan zone of a prominent SW displacements of the order of ∼5mm/yr while the regional convergence direction is NW-SE with a rate of ∼4 mm/yr. With this displacement perpendicular to the regional convergence direction, the Rif appears to have kinematics independent of the African-Eurasian convergence (Poujol, 2014).

For decades, geological and geophysical studies in the Western Mediterranean region including the Rif have been carried out in an attempt to understand the deep mechanisms that are resulting from the convergence of the African and Eurasian plates and to explain the current deformations observed in the Rif-Betic arc. Many different geodynamic models have been proposed using various approaches: gravimetry, tomography numerical modeling, paleomagnetism, seismic anisotropy, seismotectonics,... (e.g: DUGGEN et al., 2005; Faccenna et al., 2004; Fadil et al., 2006; Gutscher et al., 2002; Jolivet et al., 2008; Lonergan and White, 1997; Spakman and Wortel, 2004), but the tectonic situation remains a subject of debate.

The Rif region is the site of very active instrumental seismicity (**Figure 1-2_page 19**), but no detailed work on the attenuation of coda waves and liquefaction potential occurrence has been made in a regional scale. This seismic activity is also notable through the historical seismicity as evidenced by the earthquake of intensity MSK VIII (Medvedev–Sponheuer–Karnik scale) (Mw=6.2) occurred on November 27, 1755 in the cities of Fez and Meknes (southern Rif), 26 days after the devastating earthquake of Lisbon responsible for the death of more than 100 000 people on the European and Moroccan coasts. Closer to the study region, on May 26, 1994, the region of Al-Hoceima, located on the northeast coast of Morocco, shook under the effect of an earthquake of magnitude Mw=5.8-6 destroying many houses in the city of Al-Hoceima and in the surrounding countryside. Ten years later, on February 24, 2004, a deadly earthquake of magnitude Mw=6.3-6.5 also occurred in the province of Al-Hoceima and resulted in the death

of more than 600 people and the destruction of 2500 homes. What is more, it was felt more than 300 km from the epicenter.

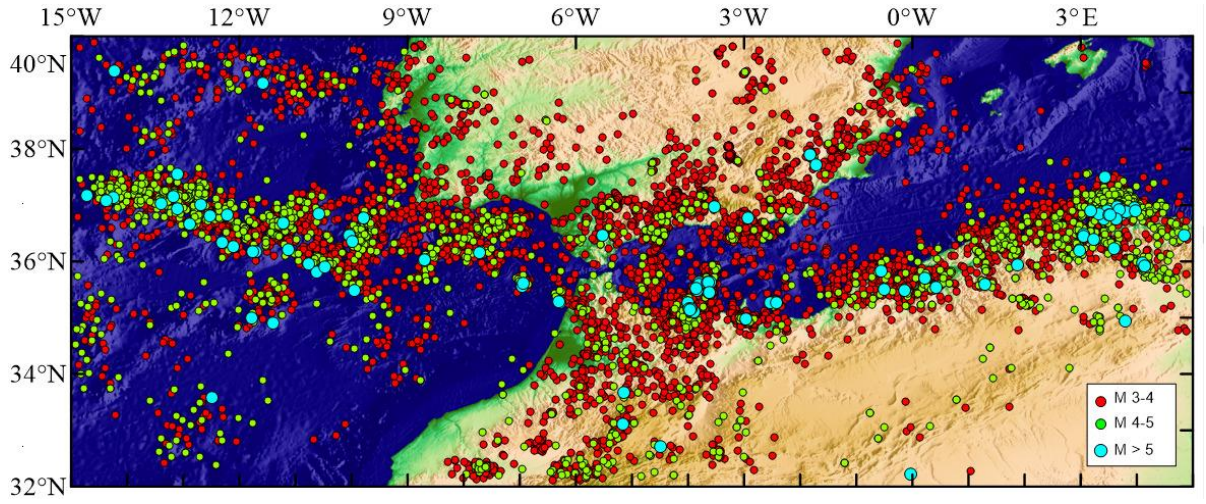

Figure 1-2: instrumental seismicity map since 1990 for magnitudes from 3 to 7 in the Mediterranean area (Catalogue de IGN).

1.3 Seismotectonic overview of the Rif chain

The Rif Range the northern Rif is marked by coastal uplift in the order of ~0.1-0.2 mm/yr along the entire Mediterranean coast (Kadiri et al., 2010; Meghraoui et al., 1996; Morel and Meghraoui, 1996). Associated with these uplifts, a series of normal faults, sometimes with transtensional components, of N-S to NNE-SSW direction that deform the upper part of the crust, in the form of horsts and grabens with Quaternary filling, up to one (or more) level of detachment at depth inherited from the phase of emplacement of the nappes. This mechanical stratification of the crust produced by the stacking of levels of different rheology, would be the origin of the differences observed between the kinematics of the faults that break the surface (normal faults) and the seismic activity (Galindo-Zaldívar et al., 2009). In addition, the authors explain the regional uplift by the presence of large folds in the upper part of the crust. Some normal faults aligned with the coastline and strongly towards the Alboran Basin have been described along the Maghreb margin on land and at sea (Ait Brahim, 1991; d'Acremont et al., 2014; Meghraoui et al., 1996; Romagny et al., 2014). The two major faults Nekor and Jebha oriented ~NE-SW direction, would be in the first glimpse responsible for the establishment of the SW-trending thrust sheets in the Miocene (Chalouan et al., 2006), that obliquely intersect the Rif Range. Seismic activity associated with these faults is almost non-existent and their activity during the Quaternary is still debated (Benmakhlouf et al., 2012; Galindo-Zaldívar et

al., 2009; Morel, 1987; Tejera De Leon, 1997; van der Woerd et al., 2014). Through reconstruction of the early Plio-Quaternary topography and the observed offsets on the Villafranchian terraces, (Meghraoui et al., 1996) had inferred a shortening rates of about 2 mm/yr on the Nekor and the Jebha faults since the Pliocene. The Jebha Fault appears to extend into the Mediterranean on the Alboran Wrinkle Fold with a reverse fault geometry, and on the Atlantic coast, south of Larache, where it appears to behave as a dampening sinister fault with folds oriented N140 (Meghraoui et al., 1996). The southern Rif is characterized by compression associated with senestial rifting along ~E-W orientation with folds and thrusts. This active Pliocene thrust front marks the boundary between the Rifan Range and the Middle Atlas/Meseta. It affects the Plio-Quaternary deposits and seems to be currently extending southwards over the foreland basins (Saiss, Rharb,...) (Bargach et al., 2004; Chalouan et al., 2006; Moratti et al., 2003). The western part of the Rif has been little studied in terms of active tectonics, only the neotectonic studies of (Morel, 1992, 1987) indicate the presence of a normal fault with~E-W orientation in dipping north in the Tetouan area and a succession of parallel folds NNW-SSE oriented folds acting as ramp propagation folds (Zakir et al., 2004). A recent study by Leroux-Mallouf,R. 2013 consistent with (Morel, 1987) suggests a recent tectonic activity in the Larache area resulting in folds associated with blind faults of N-S/NNW-SSE direction inherited from older deformations. The Quaternary deformation in the Rif seems to be globally governed by NNE-SSW, N-S and NNW-SSE shortening directions (Brahim and Chotin, 1984; Frizon de Lamotte et al., 1991; Morel, 1987), reflecting either the continuation of nappe movements south-southwestward (Frizon de Lamotte et al., 1991; Morley, 1992), or the convergence of the plates, or the concomitance of the two.

1.4 Geographic situation of the Rif chain

The Rif Mountain range is a 300 km long and 100 km wide alpine range located in the northern region of Morocco that extends between 34-36˚N in latitude and 2-7˚W in longitude. It is a highly contrasting mountain range where the humid forested landscapes of the west are contrasted with the semi-arid and steppe-like massifs of the east. The western and central regions are exposed to both oceanic and Mediterranean disturbances and are therefore very rainy (>1500 mm of precipitation per year near the town of Ketama), in contrast to the eastern part which is subject to a semi-arid Mediterranean climate and receives only 200-300 mm/year. Although this range is currently considered active, the geological terrain being mainly composed of soft rocks such as clays, marls or shales, it presents rounded and progressive reliefs where the term "badlands" (land in the form of landscapes remains with little vegetation and

cut by deep gullies) takes on its full meaning (**Figure 1-3_page 22**). The Jebel Tidirhine located on the limestone units is the highest point of the Rif with an altitude of 2456 m, for an average altitude of the chain below 1000 m.

Figure 1-3 Rif chain as looking from a road between houceima and nador (google maps)

1.5 Seismic Network (TOPO-IBERIA)

We can estimate the annual number of seismic shocks up to a few hundred concerning the Rif territory and the bordering areas. Most of these shocks are not felt by man due to its weak magnitude. These chocks express a tectonic activity which is manifested most often by the reproduction of ancient and recent crustal accidents under the influence of regional overlaps.

Compared to the world, the seismicity of the Rif can be considered as high. A detailed knowledge of the region seismicity is essential to understand the crustal movements that affect it.

The region of the study has been a subject of a seismic network that has been established by the scientific institute of rabat and the jaume almera institute of Barcelona. This seismic network had set up as part of TOPO-IBERIA project who provided 19 broad band station that has been mobilized according to the need in data. The scientific institute has been involved in international cooperation projects since 2007. These projects have allowed the renewal and consolidation by a huge network, of not only the studied area but also of all the Moroccan territory, via the observatories with recent equipment. The establishment of a dense network in the northern part of Morocco by more than 80 temporary seismic stations (**Figure 1-4_page 22**) that give a greater coverage / quantity of data and explains the need to constitute a rich seismic database useful for the research community. In our case 15 seismic stations has been

established to collect seismic signals in order to enhance the accuracy of the studies that require more collection of data in the studies zone.

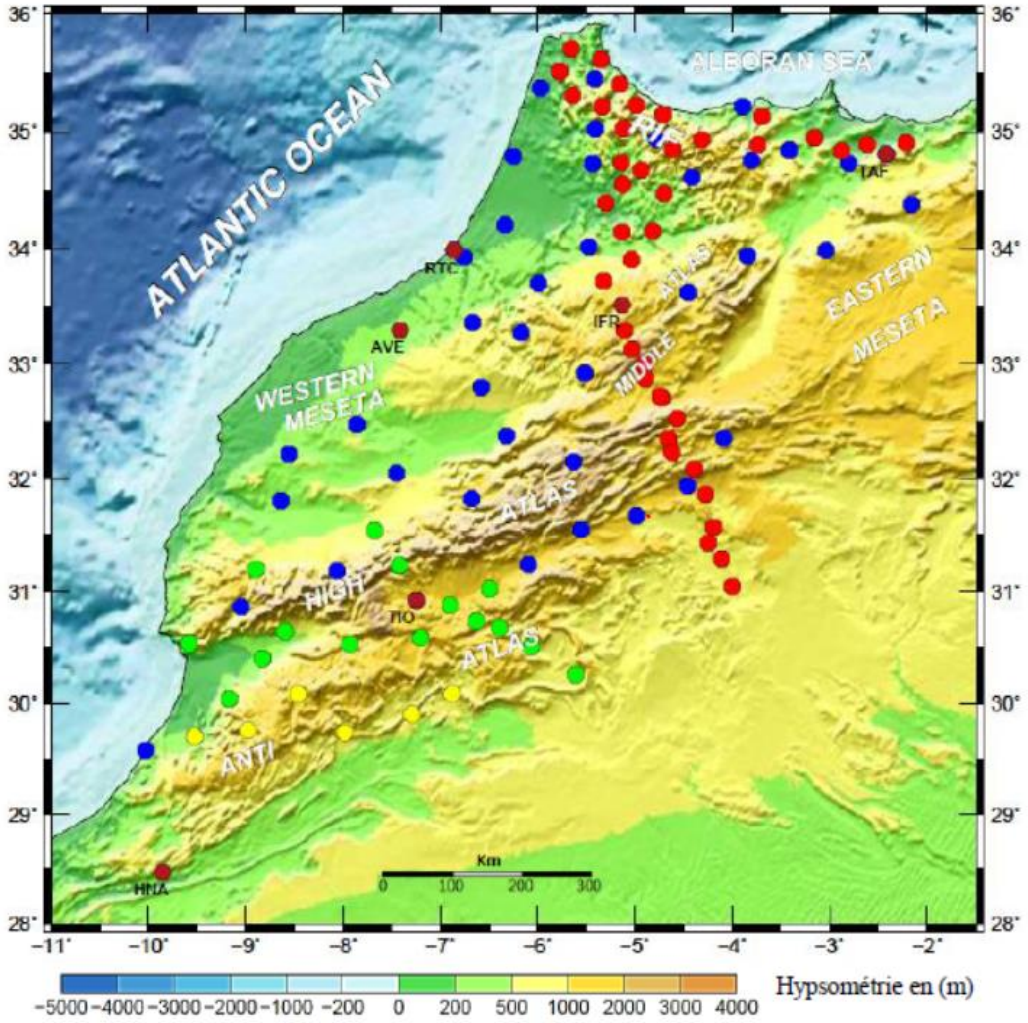

Figure1-4: Deployment map of temporary seismic stations acquired in cooperation projects with the scientific institute. (EL FELLAH 2015)

1.6 Instrumentation

The seismic station, called seismograph, is a mandatory device intended to measure all kind of earth movements with the need to give the best possible representation of the large scales of amplitude and duration, with the minimum of disorder and the maximum time precision. The seismograph contain an inner part named as seismometer which can be theoretically simulated as a pendulum, nevertheless it is often used synonymously to refer to a seismograph which is common confusion. This device can output a seismogram which is the recording of ground movement. In the case of an earthquake it can be in the form of a signal with a horizontal axis that refers to time and vertical axis that refers to earth displacement. With the absence of any source of shaking, the seismograph illustrate a straight line with a small tremor that would be caused by local disturbance called ground noise.

1.7 Seismic station operating system

A seismic station is designed as a measurement chain (**Figure 1-5_page 23**), i.e. a system whose description and analysis allow to define the input-output relationship, it integrates a multitude of sub-sets (El Fellah, 2015): Sensor, acquisition system, reference time, signal treatment, signal processing, data storage, control unit …

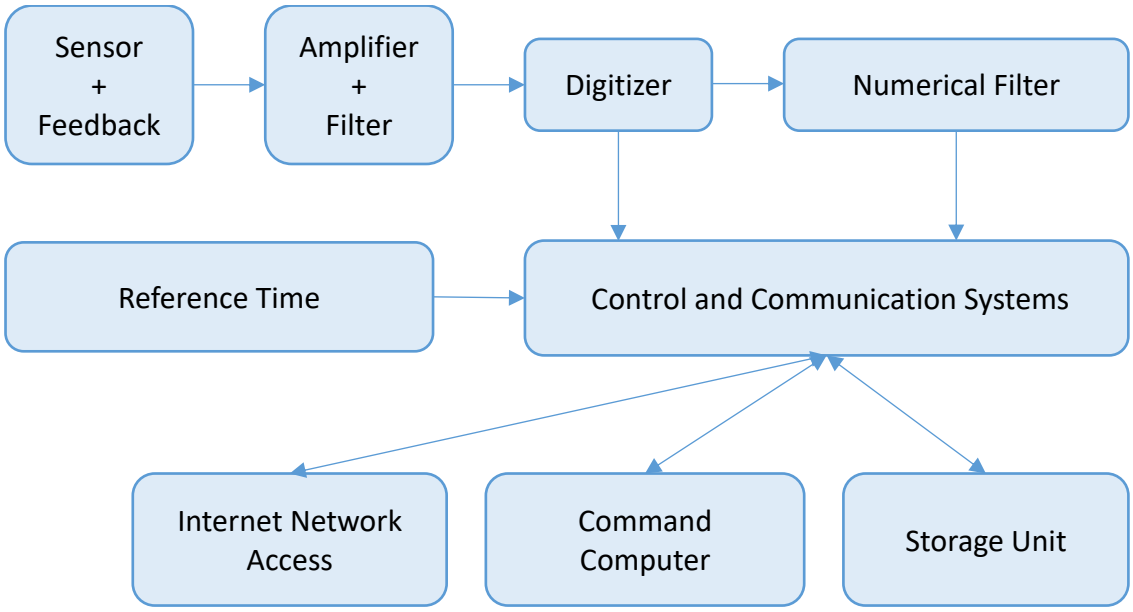

Figure 1-5: Different mechanism chain of a seismic station

1.8 Sensor

Called also seismometer, is a sensitive device to a given phenomenon capable to transform an observational physical state into a measurable physical quantity. It is a mechanical system endowed with a movement Sensor. The mechanical system is generally an oscillating system in the form of whether a rotational pendulum, translational pendulum or a translational mass with springs. The movement Sensor can be generally of two types: displacement Sensor or electromagnetic velocity Sensor.

The most used seismometers are:

- Short period seismometer whose system is said to be passive (no internal electronics), it includes a translation mass and an electromagnetic sensor. This electromagnetic or short period model (**Figure 1-6_page 24**), with a moving coil in the air gap of a circular magnet. This coil is characterized by; frequency of 1 Hz, damping 0.7 which generate a constant rotation speed of 145 v/m/s, manufactured by the Kinemetrics company. Another model of the short period seismometer named Mark L4 (natural frequency 1 Hz, damping 0.7 and constant generator 175 v/ m/s) from Lennartz, characterized by its small size and good conditions of functioning. A third model is called the Geotech S13 model also has a natural frequency of 1 Hz and a constant generator of about 629 v/m/s. The signal conditioning unit has an amplification and modulation system. From the seismometer the signal passes through an amplifier, with a range of 30 dB - 90 dB in 6 dB steps.

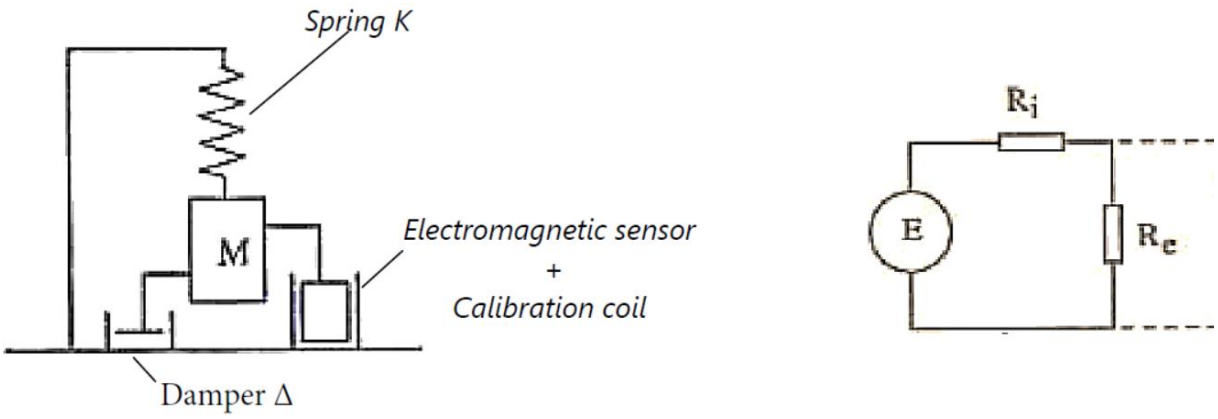

Figure 1-6: Vertical seismometer and its equivalent circuit of the electromagnetic generator

- Broadband seismometer with an active system (Need to provide energy) electronically controlled and includes a rotation pendulum, a displacement sensor, an analog filter, servo motor and re-centering motor. The Electronic Model or Broadband Seismometer with an active three-component system components is defined as capable to detect ground motion over a wide band of frequencies, hence the term "Broadband". These sensors are most often used in passive experiments, recording the weak motions of regional and teleseismic earthquakes, as well as ambient noise.

These modern seismic sensors use the negative feedback force to keep the mass motion small (as shown in **Figure 1-7_page 26**). This helps avoid problems with mechanical imperfections in the sensor.

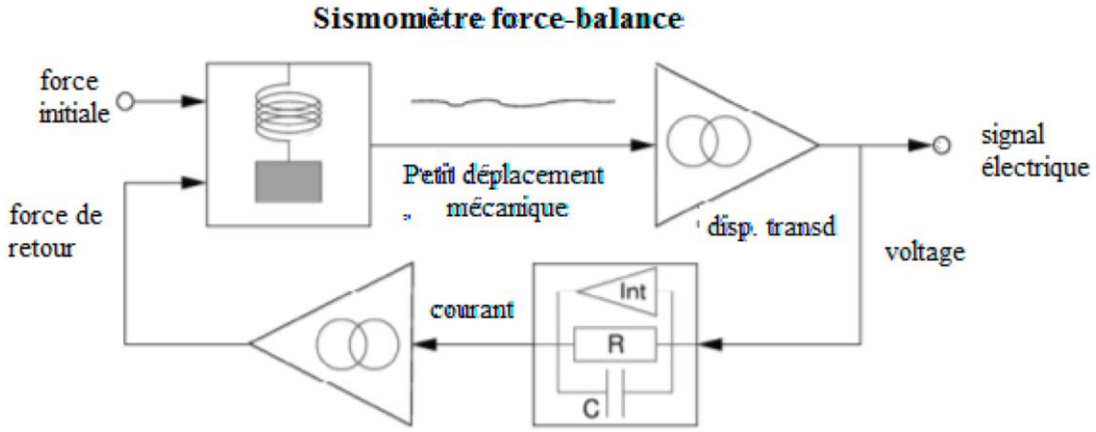

Figure 1-7: Functional diagrams of return seismometers (broadband). Ideally, in this configuration, the mechanical suspention and the displacement sensor do not detect the full aplitude of the ground motion, which is present only in the return path.

Furthermore, among the various type of broad band seismometers operated in the different seismic network projects (Streckeisen STS-2, Nanometrics Trillium 120, Guralp CMG-3T …), the Nanometrics Trillium 120 broad band sensor (**Figure 1-8_page 26**) was the one that has been used to gather the data exploited in this work. For that, we will proceed to make a brief description of the Trillium 120.

- **Broadband seismometer: Nanometrics Trillium 120**

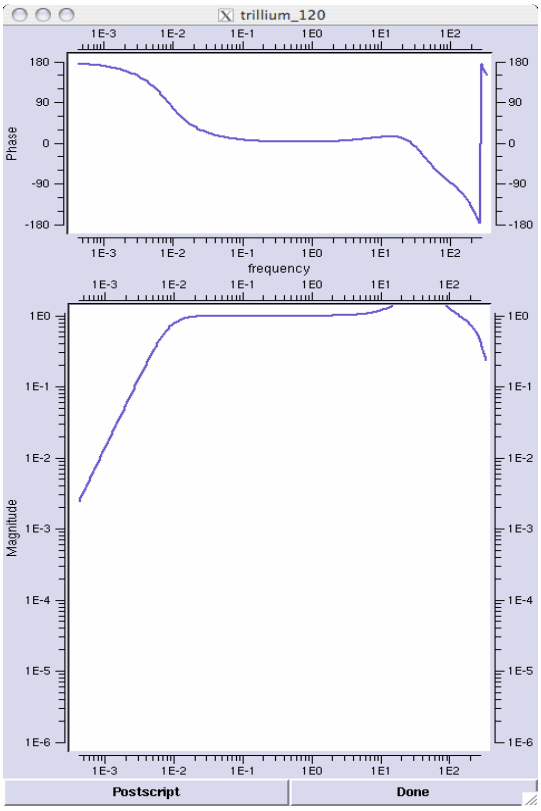

a: Nanometrics Trillium 120	**b**: Trillium 120 response characteristics

Figure 1-8: (a) – Nanometrics Trillium 120 broadband station.(b) - response characteristics of the STS2 seismograph.

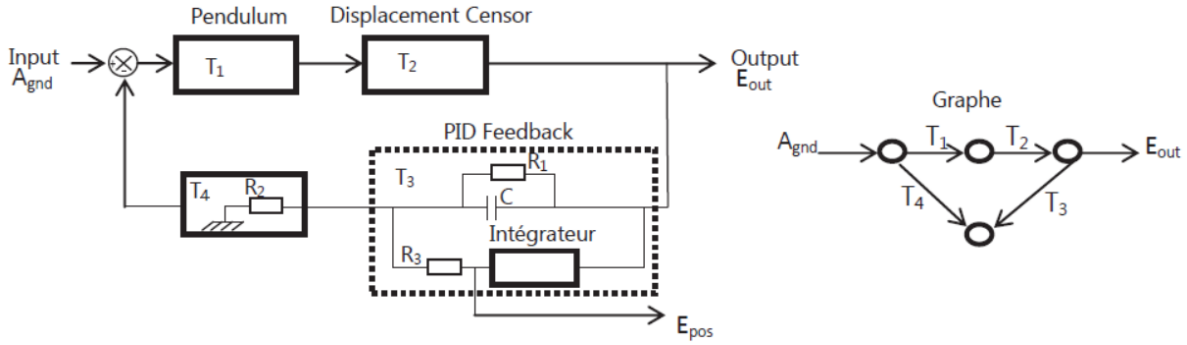

Figure 1-9: Electronic functional scheme with the seismometer graph (El Fellah 2015)

The Nanomectrics Trillium 120 seismometer: The NT-120 broadband seismometer (**Figure 1-8_page 26**) is used for the installation of seismic stations recording continuous data along the year of 2014. It has been shown that, at some sites, the vertical component of the NT-120 seismometer in the 1-5 MHz band is only 6-10 dB less sensitive than NT-120 (Widmer-

Schnidrig, 2003), this difference is often between 20 and 25 dB (e.g., Berger et al., 2004 Hanka, 2000) has shown that the sound performance of the NT-120 over long periods of time can be significantly improved by extensive extended thermal shielding.

The principle of the NT-120 seismometer is to respond to a free oscillator with a period of 120 seconds (0.008 Hz), with a differential feedback, the output is proportional to the speed of the ground between a periods of 120 s (0.008 Hz) to high frequencies 50 Hz (period 0.02 s). NT-120 seismometer contain three identical sensors with electronic and power circuits mounted in a cylindrical housing (23 cm diameter and 26 cm height).

In general, seismometer calibrations are often performed prior to the experiments, because their dynamic parameters may vary during transport and/or decay as a function of the time of use. A practical method for the calibration of seismometers using a "test table" device designed by Professor Wielandt, which can be used to evaluate the frequency response and sensitivity of seismometers (Wielandt, 2002).

Conclusion:

In the present chapter, we have talked about the historical seismicity in the northern of morocco which shows the destructive earthquakes near to the Al Houceima city in the 1994, 2004 and 2016. Furthermore, recent geodetic data has shown a significant displacement in the order of 5 mm per year which can explain the huge amount of earthquake in the region of the study. To investigate and to estimate the annual number of seismic shocks we used the seismic network of Topo-Iberia. This network allowed us to study the region of the Rif using data of earthquake registered In 2014.

A LITERATURE REVIEW OF ATTENUATION OF CODA WAVES

2.4 Introduction

The ground motion produced by an earthquake recorded in a seismic station, can be described as the convolution of the combined effects of the seismic source, the propagation path and the site effect that reflects the local effects of the environment on which the station is installed.

The impact of the propagation path on the ground motion is directly related to the attenuation of seismic waves. Therefore, the study of seismic wave attenuation is essential to study the seismic hazard and to evaluate and predict strong ground motions. One of the aimed objectives in this report, is to study the quality factor variations of the seismic waves, into five lapse times, different frequency band, and in different geological environments according to the frequency contained in the seismic signal.

The quality factor Q, dimensionless, is inversely proportional to the attenuation, which means that the seismic waves are strongly attenuated for regions with a lower quality factor Q and vice versa.

For better understanding of the attenuation of seismic wave phenomenon, we can compare a particle ground motion in a linear direction that belong to soil (**Figure 2-2_page 31**), to a mass-spring system with linear friction (**Figure2-1_page 30 and Figure 2-3_page 31**). Both, the particle and mass spring system can be modeled with the following equation:

$$m\frac{\partial^2 u(t)}{\partial t^2} + \gamma m\frac{\partial u(t)}{\partial t} + ku(t) = 0 \qquad \textbf{(2.1)}$$

Where $u(t)$ the measured displacement from the balance position and γ is is the Damping factor. While m is the mass and K is the of the spring stiffness.

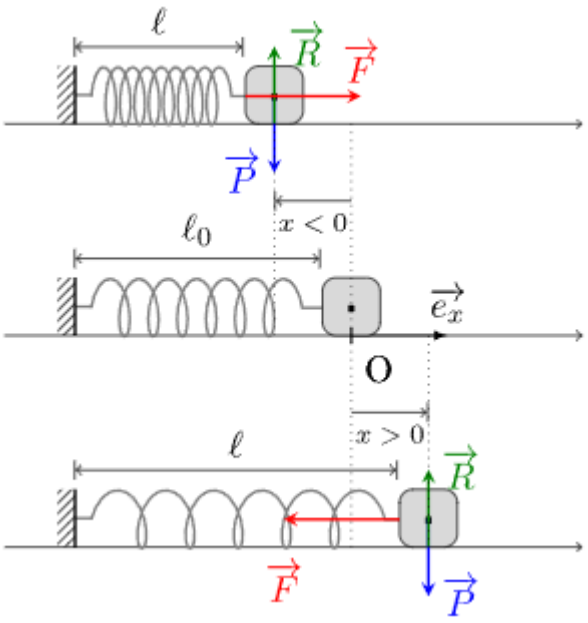

Figure2-1 : A simple example of a mass-spring system with linear friction

The damping factor is defined by the ratio of the natural frequency F0 and the quality factor Q as $\gamma = \frac{\omega_0}{Q}$ the natural frequency is determined by the relation between k and m, as $\omega_0{}^2 = \sqrt{\frac{k}{m}}$

And the eq 1 become:

$$\frac{\partial^2 u(t)}{\partial t^2} + \frac{\omega_0}{Q}\frac{\partial u(t)}{\partial t} + \frac{k}{m}u(t) = 0 \qquad (2.2)$$

For this second order differential equation, the general solution is:

$$u(t) = A_0 e^{ipt} e^{\frac{-\omega_0 t}{2Q}} \qquad (2.3)$$

A0 : initial Amplitude

$e^{\frac{-\omega_0 t}{2Q}}$: The attenuation factor caused by friction

e^{ipt} : Harmonic part

Q : Quality factor inversely proportional to damping factor

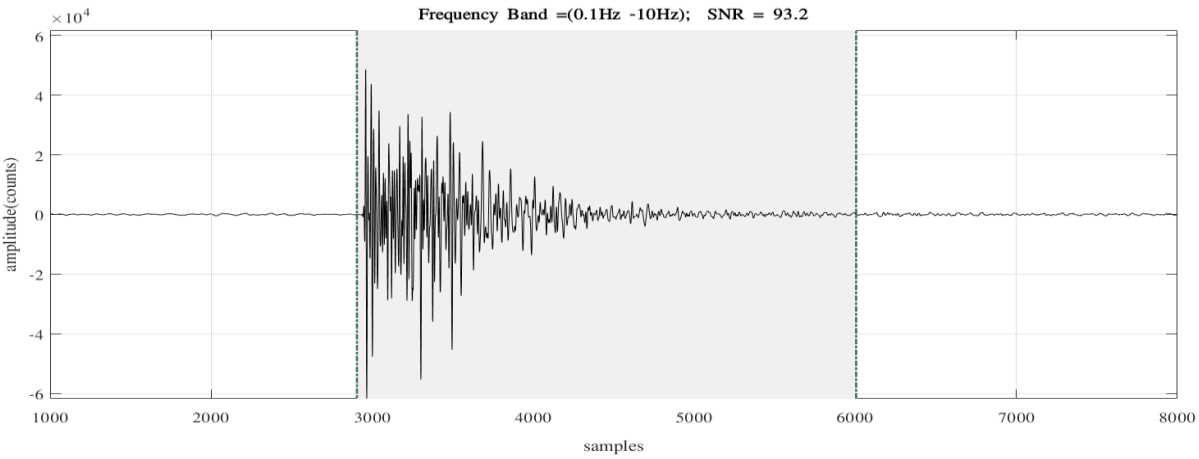

Figure 2-2: Actual behavior of a partical ground motion excited by an earthquake

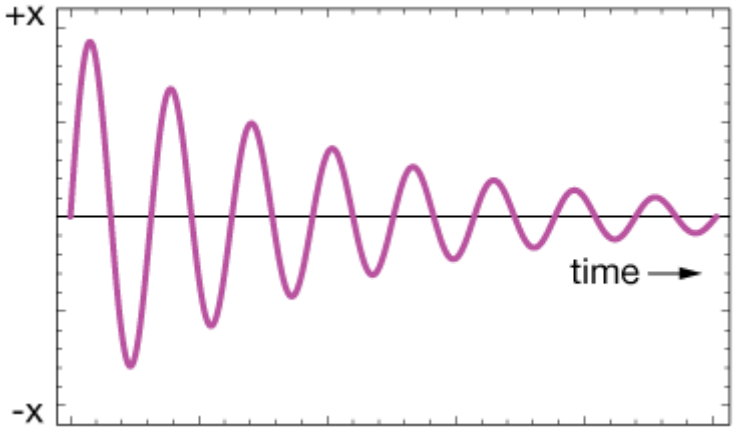

Figure 2-3: The harmonic oscillator model curve of mass-spring system with linear friction

2.5 Observations: Coda waves attenuation

In function of distance between the seismic source and the seismograph, the seismic signal sample the earth into different parts. At our planet scale, an event is called teleseismic when the distance between the epicenter and the receiver reach thousands of kilometers. Furthermore, if the event exceeds 150 Km far away from the seismic network, we can name it regional. In this manuscript we are going to be interested in earth crust characteristics. Therefore, we will utilize registered local earthquakes in an epicentral distance around 150 km or less.

In the first instance, we propose to make such observations on a registered soil movement so as to comprehend what is the relationship between seismic coda and the seismic attenuation, and why precisely seismic coda is an interesting part of the seismic signal.

2.6 Seismic coda definition (scattering intrinsic absorption)

The attenuation cannot be attributed to geometrical spreading, in contrast, it describes the decay of the wave amplitude that come about when a wave spread through real media. The attenuation can be expressed by the quality factor Q and is induced by two major springs: attenuation that come from intrinsic absorption and attenuation that is derived from scattering due to the existence of heterogeneities. Coda wave analysis can be a handy tool for discriminating between the two capital types of attenuation. (Gao, 1984) (Herraiz and Espinosa, 1987).

(Dainty and Toksöz, 1981) summarized this theory by the relation:

$$\frac{1}{Q} = \frac{1}{Qi} + \frac{1}{Qs} \tag{2.4}$$

Where Q is the quality factor value which can be obtained by experimental measurements which are based on the decay of seismic waves; Qi^{-1} express the intrinsic absorption while Qs^{-1} represents the attenuation due to scattering. Danty and Toksöz writes expression (2.4) as follow:

$$\frac{1}{Q} = \frac{1}{Qi} + \frac{gv}{\omega} \tag{2.5}$$

Where g, v, and ω are turbidity coefficient, the velocity, and the frequency of the considered wave respectively. Dainty has used the equation (2.5) to describe the quality factor behavior as well as several authors to assess turbidity and absorption coefficients (Castellano et al., 1984; Del Pezzo and Zollo, 1984) and additionally the mean free path (Rovelli, 1983).

In a given geographical pattern it has been spotted that these factors are the key component to determine the seismic signals characteristics of local earthquakes. Long-time duration seismograms reflect a low medium absorption and a strong scattering. Contrariwise, regions with high absorption reduce the scattering phenomenon and scale down duration time on seismograms. Consequently, and for the impact of attenuation on coda waves, we can use coda recordings to estimate its attenuation value. In fact, since 1975, coda waves have proved to be a useful tool to evaluate regional Q, joining the more conventional methods based on body waves, surface waves, and free oscillations of the earth. Henceforth, and for the clarity Q

estimations grounded on coda waves will be expressed as Qc. One of the facts that supports coda waves models as S to S backscattered waves is the study of Dodaira and Tsukuba in japan that exhibit a close result between Qc estimates and attenuation of S waves Qβ for frequencies higher than 1.5 Hz (Aki, 1980).

Expression (2.4) state that the Q estimation is grounded on the decay amplitude ratio of coda waves and can be named as Qc, which contain not only scattering as elastic attenuation but also absorption as anelastic attenuation.

2.7 Single-Scattering model:

A radical work has been made by (Aki, 1969) when he assumed that the coda is a compound of backscattered surface waves caused among unfettered, homogenous and isotropic medium where the heterogeneities are arbitrarily and bi-dimensionally distributed on the surface. To take this model into account, the size of scatterers should be greater than the wavelengths with no velocity disturbance and no multiple scattering is permitted. The expression was written on the grounded of these presumptions:

$$P(\omega|t) = {M_0}^2 |\varphi_0(\omega|r_0)|^2 \, 2 \, \frac{N(r_0)}{t} e^{-\omega t/Q} \tag{2.6}$$

Where

$$S(\omega) = {M_0}^2 \tag{2.7}$$

And

$$C(\omega|t) = |\varphi_0(\omega|r_0)|^2 \, 2 \, \frac{N(r_0)}{t} e^{-\omega t/Q} \tag{2.8}$$

Where N(r0) is the number of scatterers with a radius of r0. |ϕ0 (ω|r0) | mean the Fourier transform absolute value of the displacement. The term $e^{-\omega t/Q}$ integrate the medium dissipation. $P(\omega|t)$ is linked to the measured amplitude y(t) by the expression:

$$< y^2(t) >= \sqrt{\frac{Q}{2\pi(-\frac{dt}{d\omega_p})}} P\left(\omega_p \middle| t\right) \tag{2.9}$$

The relation between P(ω|t) and the amplitude y(t) in this formula is an error function approximation with a peak at a frequency p. The peak frequency can be determined directly on

the seismogram at time t by measuring the wave period. The previous equations can be used to estimate the seismic moment of small and very small earthquakes. Also, the coda excitation is strongly related to the geology of the site where the station has been set. This inference is already proven and it will be proved in this manuscript.

Despite its simplicity, this surface wave model has been so far useful in coda analysis development. All the same, some modifications has been done to enhance the accuracy of this model on some definite purposes such as evaluating Q (Herrmann, 1980) where (Kopnichev, 1975) develop a theory to explain surface wave coda in a distance between 100Km and 3000 km. Kopnichev theory presume that:

Primary and scattered waves are short-period surface waves of the same type.

Primary and scattered waves are monochromatic with period T.

Scattering is single and isotropic.

The inhomogeneities are random and stationarily distributed in the near surface.

According to these presumptions, this theory ameliorate the model of coda across the peak amplitude through the expression bellow.

$$A_i(t, \Delta t) = \sqrt{\frac{\Delta t}{t}}\ e^{-\pi t/QT} \qquad (2.10)$$

Where A_i, Δt and t are the square root energy, the time interval and the reference time respectively. In an epicentral distance from 100 to 1800 km this ameliorated coda model could not agree more with the coda wave envelope. Furthermore, this model was the spark of the first steps to double and triple scattering analysis.

Quite a few authors (Aki et al., 1958; Aki and Tsujiura, 1959; SCHEIMER and Landers, 1974) have done some interesting studies, which was in the form of improved attempts to explain coda wave's origin. All these authors put forward two extreme models. The first one is the well-known single-backscattering model that considers the coda as the superposition of the backscattering wavelets from discrete scattering sources (Herraiz and Espinosa, 1987). The second is the diffusion model that assumes the seismic energy transfer as a diffusion process (Herraiz and Espinosa, 1987). Hereafter, attention will be heed only to the first proposed model (The single-backscattering model).

The single-backscattering model is very comparable to the surface-wave model, nevertheless it propound that body waves are the cause of coda waves appearance, which reflect a major milestone in the explanation of coda waves.

In accordance with these theories, the expression (2.11) was emerged taking the geometrical spreading and the attenuation into account due to the presence of anelasiticy in Earth for body waves.

$$P(\omega|t) = |\varphi_0(\omega|r_0)|^2 \frac{8r_0^4 \pi n_v}{vt^2} e^{-\omega t/Q} \quad (2.11)$$

Where $|\varphi_0(\omega|r_0)|$ express the amplitude spectra of the backscattering wavelet from a single scatterer at a reference distance r0. nv is the density of scatterers per unit of volume, v is the wave velocity, and t represents the lapse time. The expression (2.11) would be rewritten as follows:

$$P(\omega|t) = S(\omega) \frac{e^{-\omega t/Q}}{t^m} \quad (2.12)$$

Where $S(\omega)$ is the source term, and the term $\frac{e^{-\omega t/Q}}{t^{-m}}$ express the medium impact. t^{-m} describes the factor of the geometrical spreading. $e^{-\omega t/Q}$ should undoubtedly conveys both scattering and intrinsic attenuation effects. (Aki and Chouet, 1975) did not include the scattering for the diffusion model which is correct but not in the case of the single-scattering model. The expression below has the form:

$$S(\omega) = |\varphi_0(\omega|r_0)|^2 \frac{8r_0^4 \pi n_v}{v} \quad (2.13)$$

The $S(\omega)$ expression is originated from two terms $|\varphi_0(\omega|r_0)|^2$ and $\frac{8r_0^4 \pi n_v}{v}$. The later factor is independent of the source, it remains constant for a given r0, it also include the entire number of scatterers. In the other hand the initial factor express the intensity for a single secondary wave leaving a scatterer at a reference distance r0. A relation between the primary source and the secondary wave can be expressed as follows:

$$|\varphi(\omega|r_0)| = M_0 |\varphi_0(\omega|r_0)| \quad (2.14)$$

The M_o is the seismic moment, and $|\varphi_0(\omega|r_0)|$ is independent of source effects (Aki, 1969). ω is assumed lower than the corner frequency of the earthquake. If we assume that scatterers are uniformly distributed in space in the statistical sense holds, and the expression $|\varphi_0(\omega|r_0)|$ is constant in a given area, then variation of $S(\omega)$ will be only dependent to the difference in M_0 (Earthquakes).

2.8 Conclusion:

In the present chapter, we suggest to overview the attenuation of waves especially for the coda. Moreover, we have define the backscattering theory as a way to model the damping energy of earthquakes. We also, identify the quality factor Q as an important parameter to quantify the impact of earthquakes in a given region. After that, a case study of attenuation of coda waves will be invoked in chapter for along with the geological description of the studied area so as to experiment the single backscattering model in assessing risk of earthquake in the studied area.

A LITERATURE REVIEW OF SOIL LIQUEFACTION

3.4 Introduction

The phenomenon of soil liquefaction was first discussed in 1819 by James MacMurdo (Macmurdo, 1824) following an earthquake that struck the region between Karachi and Bombay, in the northwest of India. At that time, MacMurdo was one of the firsts in this region who describes (without using the term liquefaction) the phenomenon of water and sand ejection from the ground as well as slow subsidence movements that are today equated with the liquefaction phenomenon (Seed and Idriss, 1982). MacMurdo also compares the generated damages to structures based on different types of soils, highlighting the local influence of these on the effects of earthquakes (Seed and Idriss, 1982).

Although some studies using soil mechanics parameters were conducted by Casagrande in 1936 (Seed and Idriss, 1982), the term "spontaneous liquefaction" used by Terzaghi and Peckdid did not appear until 1948. This term of spontaneous liquefaction define a sudden change in the behavior of a loose sand deposits conducted by external disturbance, which lead the deposits from characteristics of a solid material toward a material with fluid characteristics (Poncelet, 2012).

In spite of these few descriptions of the phenomenon, the scientific interest on this issue appears only in 1964, as a result of two major earthquakes, in Anchorage (USA) and Niigata (Japan) (**Figure 3-1_page 39/40**), which caused significant damage to a number of structures which were linked, among other things, to the phenomenon of soil liquefaction.

Since then, concerns for public safety, but also for the safety of high-risk structures such as dams and nuclear power plants, have led to a great deal of research in order to develop a better understanding and predictive tools for the phenomenon. This topic still represents one of the most important, interesting, complex and controversial subjects in geotechnics (kramer, 1996).

(a)- Building overflow phenomena caused by liquefaction after Niigata earthquake 1946 (National Information Service for Earthquake Engineering, EERC, University of California, Berkeley).

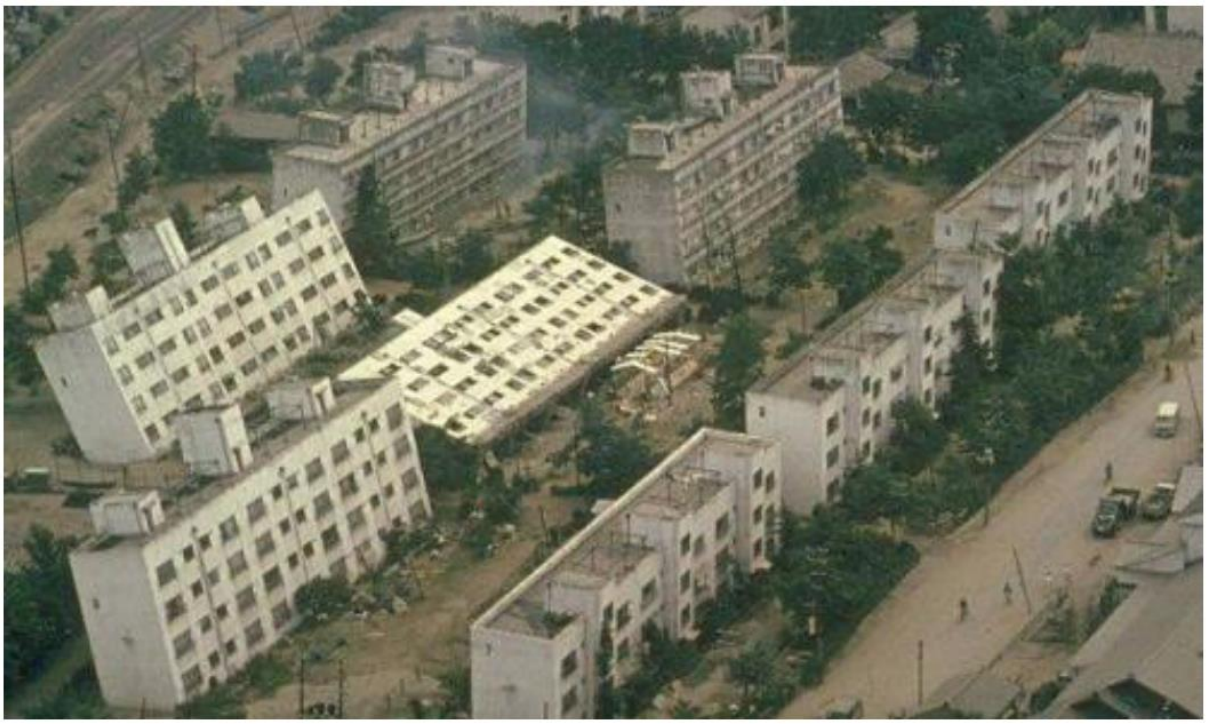

(b)- Showa bridge failure caused by liquefaction after Niigata earthquake 1964 (Steven L. Kramer, 2008).

(c)- Sand boiling evidence of the liquefaction phenomena after Niiigata earthquake 1964 (964. (Photo from National Information Service for Earthquake Engineering, University of California, Berkeley).

Figure 3-1: Liquefaction caused damage illustration after Niigata, japan 1964 earthquake, (a)- Building overflow, (b)- Showa bridge failure, (c)-soil liquefaction evidence on sand.

Figure 3-1_page 40 show the devastation effect of liquefaction phenomena after a seismic triggering. The registered impact of liquefaction occurrence in the Niigata disaster did severely affect the mechanical characteristic of soil. Thus, building overflow which is caused by the sudden loss in the bearing capacity. Furthermore, subsurface densification manifests itself on the ground surface as settlement. The induced settlement causes damage to utilities and networks such as lateral displacement of the land. Loss of shear strength induce also structures instability (dams, dikes and embankments). This instability occurs when the shear stresses required to maintain the equilibrium of a soil embankment, exceed the shear strength of that embankment (Andrade et al., 2013; Borja, 2006).

3.5 Seismic soil liquefaction phenomenon

Liquefaction is a phenomenon in which the shear strength of a soil is reduced by earthquake shaking or other rapid loading. Liquefaction occurs in powdery soils saturated with water; the presence of water causes pore pressure on the soil particles, resulting in a decrease in effective stresses in the soil and thus a decrease in its shear strength, which in the ultimate state, can become zero. Prior to an earthquake, water pressure is relatively low. However, the shaking of an earthquake can cause a considerable increase in pore water pressure to the point that soil particles can easily move relative to each other.

The phenomenon in question arise under seismic stress (possibly, at the seaside, riverside under the effect of the swell or following a seismic activity). The passage of a seismic wave causes, in certain geological formations the loss of resistance of a sandy material saturated in water in a loose state, linked to an increase of the pore pressure generated by the cyclic deformations. The sudden deconsolidation of the material results in soil collapse, making the constructions resting on these formations particularly unstable. The phenomenon of liquefaction concerns certain geological formations and geotechnical parameters, defined by their; nature, cohesiveness (compaction degree), water saturation degree, granulometry (grain size).

Liquefaction is thus effective when the pore pressures are close to the confining pressure, thus decreasing (until cancelling) the effective stresses of the material. It is therefore necessary that the material considered is saturated. Moreover, it appears that the granulometry of the considered material has a certain importance, the soils susceptible to liquefy under cyclic loading being silty to sandy.

At a microscopic scale, the phenomenon can be represented in **Figure 3-2_page 42** as, in the initial state (a), the grains are at rest; they are in a saturated environment and in a relatively loose state. They are in contact with each other, allowing the transmission forces expressed on a larger scale by the notion of effective stresses. During dynamic loading (b), a reorganization of the grains occurs. In non-conditions, this reorganization results in a pressure rise of the pore water, since the grains no longer occupy a sufficient volume to maintain the transmission of the initial effective constraints. These are therefore cancelled, which results in a rise in pressure of the pore water until the total stresses are equalized (c). The contacts between the grains are then very weak and the whole behaves like a liquid; and then the liquefaction phenomenon would occur.

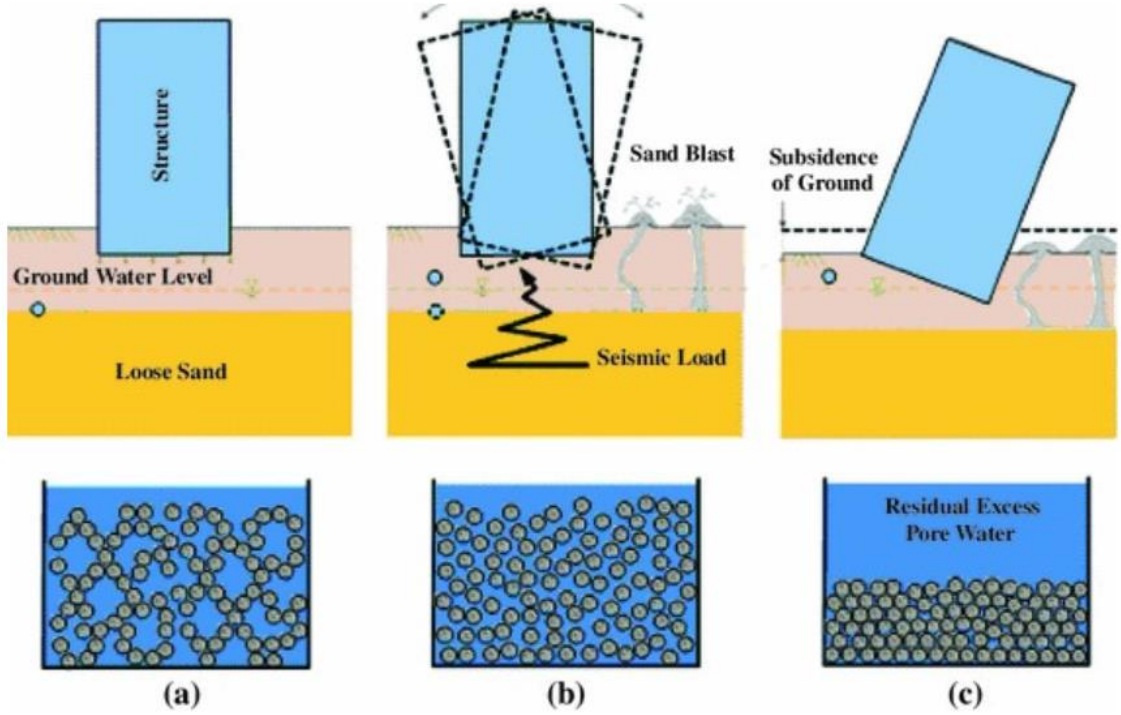

Figure 3-2: Scheme of the differential settlement of the structure due to the foundation soil liquefaction. (Soil liquefaction - description and protection measures)

Earthquake observations have provided much information on the subject of the susceptibility of certain soil types to liquefaction. Soils that have liquefied in the past may still do so by future earthquakes triggering especially in our case with the amount of earthquakes that occur in the Rif region. The study of susceptibility is related to the study of past earthquakes. It is expected that the information will be available in the form of maps on which are areas where liquefaction has occurred in the past and/or may occur in the future.

In this thesis we will look for any future liquefaction potential in the same region of the study using micro tremor measurement of the same stations that has been used to estimate coda attenuation. We will use the so called Horizontal to Vertical Signal Ratio (HVSR) method developed by Nakamura and we will deduce other parameters that are directly related to liquefaction. As for all study's methodology, we will discuss these parameters in the heed of geological and hydrogeological data region history in order to estimate the risk related to liquefaction.

3.6 Geotechnical factors influencing soil liquefaction resistance

Several factors that could influence soil liquefaction resistance, who can be weather related to physical nature or tied to environments circumstances. In general two main combined factors

could affect the triggering of liquefaction phenomenon; the first one is involve the geotechnical aspect, characterizing the susceptibility of the site to the phenomenon, while the second aspect correspond simply to the amplitude of the tripping event, i.e., the seismic hazard, characterizing the opportunity for such phenomena to take place.

3.6.1 Granulometry and angularity

Grain size has a significant effect on the liquefaction resistance of a soil. A sample with a small grain size will have a high void index, which increases the liquefaction potential. In the case of soils with a large grain size, the fine grains occupy the space between the coarser grains, which results in a more stable and resistant structure. A quick determination of the liquefaction risk of a soil could be possible by comparing its particle size curve with **Figure 3-3_page 44**. The latter shows a grading range of natural soils susceptible to liquefaction as proposed by (Hunt, 1986).

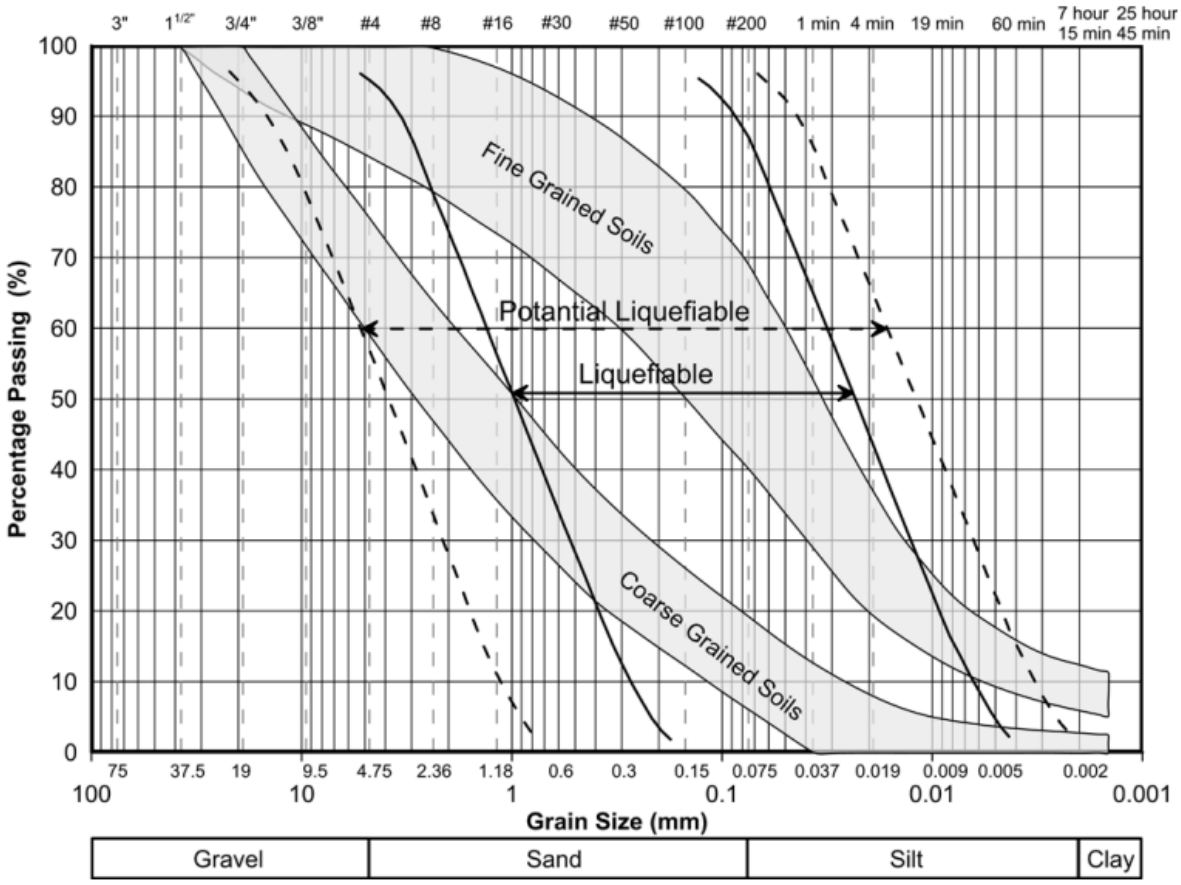

Figure 3-3: particle size distribution interval of fine–coarse grained soils ((A. Orhan et al 2013)

The shape of the grains also plays an important role, as soils with highly angular grains are more resistant to grains to stresses than spherical particles that can move more easily relative to each other. This notion must however, be taken into consideration at the time of put in

relation with the confining pressure applied to the sample studied. As a matter of fact, (Vaid et al., 1990) carried out various simple cyclic shear tests on sand samples in order to evaluate the effect of the angularity of the particles. According to their results, it appears that the resistance to liquefaction of angular sands at a low level of confining effective stress (less than 200 kPa) is higher than spherical sands for an identical relative density. When the confining stress is increased (between 200 kPa and 800 kPa), spherical sands can be stronger than angular sands depending on the relative density of the angular sands. On the other hand, for very high confining stresses (higher than 800 kPa), spherical sands are more resistant than angular sands. All in all, the angular and the spherical sand, each one has better capacity in resistance then the other depending on level degree of effective stress.

3.6.2 Saturation degree

To initiate liquefaction, the soil does not necessarily have to be in fully saturation conditions. However, the degree of saturation is another important parameter. The difference between two soils saturated at 100% and 95% respectively is far from negligible, the resistance to liquefaction can be 15 to 20% higher in the second case (Xia and Hu, 1991). The development of suction in the case of a less saturated sample could be at the origin of this an increase in strength that would lead to an apparent cohesion within the sample (James, 2009).

The degree of saturation of a sample can be determined experimentally using the Skempton B coefficient, which is designed to characterize the response of the soil to which an isotropic stress is applied. A low value indicates good saturation, the effect of the applied stress can be directly related to the soil response. (Yang et al., 2004) discussed many results from saturation studies and concluded that liquefaction resistance was increased as the Skempton coefficient decreased.

3.6.3 Deposit age

Over time, the particles will tend to rearrange themselves into a denser configuration and become cemented (Leon et al., 2006) leading to an increase in the liquefaction resistance of a deposit (Youd and Idriss, 2001). This observation has been confirmed in the case of natural (Leon et al., 2006) and artificial (Troncosso, 1986) sedimentation.

3.6.4 Hydraulic conductivity

The generation of pore pressures is one of the agents that could contribute to the development of the liquefaction phenomenon. The hydraulic conductivity is an important factor in the

initiation of the phenomenon. In the case of a medium to high conductivity, the dissipation of pore pressures may be fast enough to prevent the development of liquefaction. In the case of granular soils with a lower hydraulic conductivity, the susceptibility is normally higher. The use of drainage methods is regularly used to sort the problem out.

3.6.5 Presence of fine aggregates

Several studies that aimed to characterize the influence of the presence of fines on the resistance to liquefaction of a soil indicate that it is an influential parameter to soil liquefaction resistance. According to (James, 2009), each soil has a unique limiting value below which the resistance to liquefaction decreases with the void index of the sand skeleton and above which the resistance is relatively constant.

3.6.6 Plasticity of soil

The influence of the plasticity can be evaluated with the help of the Atterberg limits which allow to define the plasticity index IP (= WL - WP) associated to the range of water contents within which the soil behaves as a plastic material. Where WL present the liquidity limit and WP the plasticity limit. Soils with a moderate to high plasticity index are not subject to liquefaction, although they may undergo cyclic softening (kramer, 1996). The resistance to liquefaction would increase with the increase of the plasticity index value.

3.7 Methods for assessing liquefaction potential using simplified approaches

Different approaches exist to evaluate the liquefaction potential of a soil such as methods based on in situ tests or laboratory tests. An analysis of the site allows characterize the overall risk related to liquefaction. The superficial layers composed of young deposits of fine pulverulent soils where the groundwater aquifer is shallow are considered as critical. This zones are presenting a high seismic hazard to liquefaction. Chinese criteria (Chinese criteria - Wang, 1979) can help to identify soils susceptible to significant loss of strength following an earthquake. These criteria are as follows:

- Quantity of particles lower than 5 μm ≤ 15%
- Liquidity limit $W_L \leq 35\%$
- Water content $W \geq 0.9\ W_L$
- liquidity index $I_L \leq 0.75$

Although sands do not have neither liquidity limit nor a liquidity index, these criteria could apply. Further investigation of the potential risks of liquefaction can be performed using the methods presented in this section.

Before discussing the experimental laboratory and field analysis methods, it is useful to describe the Simplified Method or Cyclic Stress Method developed by Professors Seed and Idriss of the University of California at Berkeley in California (Seed, 1979; Seed and Idriss, 1970). Based on the various observations and research conducted after the 1964 earthquakes in Japan and Alaska, the method was updated in 1998 by the National Center for Earthquake Engineering Research (Youd and Idriss, 2001). It consists of comparing the average cyclic shear stress CSR caused by an earthquake on a soil element with the resistance of the soil element to the loading.

3.7.1 Cyclic stress ratio

The effect of an earthquake on a soil element can be represented by the Cyclic Stress Ratio (CSR) defined as the ratio of the average cyclic shear stress τ_{moy} to the initial effective vertical stress σ_{moy} (Seed and Idriss, 1982).

$$CSR = \frac{\tau_{moy}}{\sigma_{moy}} = 0.65\left(\frac{a_{max}}{g}\right)\left(\frac{\sigma_{v0}}{\sigma'_{v0}}\right)r_d \qquad (3.1)$$

τ_{moy} : Average cyclic shear stress [Pa].

a_{moy} : Maximum horizontal acceleration at the ground surface [m/s2]

g: Gravitational constant (9.81 m/s2)

σ_{v0} : Initial total vertical stress [Pa].

σ'_{v0} : Initial effective vertical stress [Pa].

r_d : Stress reduction coefficient according to depth

The factor 0.65 is an empirical factor, determined from observations, to represent the average value of the shear stress developed during an earthquake. This value corresponds to 65% of the maximum stress value obtained from the Peak Ground Acceleration (PGA) (Seed and Idriss, 1970).

The stress reduction coefficient r_d can be determined based on the use of **Figure 3-4_page 47** showing the value of r_d as a function of depth (Seed and Idriss, 1982; Youd and Idriss, 2001).

We can also determinate r_d coefficient based on the following equations (Youd and Idriss, 2001):

$$r_{d=1-0.00765\times z} \quad \text{for } Z \le 9.15\text{m} \tag{3.2}$$

$$r_{d=1.174-0.0267\times z} \quad \text{for } 9.15\text{m} \le Z \le 23\text{m} \tag{3.3}$$

$$r_d = \frac{1-0.4113\times\sqrt{z}+0.04052\times z+0.001753\times z^{1/3}}{1-0.4177\times\sqrt{z}+0.05729\times z^{3/2}+0.001210\times z^2} \tag{3.4}$$

Where z represent depth below ground surface in meters.

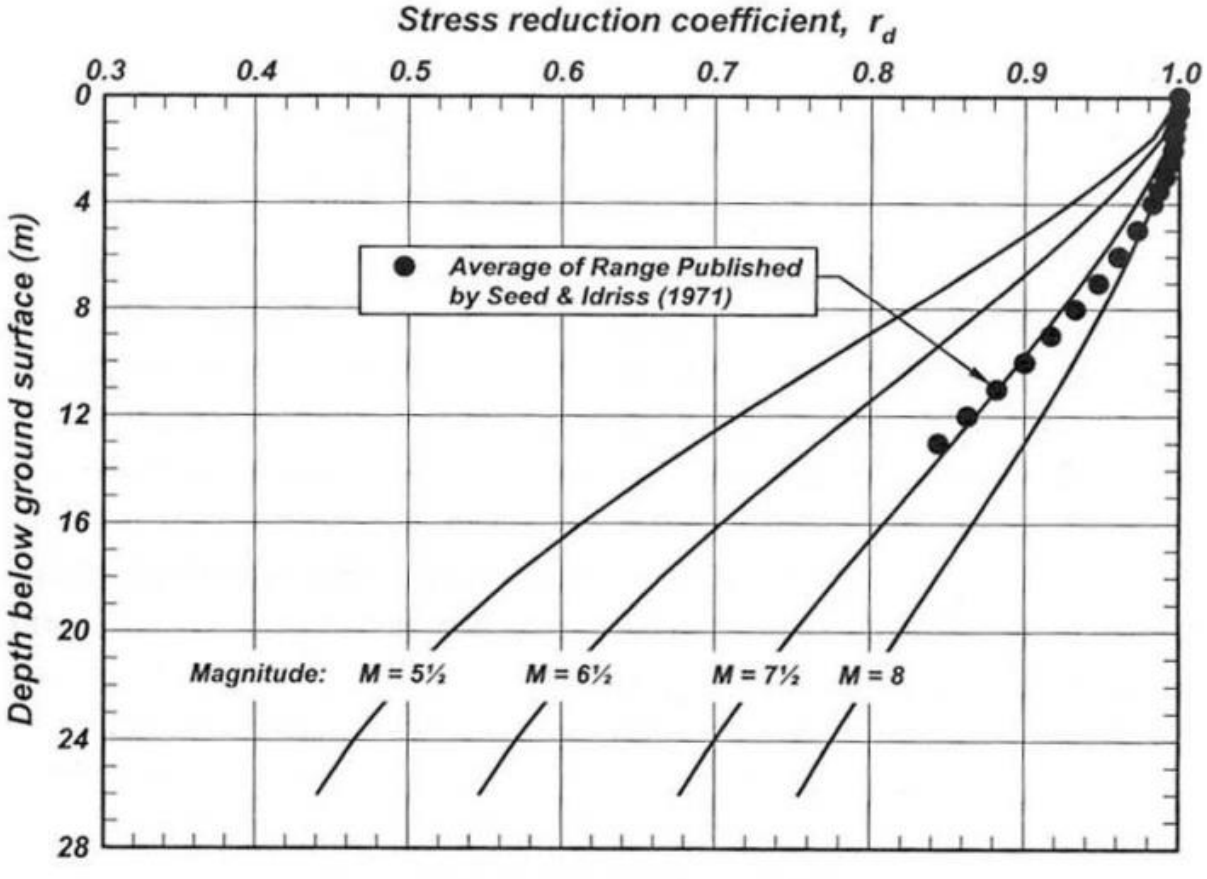

Figure 3-4 : variation of stress reduction coefficient rd with depth and earthquake magnitude (Seed and Idriss 1982)

The expressions 3.2 and 3.3 are directly deducted from **Figure 3-4_page 47**, while the expression 3.4 was proposed by Blake 1996 and published by (Youd and Idriss, 2001). Figure 3-4 shows that there is a marked difference between the possible values of rd as the depth increases. This difference is caused by the characteristics of the soil. When the depth exceeds 20 meters, this tendency increases, but the use of the simplified method is not recommended by (Youd and Idriss, 2001) for these depths. As a matter of fact, the various observations show that the effects of liquefaction are limited to the development of the

phenomenon for depths not exceeding 15 meters. However, the method is still used for prediction of liquefaction to depths of 50 m (Byrne et al., 2004).

3.7.2 Cyclic resistance ratio (CRR)

The ability of a soil element to resist liquefaction can be estimated by the Cyclic Resistance Ratio (CRR). The CRR is expressed as the quotient between the average shear strength of the soil volume and the initial effective vertical stress. It can be calculated in different ways, depending on the type of test used.

- *Standard Penetration Test (SPT)*

The standard penetration test is the most used test and consists in determining the number of strokes N necessary to drive a core drill to a depth of 30 cm, while taking reworked samples indicative of the different layers crossed. This method uses the standard penetration index $N_{1\text{-}60cs}$ where the notation associated with the value of N has the following meaning. 1 indicates a normalized value for a load of one atmosphere (100 kPa), 60 indicates a normalized value for an efficiency of 60% of the total energy supplied, cs indicates a normalized value for clean sand, i.e. without fine particles. We note that, these conditions are almost never encountered in reality. Therefore it is necessary to appropriate correction factors. In the case of clean sand, the standard penetration index $N_{1\text{-}60}$ can be determined as follows (Youd and Idriss, 2001).

$$N_{1-60} = N \times C_N \times C_E \times C_B \times C_R \times C_S \quad (3.5)$$

Where

N: Number of strokes actually needed measured at the sink

C_N: Correction factor for the effective confining stress (depending on the depth),

C_E: Correction factor for the energy transmitted

C_B: Correction factor for borehole diameter

C_R: Correction factor for rod length (whole depth)

C_S: Correction factor for the sampling method

If fine particles are present, the following correction must also be made,

$$N_{1-60cs} = \alpha + \beta \times N_{1-60} \quad (3.6)$$

The coefficients α and β are a function of the percentage of fine particles by mass (or Fines Content - FC) corresponding to the 200 sieve pass. They take the following values depending on these cases (Youd and Idriss, 2001):

$$\alpha = 0 \; and \; \beta = 1 \; for \; FC \leq 5\% \quad (3.7)$$

$$\alpha = e^{[1.76-(\frac{190}{FC^2})]} \; and \; \beta = [0.99 + (FC^{1.5}/1000)] \; for \; 5\% \leq FC \leq 35\% \quad (3.8)$$

$$\alpha = 5 \; and \; \beta = 1.2 \; for \; FC \geq 35\% \quad (3.9)$$

$N_{1\text{-}60cs}$ values greater than 30, indicate the presence of relatively dense soil, (Youd and Idriss, 2001) did not specify an expression for calculating the liquefaction resistance of the soil in place. In contrast, the values of $N_{1\text{-}60cs}$ less than 30 can be effective in determining soil resistance capacity to liquefaction for an earthquake of about 7.5 magnitude. The expression can be written as follows:

$$CRR_{7.5} = \frac{1}{34 - N_{1-60cs}} + \frac{N_{1-60cs}}{135} + \frac{50}{(10 \times N_{1-60cs} + 45)^2} - \frac{1}{200} \quad (3.10)$$

This expression can be illustrated graphically in **Figure 3-5_page 50** for the set of $CRR_{7.5}$ values corresponding to the standard penetration indices $N_{1\text{-}60cs}$ ranging from 0 to 30.

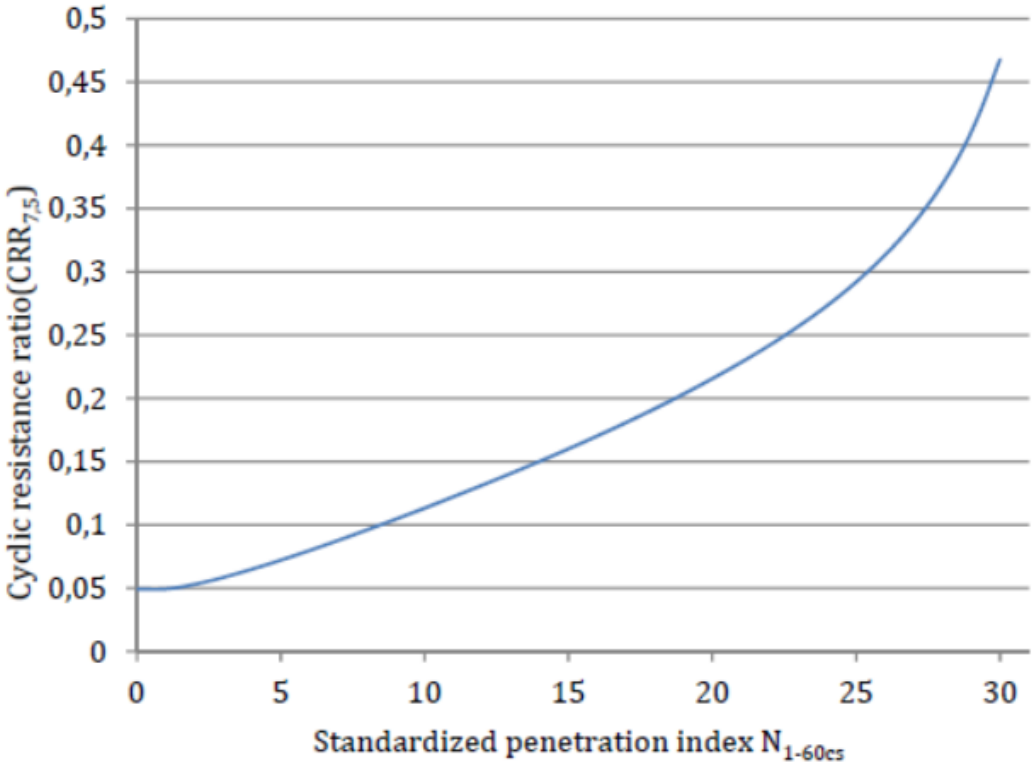

Figure 3-5: Cyclic resistance ratio CRR7,5 according to the standard penetration index N1-60cs

- *Cone penetration test*

Unlike the standard penetration test (SPT), the cone penetration test does not involve shocks and provides characteristic data of the soil in a continuous way during the cone is driven in at a constant speed (2 cm/s). Depending on the type of device, this test allows to determine the tip resistance qc and the lateral friction fs in the case of a traditional CPT to which is added the measurement of pore pressures in the case of a piezo-cone. The Seismic Cone Penetration Test (SCPT) also allows to measure the speed of shear waves emitted by a surface source. Many parameters can be determined with this type of test, but it does not allow for the collection of samples. To determine the fine particle content of the studied soil volume, it is necessary to use other probing techniques allowing sample gathering.

It is possible to determine the ratio of cyclic resistances CRR using empirical formulas where only the tip resistance is involved. For example, (Robertson and Wride, 1998) proposed the following expressions:

$$CRR_{7.5} = 0.833 \times \frac{q_{c1Ncs}}{1000} + 0.05 \;\; for \;\; q_{clNcs} < 50 \qquad (3.11)$$

$$CRR_{7.5} = 93 \times (\frac{q_{c1Ncs}}{1000})^3 + 0.08 \ \ for \ \ 50 \leq q_{clNcs} < 160 \quad (3.12)$$

The parameter q_{c1Ncs} again refers to a normalized value for a surcharge of one atmosphere (100 kPa) for clean sand. In practice, various corrections must be made to the value of the peak resistance actually obtained. They depend on the confining pressure, the content of fine particles, the type of soil and the thickness of the of the different soil layers. The details of these corrections are available in (Robertson and Wride, 1998) and (Youd and Idriss, 2001).

- *Measurement of shear wave velocity*

This is an interesting alternative to the penetration tests mentioned in the previous sections. The speed of propagation of shear waves, are known for their devastating effects during an earthquake, is influenced by the same parameters as those having an effect on the resistance to liquefaction of a soil. Indeed, the void index, the saturation, the effective and confining stresses of the soil, the loading history as well as the age of the deposit must be taken into account in the study of both cases (Youd and Idriss, 2001).

In general, high shear wave velocities imply the presence of a relatively dense soil, little or no saturated, leading to a low risk of liquefaction. The relationship between the shear wave velocity and the capacity of the soil to resist to cyclic loads can be expressed using the following expression (Andrus and Stokoe, 1999):

$$CRR_{7.5} = a \times \left(\frac{V_{s1}}{100}\right) + b \times (\frac{1}{V_{s1}^* - V_{s1}} + \frac{1}{V_{s1}^*}) \quad (3.13)$$

Where V_{s1} are the corrected shear wave velocity for 1 atm pressure (100KPa) in m/s, V_{s1}^* are limit value of V_{s1} to attend liquefaction and a and b are the adjustment parameter (dimensionless). The parameters a and b as well as the different correction factors need to be applied to obtain the parameter vs1 are presented in detail in (Youd and Idriss, 2001). This method has the advantage of being able to be used for all types of soil, particularly those composed of hard rock in which the tests previously developed cannot be used. However, some authors consider that the technique is not sufficient to determine the risks related to liquefaction (kramer, 1996). For example, the recognition of thin layers, which can play an important role in the development of the phenomenon, is relatively difficult with this method because of the imprecision of the results. Moreover, the shear strength is not directly proportional to the shear wave speed. This method can be useful as a complement to the various penetration tests.

3.8 Conclusion:

In this chapter we have defined the liquefaction phenomena as a post risk that could happen after an earthquake. Two major earthquakes in 1964, in Anchorage (USA) and Niigata (Japan) have damaged both cities in a horrible way that enhanced the scientific interest on studying liquefaction phenomena. In brief, liquefaction is defined as a process by which loose water-saturated sands behave like liquids when it is vigorously shaken. By that, soil loose it resistance and then all kind of infrastructure could be in a great danger of collapse. To investigate this phenomena and prevent the menace, different method was elaborated by several scientists. The investigation method can be separated in two different aspects, the destructive and nondestructive enquiries. This chapter has raised several destructive and experimental analysis that could help in preventing from liquefaction risk. We will also discuss the nondestructive way to estimate the liquefaction susceptibility using micro-tremor measurement in chapter five along with a case study.

ATTEUNATION OF CODA WAVES IN THE RIF, CASE STUDY

This section is devoted to the paper published in the journal of African Earth Sciences (Arab et al 2020) that proposes a study of attenuation of seismic coda waves in the Rif area, northern Morocco.

4.1 Introduction

Bounded by the Eurasian and the African plates, the northern Morocco is located where moderates tectonic activities take place. With the view to mitigate the danger of the damage caused by the earthquakes, we have tried to estimate the attenuation of coda waves in high-frequency through the back scattering model. The coda wave is basically the dropping edge of the signal, it manifests after the appearance of the P, S and the surface waves. Furthermore, the behavior of the seismic wave attenuation could be; described as the drop of energy, modeled such as a harmonic oscillation of the ground, and also quantified as a dimensionless quantity, designated by the quality factor Qc (Aki and Chouet, 1975; Knopoff and Hudson, 1964).

The complexity of estimating the quality factor is related to the intricate composition of the medium. This intricacy can be justified by the anisotropy, the anelasticity of the system and also with the small scale of heterogeneities in the inspected region. The presence of these three-fold issues is due to the existence of a considerable number of faults and macro fractures all near in the proximity of AL-Houceima city (Gil et al., 2014).

Several studies and research on attenuation around the world have managed to inspect the properties of plenty seismic regions (Aki and Chouet, 1975; Azguet et al., 2019; Bora et al., 2018). Aki and Chouet were one of the firsts who estimated Qc from the coda wave. These studies achieved computing the quality factor adopting the single backscattering model and revealing that the Qc parameters are strongly dependent with the frequency and lapse time.

A few studies has been done on estimating the quality factor by examining coda waves in the northern morocco (Boulanouar et al., 2017, 2016). According to these studies the Qc values are also dependent with the frequency, which shows a great heterogeneities of the medium in the RIF region, as well as a complex lithosphere subduction (Gutscher et al., 2012).

The study of attenuation of coda waves aims to characterize the crustal structure in the Rif region. The complexity of the crust geology and the sophisticated ground behavior push us to dig more deeply than before, in order to obtain additional information about the crust and the lithosphere under each particular station. The crust investigation in the Rif area, is a big contribution to Moroccan seismology. This study would help to spot crust anomalies and support previous geodynamic models (Baratin et al., 2016; Gutscher et al., 2002; Timoulali et al., 2014) for better understanding of the earth structure. Furthermore, it would be beneficial for construction so as to assess the seismic hazard and mitigate risks.

In this work, we estimated the attenuation of coda waves in the northern morocco as a function of frequency and lapse time for local earthquakes. It will be computed through the single back-scattering model by inspecting a massive number of local earthquakes during 2014 using the topo Iberia network. We are also willing to show the lapse time window and frequency dependence to the quality factor. Moreover, we suggest comparing results of the Qc features with other regions In the world.

4.2 Tectonic setting

Due to the complex tectonic interactions history between the African and Eurasian plates, The Gibraltar Arc system takes place in the end of the western borders of the Alpine orogenic belt (Morley, 1987), which contains the Alboran Sea and surrounded by the Betic-Rif-Tell orogen. The estimated crustal thickness beneath the Rif cordillera varies from a maximum of 36 km and decline to 30 km toward the border with the southern part of Alboran Sea (Torne et al., 2000), it is characterized by deep sedimentary and composed from three main structural domains cited from north to south; the internal zone, the Flysch Nappes and the external zone. Each one of these geological structures is a result of complex tectonic movements during eras (Chalouan et al., 2008; El Fellah et al., 2019).

- The internal zone consists of upper and lower plates and it contains Paleozoic rocks covered by Mesozoic-Cenozoic remnants(Chalouan et al., 2008, 2001).
- The complex Nappes of Flysch are composed from two major Nappes, the Mauretanian Nappes and the Massylian Nappes on which are formed in the late Mesozoic (upper and lower Cretaseous), Eocene-Oligocene and the early Miocene(Chalouan et al., 2008; de Capoa et al., 2007).
- The external zone is devided to three structural zones, the Intrarif, Mesorif and Prerif and it is manly composed from Cretaseous and Tertiary (Andrieux, 1971; Chalouan et al., 2008) (**See Figure 4-1_page 56**).

During 1994-2019 period three destructive earthquakes occurred on 2016 January 25th (Mw 6.3), 2004 February 24th (Mw 6.4) and 1994 may 26th (Mw 6.0) and took place in the Rif region near Al Houceima city (**Figure 4-2_page 57**). The last earthquake didn’t cause a huge

damage comparing to the two earlier earthquakes due to his offshore location and was only felt in the coastline of the Rif region.

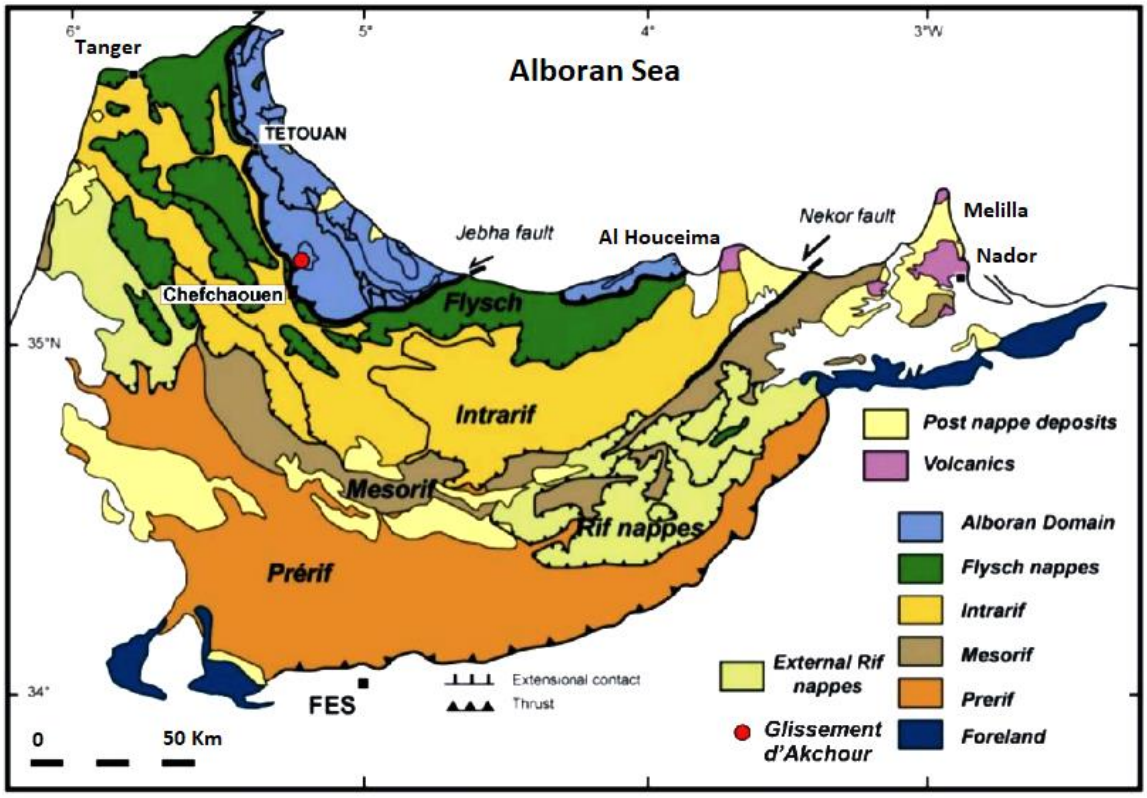

Figure 4-1: The main geological formations of the Rif region (Negro et al., 2008), modified.

While the earlier earthquakes resulted in a big loss of life and caused a serious damage to infrastructure due to their inland location.

Moreover, comparing to other regions around the world this zone of the Iberian-African collision is characterized by moderate seismicity. As seen in (**Figure 4-2_page 57**) the seismicity is mainly focused all around Al Houceima city in a radius of 50 km approximately, in the south of Nador city and in the north-east of the coastline between Jebha and Tetouan city.

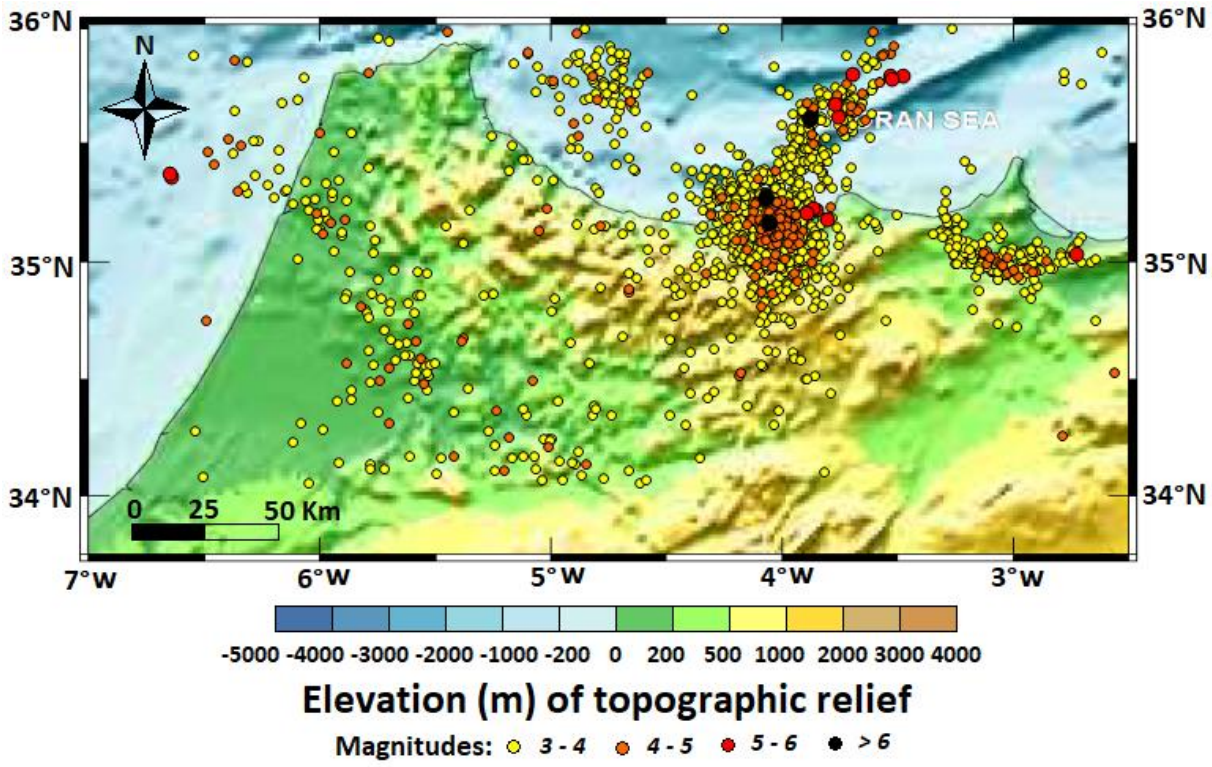

Figure 4-2: Topographic map shows the seismicity of the Rif region during 1994 -2019 period, the black circles show Al Hoceima earthquakes of 2016, 1994 and 2004 from north to south respectively (The localizations of these earthquakes were taken from Instituto Geografico National (IGN) catalogue).

4.3 Network and data

The Topo Iberia seismological network was supported by the Topo Iberia project where 20 stations were deployed in the northern morocco in 2007. This project was managed and operated by the scientific institute of Rabat and Jaume Almera institute of Barcelona, which has the vocation to carry out studies and research in the northern Moroccan territory in matters of geophysics. The seismological network which provides us data, consists of thirteen temporary redeployed stations in 2013 (**Figure 4-3_page 58**). This provides the convenient data for the Rif area and explains the need to build a rich and useful seismic database for the research community. Several studies has been carried out thanks to the collected data from this collaborations such as (Carbonell et al., 2015; El Fellah et al., 2019; Ouchen et al., 2018; Palomeras et al., 2017) (see **Table 6-3_page 110**) .

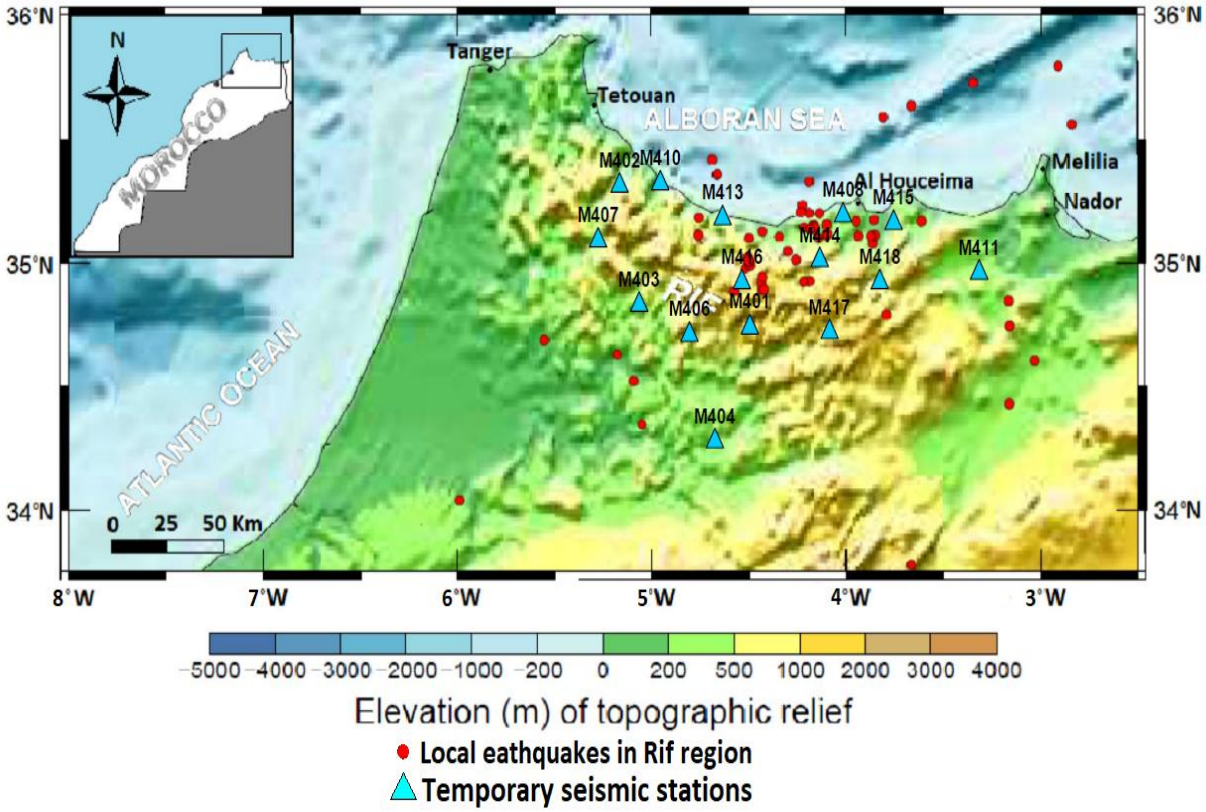

Figure 4-3: Topographic map showing the temporary broadband stations network with cyan color deployed during 2014 and the 70 gathered local earthquakes with the red color recorded during 2014.

In this study, we used 70 local earthquakes collected in the year of 2014 (**Table 6-4_page 110**) and recorded by 15 broad-band stations equipped with nanometrics Trillium 120P seismometers and Taurus data loggers sensors. The obtained data is sampled as the rate of 100 samples per second continuously. The magnitude of the local earthquakes is spanning between 2 and 5(Ml). To avoid unqualified results we purely selected signals for a good SNR (signal to noise ratio). The source parameters of the selected data were manually determined by Seisan software. Using Alba Gil (Gil et al., 2014) velocity model we located the 70 local earthquakes (**Figure 4-3_page 58**). We examined only the vertical component due to the slight dissimilarity between the vertical and horizontal components of coda waves (Sato and Fehler, 1998; Sedaghati and Pezeshk, 2016) (see **Table 4-_page 70**).

4.4 Methods

To measure the seismic wave attenuation of the signal, we adopted the single backscattering model which is elaborated by Aki and Chouet (Aki and Chouet, 1975). The coda wave is extremely dependent on the local geology of the medium. Moreover, the coda band would be thinner on the hard grounds (high level of density) than the sediment (Aki and Chouet, 1975).

As there is not just one origin of coda waves, we are looking for quantifying the attenuation that results from the scattering of the reflected S-waves when they propagate through the hazardous heterogeneities distribution in the crust(Aki, 1969; Rautian and Khalturin, 1978). We can express the seismic attenuation as a function of frequency as follows (BRIAN J. MITCHELL, 1981):

$$Q_c(f) = Q_0.(f^n/f_0) \quad (4.1)$$

Where $Q_c(f)$ represents the quality factor of coda wave dependency with frequency, Q_0 is the quality factor value at frequency f_0 (f_0=1Hz) while n is the covariate frequency parameter and varies with the variation of the medium characteristics.

The coda wave amplitude (A_c) is dependent on the central frequency f and the lapse time t where it can be measured as the double arrival time of the S-wave from the earthquake origin time and it can be illustrated using the following equation (Aki and Chouet, 1975):

$$A_c(f,t) = S(f).t^{-\varphi}e^{(-\pi ft/Qc)} \quad (4.2)$$

Where S(f) is the source factor of coda at a certain frequency f, φ is the geometrical spreading parameter which varies depending on the type of wave (φ=1 for body waves, φ=0.5 for surface waves and φ=0.75 for diffusive waves) (Rautian and Khalturin, 1978), Qc is the coda waves quality factor. As the coda waves were acquired from the backscattering of body waves, the geometrical spreading parameter in our case would be φ=1. By taking the natural logarithm of Eq. (4.2) and readjusting terms, the equation can be written as follows:

$$ln[A_c(f,t).t] = ln[S(f)] - (\pi ft/Qc) \quad (4.3)$$

$$ln[A_c(f,t).t] = \alpha - \beta t \quad (4.4)$$

The Eq. (4.3) is considered as a linear equation where $\beta = \pi f/Qc$ and $\alpha = ln[S(f)]$. In this respect, β is the linear least square slope plot of $ln[A_c(f,t).t]$ versus t in a given frequency. The quality factor is derived from the root mean squares (RMS) of the signal amplitude along with the corresponding lapse time. The coda wave's depth can be computed considering the distribution of coda waves in an ellipsoidal volume. Thus, the total surface of an ellipsoidal volume on which the coda waves are distributed can be rewritten as follow:

$$x^2/a^2 + y^2/b^2 = 1 \quad (4.5)$$

Where, $a = vt/2$ and b = $\sqrt{a^2 - D^2/4}$. The v, t, and D parameters represent velocity of S-waves, lapse time window average length and the average of hypocentral distance respectively. The lapse time average can be described as $t = t_0 + W/2$, where t_0 is the starting time of coda wave and W is the window length of coda wave.

The lower border of the ellipsoidal volume is the maximum penetrated depth by the estimated coda wave (Havskov et al., 1989) and can be represented as $d = h + b$ where h is the average earthquakes depth.

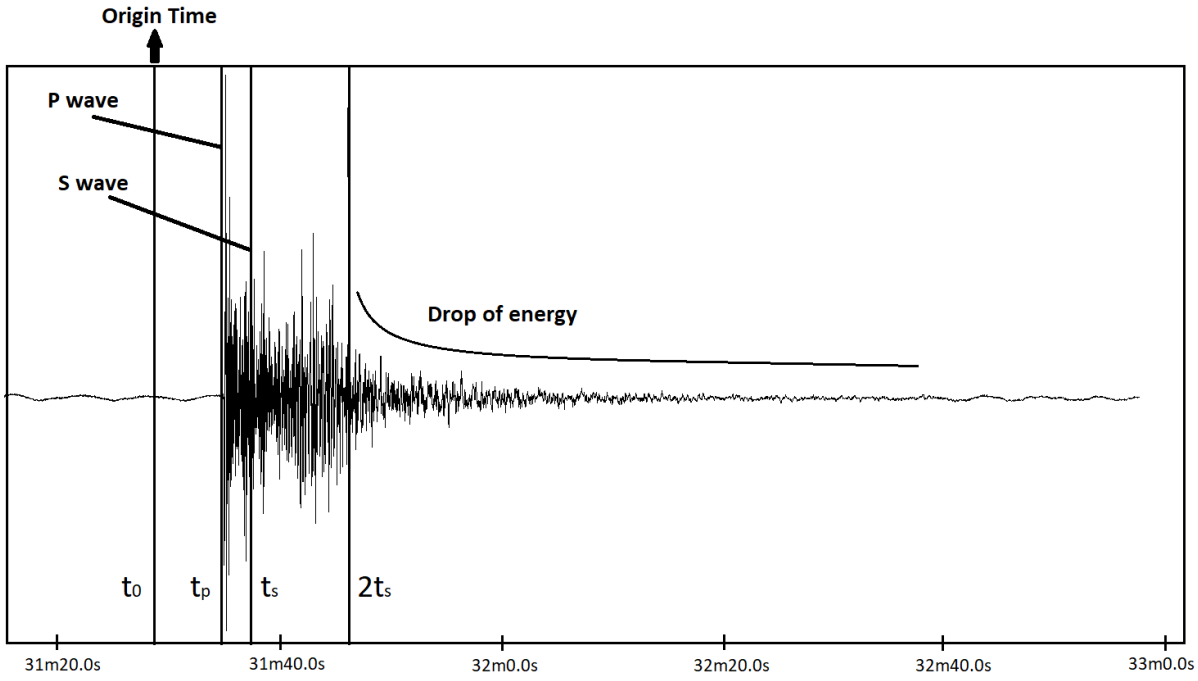

Figure 4-4: Example of seismogram for the earthquake recorded on the 7th of April 2014 at 13:31:26 at the station M418 with magnitude 2.4 showing the origin time, arrivals of P and S and the Coda.

4.5 Results and discussion

To compute the frequency-dependency attenuation parameter of coda waves in the Rif region we applied the single back scattering model of Aki and Chouet (Aki and Chouet, 1975).

Considering Aki and Chouet model, we analyzed vertical motion component of seismograms at six frequency bands 1.5, 3, 6, 9, 12 and 18 Hz using Butterworth filter under five lapse time windows (20, 30, 40, 50 and 60s). As plotted in **Figure 4-4_page 60** the length of lapse time window starts from t = 2ts. The ts is the duration from the origin time until the start of the S waves.

Table 6-1_page 108 shows the estimated quality factor values at 15 stations with their standard deviation. Also, the Qc mean values of the whole study zone at different central frequencies for five lapse time. As overviewed in the **Figure 4-5_page 62** the global average Qc values, with their standard deviation, upward from 157 ± 15 at 1.5 Hz to 1787 ± 807 at 18 Hz for 60s lapse time windows. The Q_0 and n values were estimated as function of lapse time from the empirical power law equation in the form of $Q_c(f) = Q_0.f^n$. **Table 6-2_page 108** displays values of Q_0 and n for five windows length, where the Q_0 average values varies from 136 ± 17 at 60s to 41 ± 7 at 20s lapse time and n average values fluctuate from 0.68 ± 0.06 at 60s to 0.92 ± 0.1 at 20s lapse time.

4.5.1 Dependency with frequency

For the whole study region, the Qc value is set as $= (41.21 \pm 6.95)f^{(0.92\pm0.1)}$, $Qc = (55.38 \pm 7.37)f^{(0.85\pm0.09)}$, $Qc = (75.33 \pm 10.07)f^{(0.8\pm0.07)}$, $Qc = (100.88 \pm 12.06)\, f^{(0.74\pm0.07)}$ and $Qc = (136.47 \pm 17.72)f^{(0.68\pm0.06)}$ for 20, 30, 40, 50 and 60s lapse time windows respectively. In these previous values we distinguish a rise of Qc with the increase of frequency for all 15 broad-band stations (**Figure 4-5_page 62** and **Figure 4-6_page 63**). From that, we can conclude a strong Qc dependency to frequency which can illustrate the high degree of heterogeneities in the entire medium (Aki, 1969). Furthermore, we also observe a potent relation between tectonic activity level and parameter of frequency dependency n, where our frequency parameter n is less than 1. This correlation between n and Qc has been confirmed by several research around the world, where the n value is high for tectonically active regions and low for more steady areas (Akinci et al., 1994; Roecker et al., 1982).

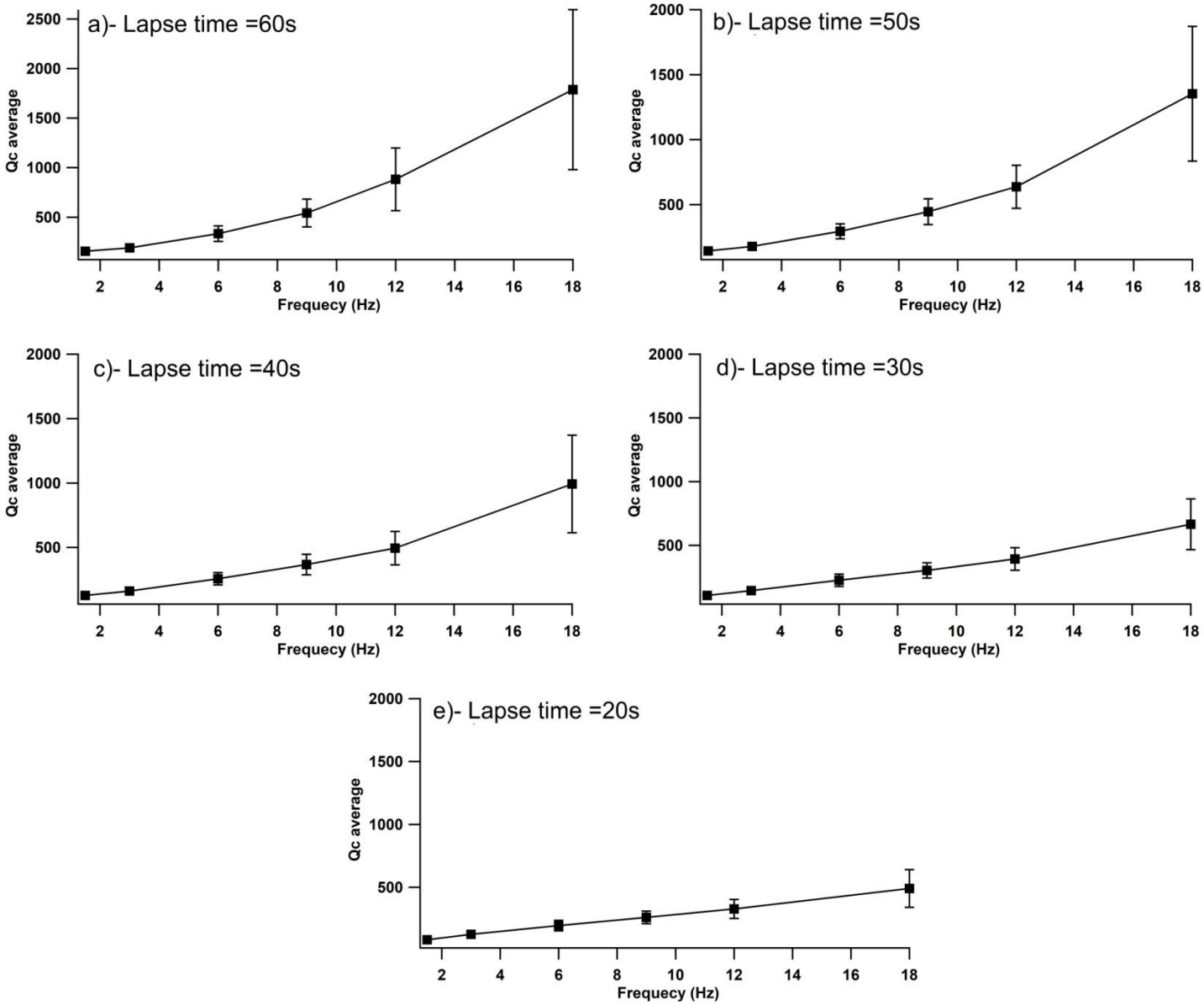

Figure 4-5: The Qc average for the whole zone of study in function of frequency within 60, 50, 40, 30, 20s lapse time.

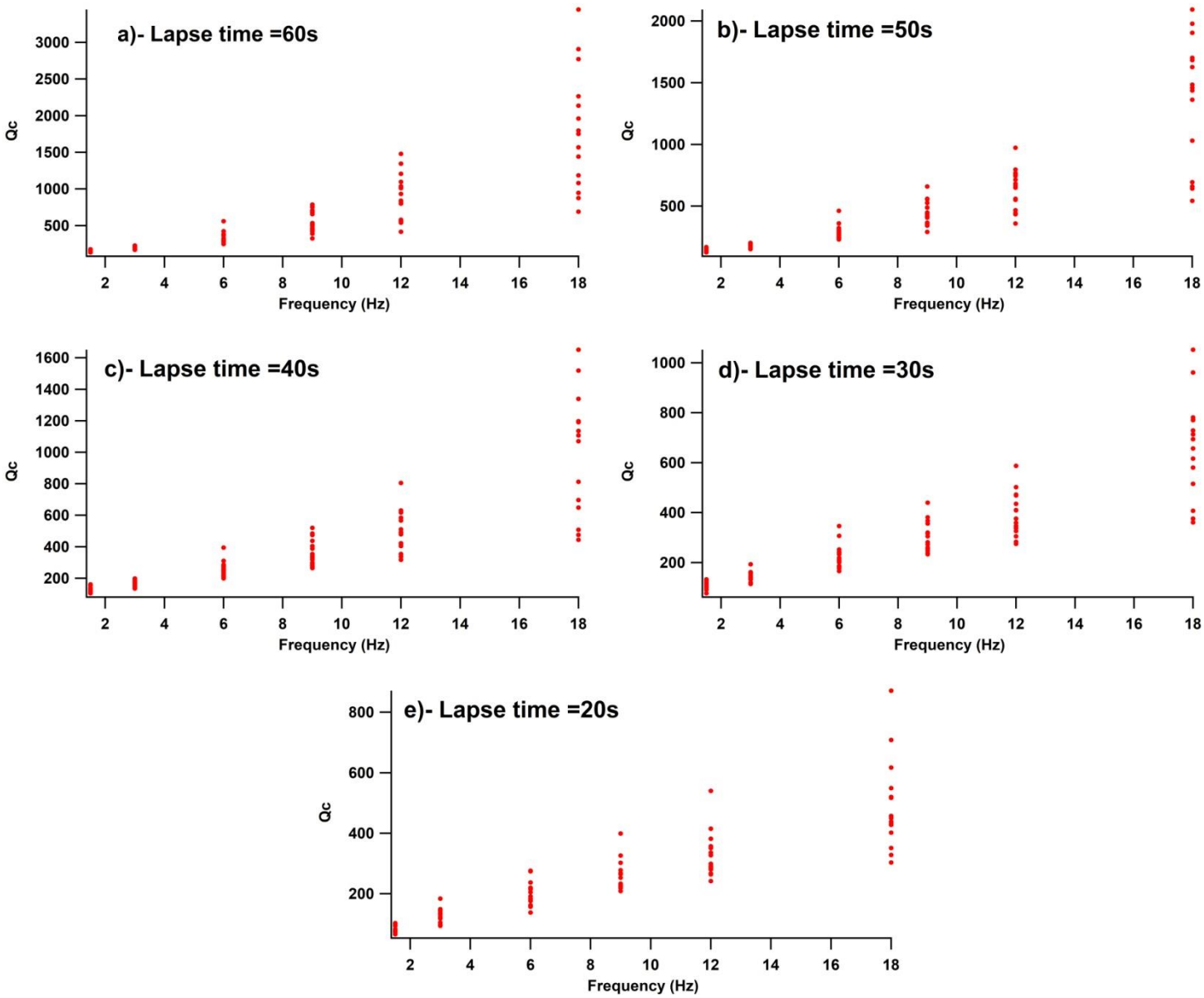

Figure 4-6: Qc value for all stations with the frequency in 60, 50, 40, 30 and 20s lapse time.

4.5.2 Dependency with lapse time

Table 6-2_page 109 indicates Q_0 and n values for the five selected lapse time windows and both Q_0 and n standard deviations. We notice that Q_0 increase with the increase in window length, whereas the frequency parameter n decreases (**Figure 4-7_page 64, Figure 4-8 and Figure 4-9_page 65**). Q_0 and n values, show a huge heterogeneity of the entire medium of the Rif region and considered it as a tectonically active region. Since there are generally less heterogeneities in larger depths, the attenuation Q_0^{-1} and frequency parameter n should be thinner, which is the case in our study.

From the previous results, we can obviously infer that the Qc values increase with the rise of lapse time. Identically to other inferences in different regions (Azguet et al., 2019; Boulanouar et al., 2017; Del Pezzo and Patanè, 1992; Giampiccolo et al., 2002). We can also confirm the quality factor dependency with lapse time and also with depth. It is considered as well, that the Q_0 is more significant in the larger windows length than the smaller, due to the low value of attenuation in the deeper depths and inversely when the waves are scattered in the shallow part of the crust.

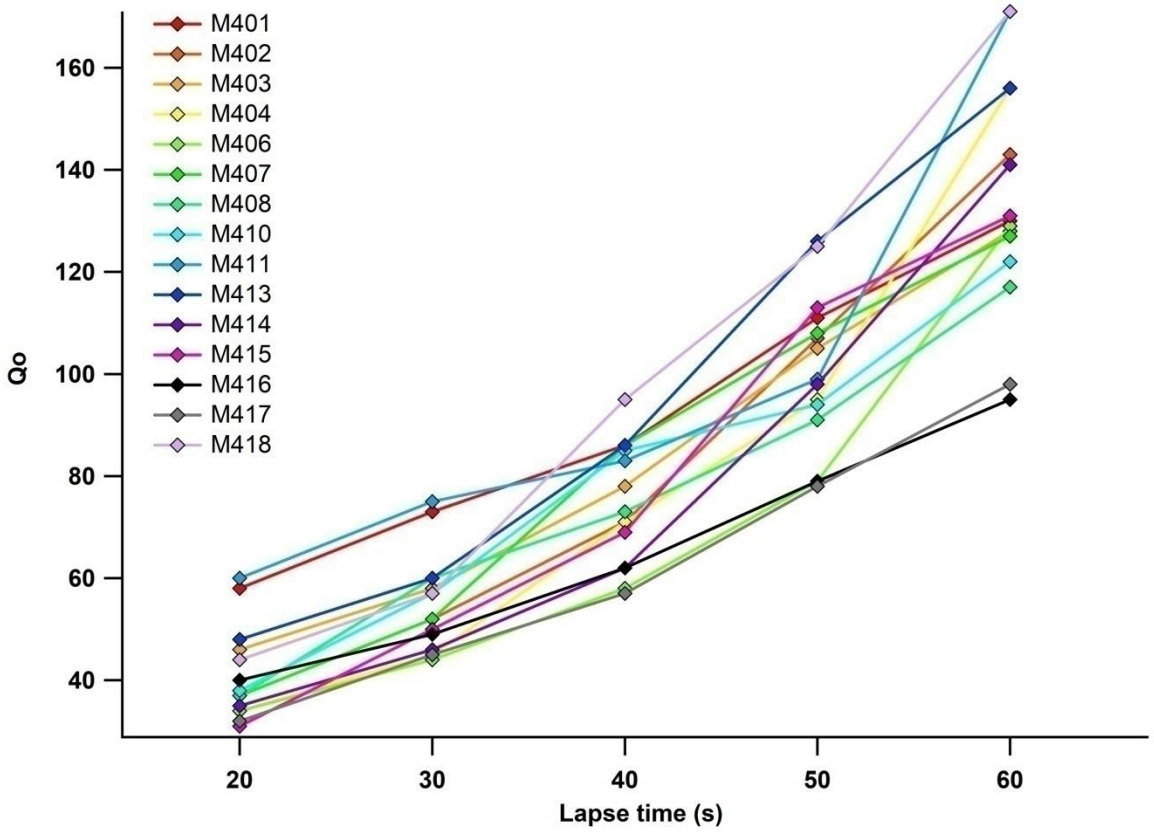

Figure 4-7: Plot of Q_o with lapse time for all stations.

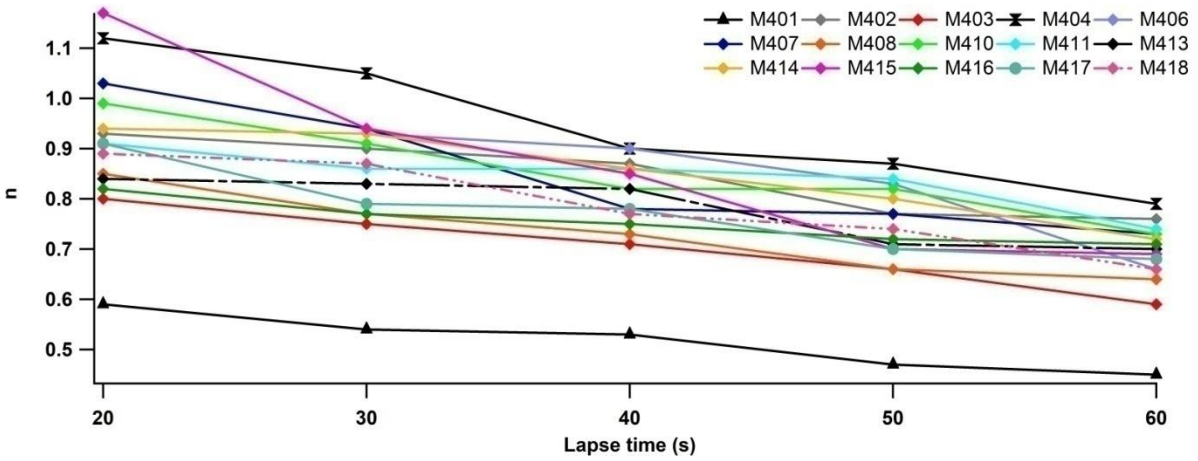

Figure 4-8: Plot of n with lapse time for all stations.

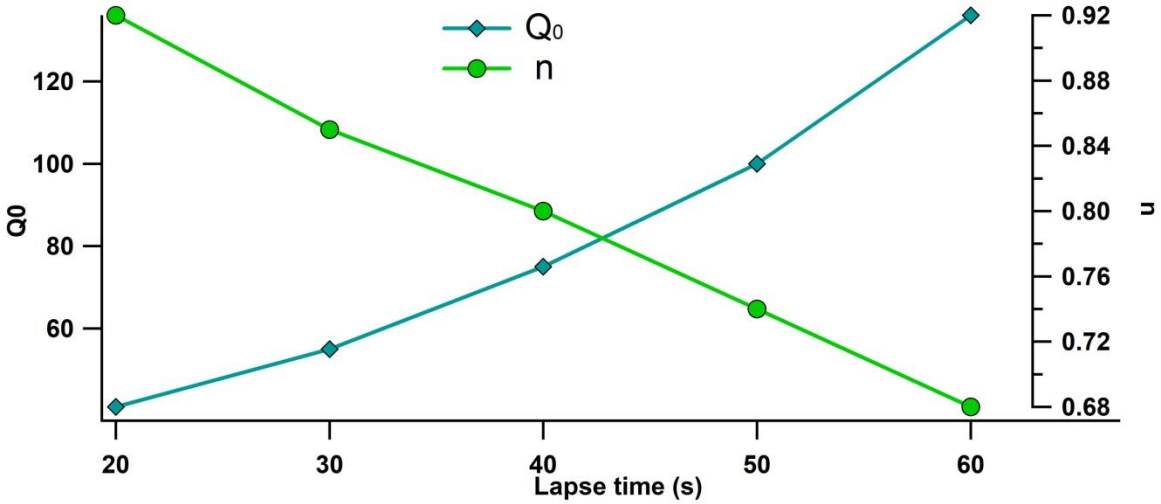

Figure 4-9: Plot of the average of Q_o and n in function of lapse time.

The variation of the quality factor in the Rif region can be described as highly fluctuating, especially in the lapse time of 20s. Moreover, the high variations of the quality factor in 20s window length can be related to the high heterogeneity in the shallow part of the crust. Comparing to the other window length, the variation of quality factor values for all stations get lower when the lapse time rises. This finding can be explained by the high penetration of waves to the deeper layers, and since the lithosphere become less heterogeneous with the rise of depth, the quality factor of high window length become less fluctuating. Erreur ! Source du renvoi introuvable.**Figure 4-10_page 67** and Erreur ! Source du renvoi introuvable.**_page 68** show the average values of the Q_0 and the n parameter for 70 earthquakes recorded in 15 temporary stations with five lapse time windows. For the 20s window length, it is noted that the quality factor value for M415 and M417 stations has the lowest values of all the others. In contrast the stations M401 and M411 have the highest quality factor. While for the 60s window length, it is observed that the lowest quality factor values go to the stations M416 and M417, and the highest

values go to the stations M411 and M418 comparing to all stations. For the 20s lapse time, it is seen that the lowest n value is for the stations M401, while the highest n value goes for the stations M404 and M415. The lowest frequency parameter value for 60s window length goes to station M401, whereas the highest n value goes to the station M404 (see **Figure 4-10_page 71**).

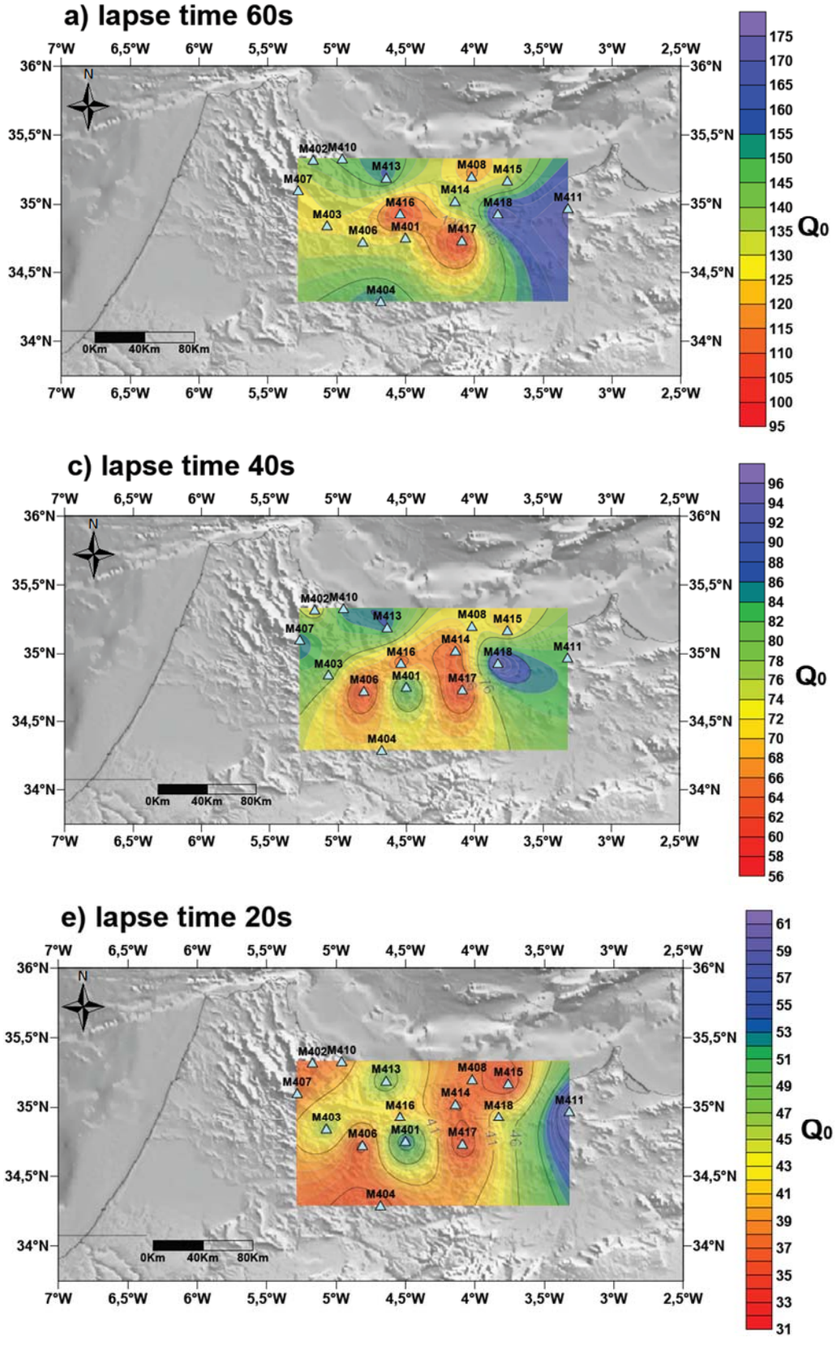

Figure 4-10: From (a) to (e) are the spatial distribution of coda Q_o. Triangles in cyan color are the deployed stations. The scale is indicating the maximum and minimum values of Q_o.

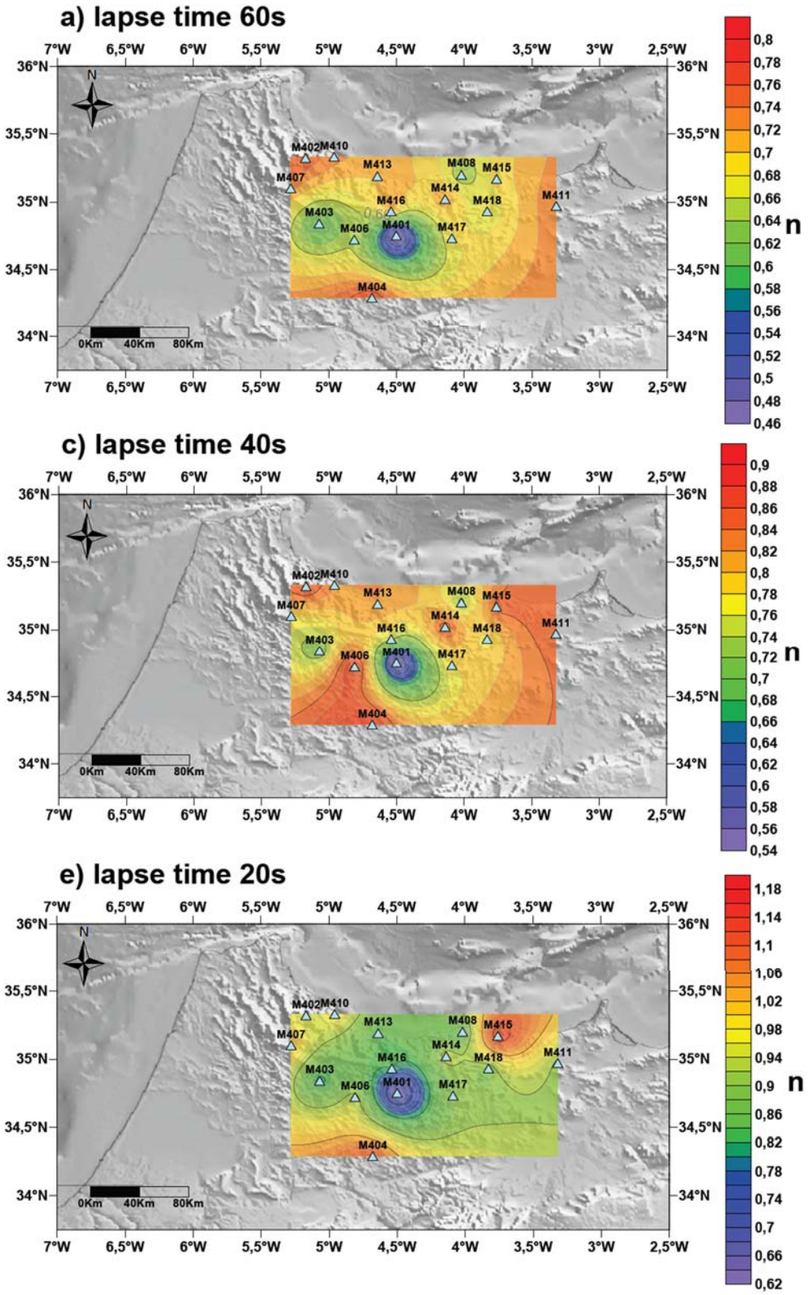

Figure 4-11: From (a) to (e) are the spatial distribution of frequency parameter (n). Triangles in cyan color are the deployed stations. The scale is indicating the maximum and minimum of the frequency parameter (n).

This variation of Q_0 between all deployed stations can reflect the complexity of the medium and the high variation of geological structures from station to another especially in the shallow parts of the crust.

4.5.3 Correlation with the tomographic and the geodynamical model

Under the stations M402, M410 and M413 the quality factor estimation is about 170.9, 173.3 and 176.5 respectively for 60 second lapse time. The lapse time of 60 sec correspond to the upper crust depths exceeding 30 km (El Fellah et al., 2019). The same paper show high velocity level due to the existence of less heterogeneities and high density in this depth. On all this reasons we can conclude that the quality factor should be high under these three stations (M402, M410 and M413).

The depth in between 45 and 60 Km contain manly positive anomalies features with a velocity of about (7.5-8.0 Km/s) associated to lithosphere body that has descended into the upper mantle (Timoulali et al., 2014). This geodynamic model can lead us to the same conclusion of the existence of high velocities due to high density in this range of layers. So as for the gravity model of (Baratin et al., 2016) the maximum thickness is beneath the peak of gravity anomaly which is about 40Km. All these models can prove the correctness of the quality factor estimation in this study.

4.5.4 Comparison with other results

To compare results with other regions, it is prefers to choose those who are similar in lapse time window. The previous attenuation results of several study spots have come down to the conclusion that the tectonic active regions are described by a low quality factor in the vicinity of 1Hz (Q_0), addition to that a high values in the frequency parameter (n), and vice versa for tectonic stable regions (Azguet et al., 2019; Bora et al., 2018; Boulanouar et al., 2017). Numerically, the active tectonic regions have Q_0 values that are less than 200 ($Q_0 < 200$), while the coefficient of the frequency dependency is more than 0.8 ($n > 0.8$) (Aki and Chouet, 1975; Azguet et al., 2019; Gupta et al., 1995; Havskov et al., 1989; Woodgold, 1994). On the other hand, the Q_0 values for inactive tectonic regions are higher than 600 ($Q_0 > 600$) and for n is lower than 0.5 ($n < 0.5$) (Atkinson, 2004; Hasegawa, 1985). For the regions that are regarded as a moderate tectonic areas, Q_0 values are set between 200 and 600 ($200 < Q_0 < 600$) and n between 0.4 and 0.7 ($0.4 < n < 0.7$) (Kumar et al., 2007; Pulli, 1984; Roecker et al., 1982; Sedaghati and Pezeshk, 2016).

In this study, the average of Q_0 and n for the whole zone of examination is 75 and 0.8 respectively for a window length of 40s. As the $Q_0$is less than 200 and n is near to 0.7 we can define the Rif region as a tectonic active region. This location of study is more tectonic active comparing to central USA and New England (Pulli, 1984), and less tectonic active than Washington and United states (Havskov et al., 1989). Our results are nearly the same as Parfkfield, California (Hellweg et al., 1995). As seen in the **Table 6-4_page 110**; Parkfield, California In united states (Hellweg et al., 1995) and The Rif, Morocco (the study zone) is the most tectonic active comparing to other regions. This active seismicity can reveal a huge variation of heterogeneities and a complex geological-geophysical structure.

Seismicity	Region	Q0	N	Source
Active	Washington, United States	63	0.97	(Havskov et al., 1989)
Active	**This study**	**75**	**0.8**	**-**
Active	Parkfield, California, United States	79	0.74	(Hellweg et al., 1995)
Active	Zagros, Iran	88	0.9	(Rahimi and Hamzehloo, 2008)
Active	Charlevoix, Quebec Canada	91	0.95	(Woodgold, 1994)
Active	the Garhwale-Kumaun Himalaya	119	0.99	(Mukhopadhyay and Sharma, 2010)
Active	SW of High-Atlas, Morocco	120	1.01	(Azguet et al., 2019)
Active	Garhwal, Himalaya	126	0.95	(Gupta et al., 1995)
Active	Northern Morocco	139	0.86	(Boulanouar et al., 2017)
Moderate	New England, United States	460	0.4	(Pulli, 1984)
Moderate	South Indian Peninsular Shield	535	0.59	(Kumar et al., 2007)
Moderate	New Madrid	598	0.54	(Sedaghati and Pezeshk, 2016)
Stable	NW Iberia	600	0.45	(Pujades et al., 1990)
Stable	Northeast United States	900	0.35	(Singh and Herrmann, 1983)
Stable	Central United states	1000	0.2	(Singh and Herrmann, 1983)

Table 4-1: Quality factor and n parameter for different regions around the world.

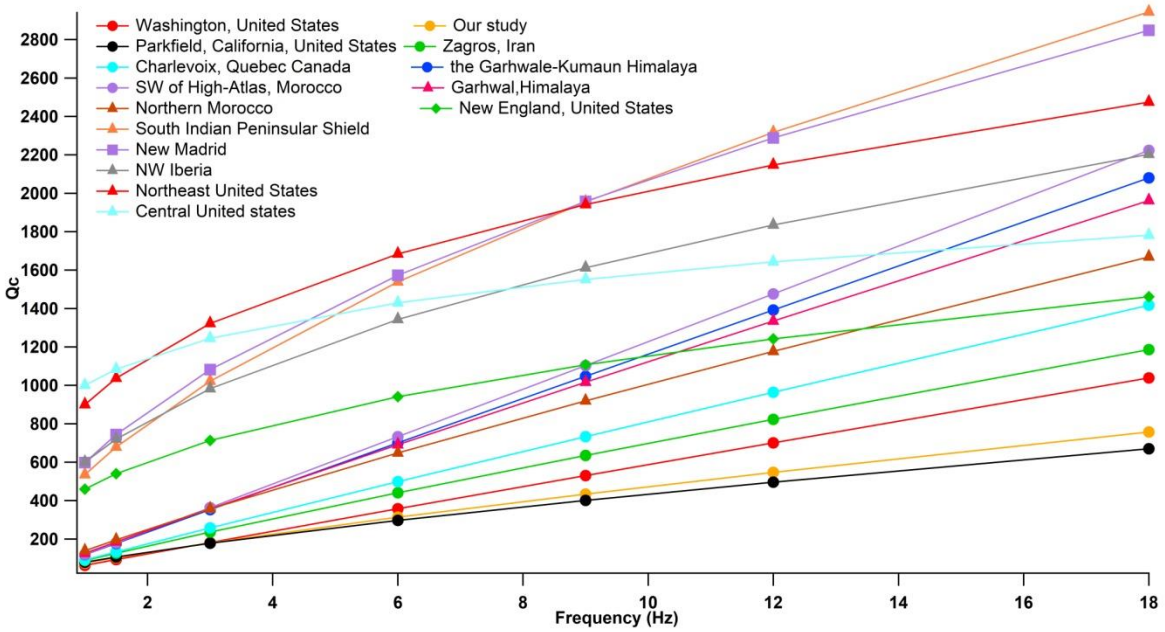

Figure 4-10: Comparison of quality factor values of the Rif region with other regions around the world.

4.6 Conclusion

In this study, we suggest the examination of the attenuation of coda waves in Rif region using the single back scattering model of (Aki and Chouet, 1975). For that, we used 70 earthquakes collected during 2014 and recorded by 15 broadband seismic stations deployed in the Rif region. The average Q_c values for this zone are strongly dependent to frequency, which shows an extreme heterogeneity in the region. The estimation of the frequency dependency relationship for this location is of about $(75.33 \pm 10.07)f^{(0.8\pm0.07)}$ for 40s lapse time. The covered surface area for the obtained results of Q_c is 25.17 x 10^3 Km2. The increase of quality factor and the decrease in frequency parameter with lapse time window reflect strong frequency dependency to quality factor, and since the lapse time window is in another words the depth of the traveling scattered waves, we can say that the shallow layers of the earth are more heterogeneous comparing to the deep parts. The estimated Q_c and frequency parameter n values state that the Rif region takes part of the high seismic activity cluster.

To sum up, the dense seismic broadband stations network used in the present study which covers the Rif area, gives a reliable Qc and n values. This massive data quantity recorded during 2014 will reveal a huge missing part of crust and allow us a better understanding of the medium and it's tectonic.

It would be a huge contribution to seismic hazard assessment and engineering seismology (Jin and Aki, 1988). Also, this work would give us the opportunity to run the first extensive exploration of the complex earth structure in the northern Morocco precisely the Rif region which we formerly didn't have the possibility before.

INVESTIGATION ON THE LIQUEFACTION POTENTIAL IN THE RIF, CASE STUDY

This section is devoted to the paper published in Arabian Journal of Geosciences (Arab et al 2021) that proposes a study of Estimation of liquefaction potential in the region of Rif, northern Morocco.

5.4 Introduction

Earthquake hazard, in its concise definition, can be introduced as any agent and/or event of which the association to earthquake risk (which is the exposure probability to earthquake hazard) of affecting vulnerable structures, may have negative consequences on the normal living activity in a given area. These consequences include tectonic deformations, ground shaking, landslides, liquefaction, tsunamis, etc. Earthquake hazard planning thus includes identifying sites where these risks are present (Stein and Wysession, 2003). Liquefaction is one of the main causes of instability in buildings and structures during and after earthquakes i.e. aftershocks. This phenomenon has always occurred simultaneously with earthquakes, but since the 1960, the mechanism behind it has started to be investigated and deciphered. In this context, two well-known large earthquakes occurred in 1964 the Niigata (Japan) and Alaska (USA) (Satake and Abe, 1983; Youd, 2014) and produced an enormous amount of liquefaction. Since then, Seismic-induced liquefaction has drawn extensive attention in academic and engineering fields.

In a nutshell, liquefaction is defined as a process by which loose water-saturated sands behave like liquids when it is vigorously shaken; under normal conditions, the sand grains getting friction with each other, and water fills in the interstitial pore spaces. Strong shaking moves the grains apart, and hence the soil behaves like a slurry fluid similar to “quicksand” (Stein and Wysession, 2003).

On the basis of both the field observations and laboratory tests, abundant methods have been developed and great progress has been performed in order to evaluate the liquefaction potential for particular soil types, which serves well the seismic microzonation advances.

Several studies and research on liquefaction have been carried out using different methods. As an example of investigations, laboratory tests were performed by (Chiaro et al., 2012); (Hird and Hassona, 1990); (Sivathayalan and Ha, 2011); (Vaid et al., 2001) and (Yang J. and Sze H. Y., 2011) to investigate the effect of initial shear stress on liquefaction resistance. (Juang et al., 2012, 2003, 2002), (Kayabasi and Gokceoglu, 2018); (Sonmez et al., 2008) and (Yuan et al., 2004) have evaluated the soil liquefaction analysis based on the database of case histories obtained by different test methods (CPT and SPT et al.). (Idriss and Boulanger, 2006); (Juang et al., 2008); (Poulos et al., 1985) and (Seed and Idriss, 1971) presented simplified procedure for evaluating liquefaction potential. (Byrne et al., 2004); (Elgamal et al., 2002); (Popescu and

Prevost, 1993); (Ye et al., 2007) and (Zhang and Wang, 2012) realized liquefaction studies by means of numerical simulation method.

Ambient seismic noise or micro-tremors are a slight ground motions with displacement amplitudes of about 0.1 to 1 μm and period range of 0.1 of a second to 10s (Kanai and Tanaka, 1961). Recently, to assess potential hazards associated with ground failure or liquefaction, the vulnerability index (or Kg value) that is derived from micro-tremor data may be evaluated and used as a key value (Akkaya, 2020; Choobbasti et al., 2015; Khalqillah et al., 2019; Rezaei and Choobbasti, 2014; Sunaryo, 2017).

Amongst the various approaches to micro-tremor study, the HVSR technique introduced by Nakamura (Nakamura, 1989) was adopted for this investigation because of the trusted results of its application.

This technique has been described in a number of papers e.g. (Bour et al., 1998; Lermo and Chávez-García, 1994, 1993; Teves-Costa et al., 1996). The aim of this study is to verify the utility of the soil vulnerability index proposed by Nakamura (Nakamura, 1996) as a proxy of liquefaction susceptibility. For this purpose we investigate the use of ambient noise, using horizontal-to-vertical spectral ratio (HVRS) and calculate Kg values. This investigation is based on data provided from 15 broadband stations during 2014 and located upon different geological units across the Rif region in the north of morocco. These data provide an opportunity for studying for the first time the liquefaction sites in the study region (**Figure 5-1_page 76**), which was never done before. The results will be interpreted in the context of geological structure and liquefaction investigation.

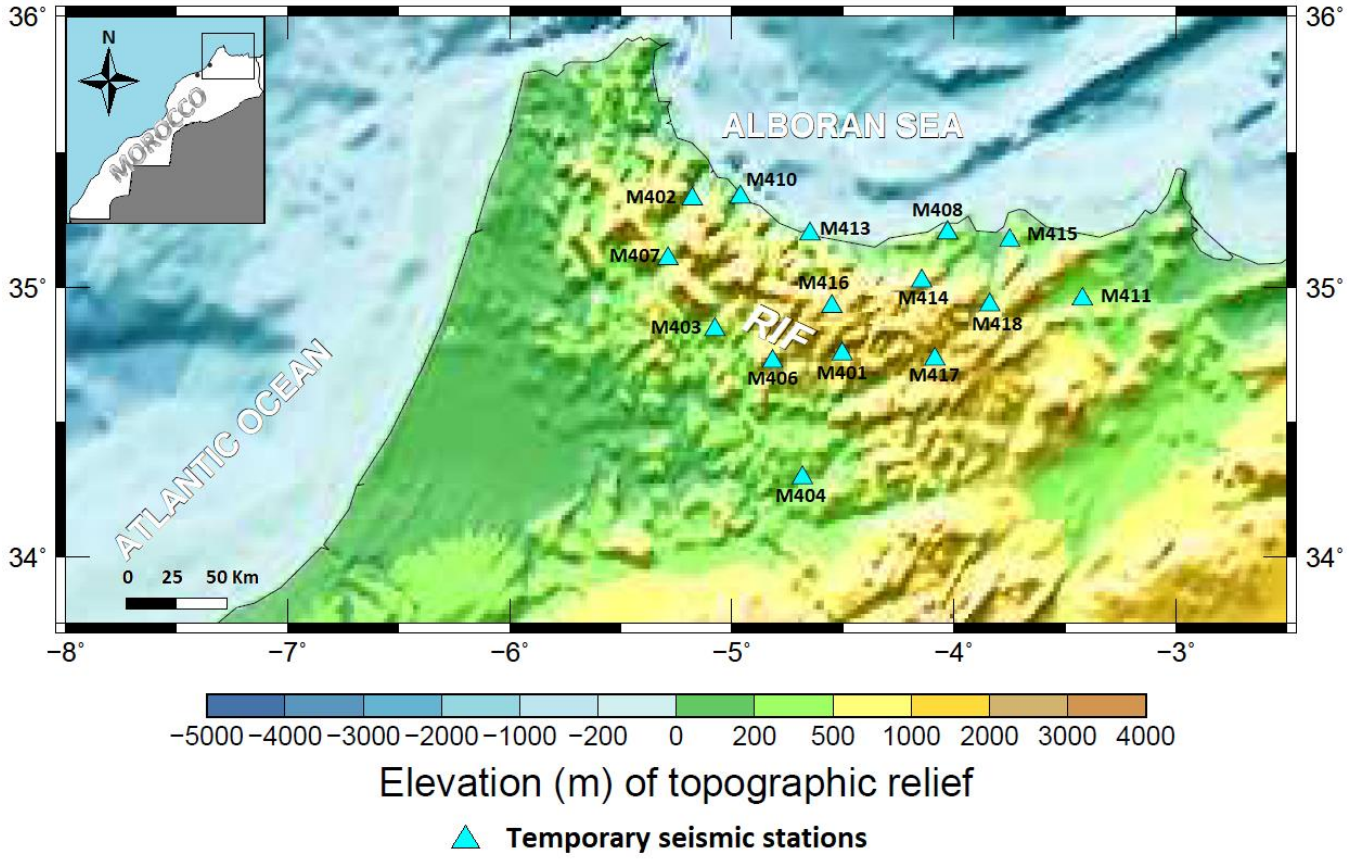

Figure 5-1: Topographic map showing the temporary broadband stations network with cyan color deployed during 2014.

5.5 Geological setting

On the grounds of tectonic contact between African and Eurasian plates, the Gibraltar Arc system is occurred in the end of the western boundaries of the Alpine orogenic girdle (Morley, 1987), which consist of the Alboran sea and the Betic-Rif-Tell orogens. The Rif cordillera is originated throughout the Miocene and can be divided into three main structural domains; the internal zone, the maghrebian flyschs domain and the External zone where each domain contain principally a lot of geological intricacies (Chalouan et al., 2008; Platt et al., 2013; Vergés and Fernàndez, 2012).

The internal zone is considered as the most complex zone in the Rif cordillera and it is incorporated mainly from dorsal calcaire which represent relic of the former southern passive margin of Mesomediterranean Block with Mesozic-Cenozoic calcareous layers, Ghomaride nappe which consists mainly of Paleozoic metamorphic rocks with a remnant of Mesozoic-Cenozoic front and Sebtide nappes which are in the form of deep crustal rocks such as mica-

schists, migmatites and granulites associated with Ronda/Beni Bousera mantle peridotites (Chalouan et al., 2008). The flysch domain is containing sediment deposits where it was formed in an oceanic through with a slim continental crust (Luján et al., 2006). The external zone is formed by the Mesozoic and Tertiary sedimentary rocks, distinguishing three structural zones Intrarif, Mesorif and Prerif (Chalouan et al., 2008; Mancilla et al., 2012). The complexity of the Rif's geology is due to the stacking of nappes and units and also its complex tectonic movements during eras (Chalouan et al., 2008; El Fellah et al., 2019). Moreover, it resulted in a several surface morphologies and complex structures. We have also to mention that the sediment thickness is remarkably increasing from east to west (Gil et al., 2014) with the increase of the continental crust in approximately the same direction. What is more, crustal thickness underneath the Rif cordillera varies from a maximum of 36 km and decline to 30 km from south to north (Torne et al., 2000). **Figure 4-1_page 56** distinguishes the principal structural lines

of the Rif belt

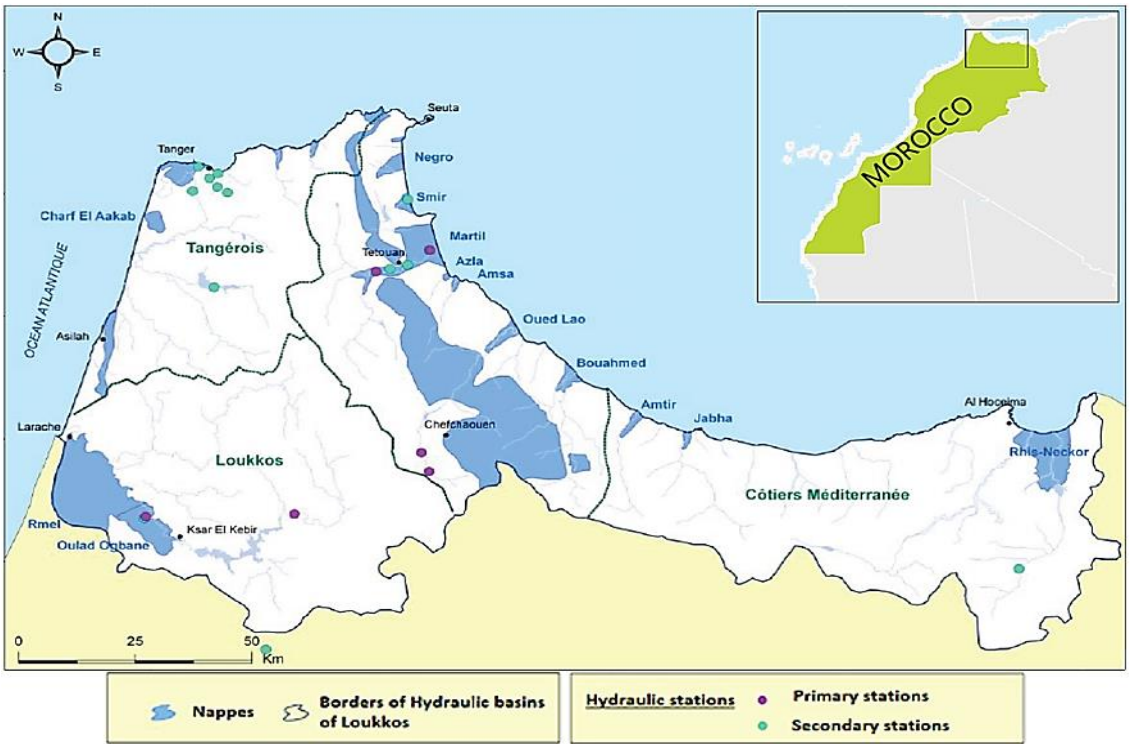

Figure 5-2: The principal hydraulic basins in the Rif, Loukkos zone (ABHL, 2014).

5.6 Datasets

This seismic ambient noise study was carried out using 15 seismic stations implanted in the Rif area, north part of Morocco. The measurement was done using broadband and three-component seismometers type equipped with Nanometrics Trillium 120 P and Taurus data loggers sensors. The data used in the present work are recorded during the Topo Iberia project (Arab et al., 2020; El Fellah et al., 2017), which was conducted in 2014 covering the main zone of the Rif, localized between the longitude 34°N to 35.50°N and the latitude of 3.2°W to 5.3°W (**Figure 5-1_page 76**). The data were analyzed using GEOPSY software (Wathelet et al., 2020) to compute the HVSR (**Figure 5-3, a, b** and **c_page 79**) and to calculate the fundamental frequency and the soil amplification factor (Abd el-aal, 2018; Bard, 1999; Fergany and Bonnefoy-Claudet, 2009; Gosar, 2007; Nakamura, 2008, 2000, 1997; Ouchen et al., 2018).

a)-

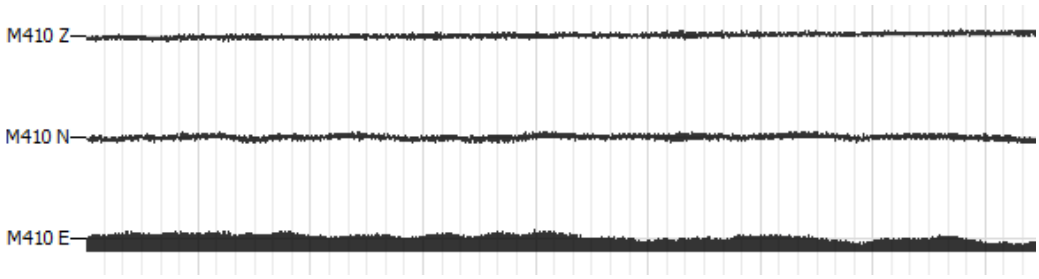

b)-

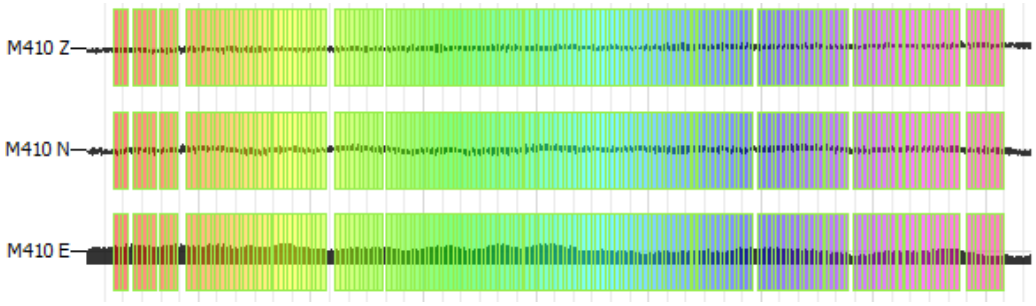

c)-

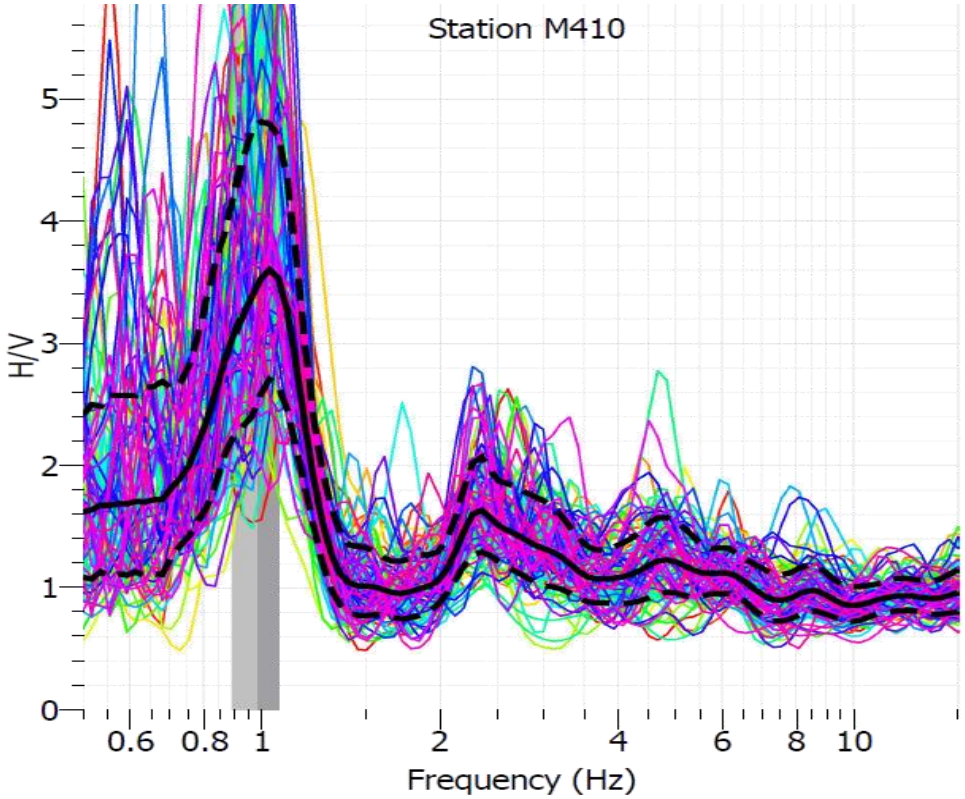

Figure 5-3: HVSR routine process on geopsy software. (a): A sample of seismic noise in the vertical and the horizontal components of the station M410. (b): The chosen lapse time windows of noise with rainbow colors in the three component of the M410 station. (c): Examples of the H/V spectral ratio curves of M410 in the investigated area. The continuous line is the average amplification value and the dashes lines are the maximum and minimum amplification. The colored curves represent the number of the time windows used for this station.

5.7 Methodology

The HVSR technic, which is grounded on Nakamura's (1989) methodology (Nakamura, 1989), is based on the assumption that the spectral ratio between the horizontal and vertical components of micro-tremors, is an approximation of the soil transfer function. To get to this, Nakamura relied on the following assumptions:

- Micro-tremors mainly propagate as Rayleigh wave trains.
- The effect of Rayleigh waves is similar for horizontal and vertical surface components.
- Artificial noise spreads many times like Rayleigh waves.
- The vertical and horizontal components of micro-tremors (in their origin) are considered similar.
- These micro-tremors are amplified by the soft surface layers of soil accumulated on a hard stratum.
- It can be considered that the horizontal component of the micro-tremors is amplified by the multi-reflection of the S wave and the vertical component by multi-reflection of the P wave.
- The vertical component of micro-tremors is not amplified by horizontal layers. The proposed methodology sought to eliminate the effect of Rayleigh waves to describe the transfer function based on internal waves.

The processing to calculate the HVSR goes through five stages; (a) first is to take the 3 components of an ambient noise signal, (b) select the most stationary seismic noise windows with sufficient length in the recording, (c) calculate the Fourier spectra of each component and each window; then smoothing, (d) calculate the average "H" of the 2 horizontal components - for each selected window, (e) compute the H/V ratio for each selected window, (f) And finally calculate the mean and standard deviation of the H/V ratios on all the selected windows. The maximum of the H/V ratio corresponds to the fundamental frequency and the corresponding amplitude is the fundamental amplitude. **Figure 5-4_page 81** show the flowchart of the data processing as shown below.

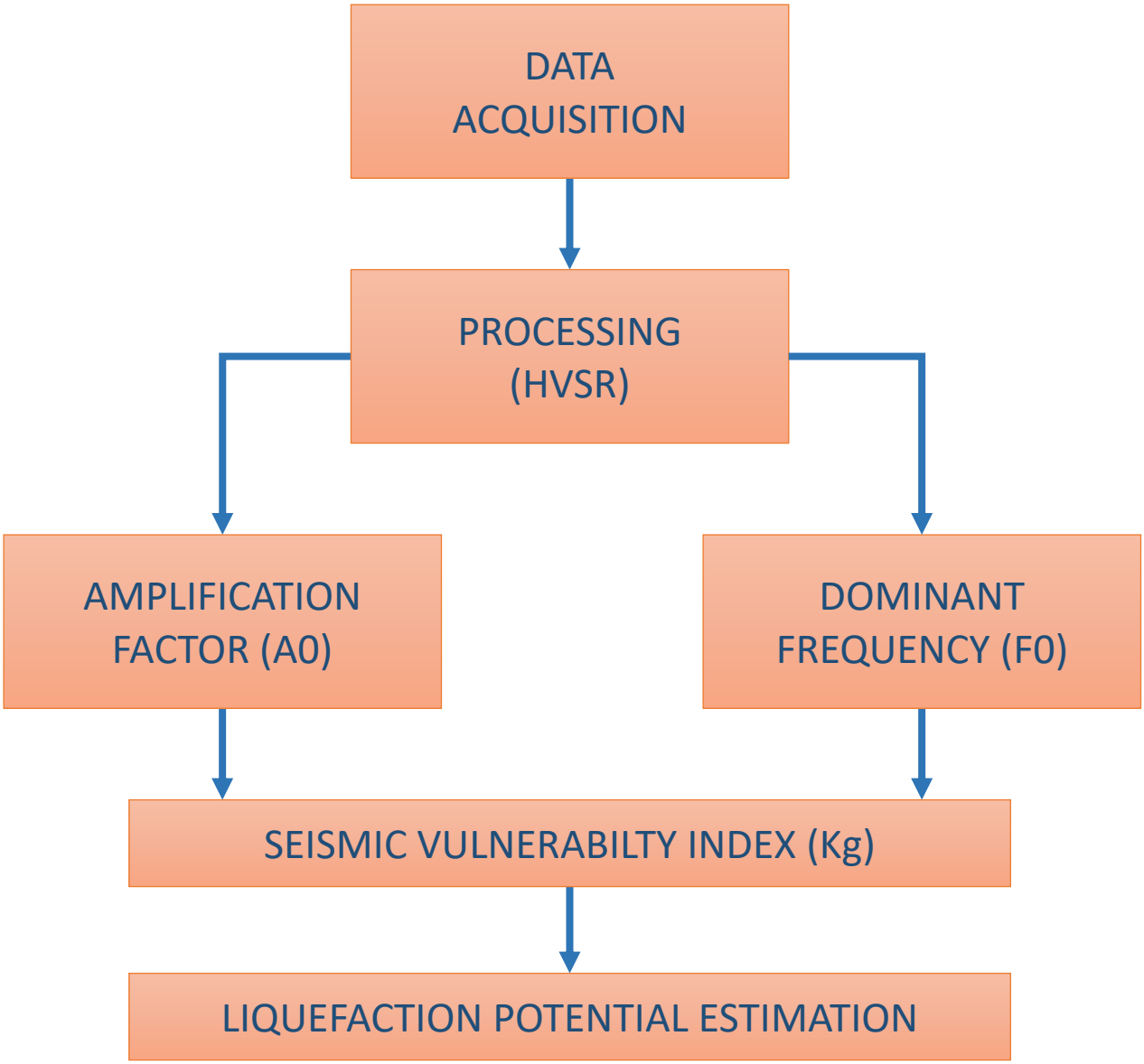

Figure 5-4: Flow chart of general processing for liquefaction potential estimation.

From the fundamental frequency obtained by HVSR method, we calculate the Thickness in each station, giving by this formula:

$$Z = a \times F_0^b \quad (5.1)$$

To determine the values of the coefficients ”a” and “b” we used a MATLAB Program developed by Abd el-aal (Abd el-aal, 2018), to perform a nonlinear regression fit of Thickness with 95% confidence bounds and the parameters obtained are a=90 and b= -1.45.

Nakamura made also measurements of regular micro-tremors at the sites affected by the Loma Prieta (USA) earthquake in 1989 (Harris, 1998) since there were signs of liquefaction. In his analysis he proposed the vulnerability index “Kg value” which corresponds to the level of deformation of the soil (Nakamura, 1996). He also concluded that the Kg value is related

specifically to the loss of the shear stress of the soil, where very large soil deformation can generate liquefaction (Nakamura, 1996). Therefore, it can be understood that the Kg value corresponds directly to the level of damage.

Ishihara, K. (Ishihara, 1978) stated that with unitary deformation of the surface layer in the order of the soil, shows its elasticity characteristics and does not show changes in state. However, in the range of deformation between, the soil enters a plastic range presenting cracks and differential settlements, in the case of deformation greater than the ground it passes from its creep limit to rupture and it is destroyed presenting landslides and liquefaction.

The Kg values are simply calculated from the Fundamental Frequency and the Fundamental Amplitude obtained from the HVSR calculation ratio, it is defined by the following formula:

$$K_g = A_0{}^2 / F_0 \quad (5.2)$$

Where Kg is the vulnerability index, A_o is the Fundamental Amplitude and F_o is the Fundamental Frequency.

In this way, it can be seen that the most liquefied points are those that are above the high vulnerability index Kg (in our case Kg=11.93), this method is used in several studies after Nakamura to evaluate liquefaction factors (Rezaei and Choobbasti, 2014; Saita et al., 2012).

We compute the strains of ground (γ) from the vulnerability index Kg by the following expression:

$$\gamma = K_g \times \alpha \ [in\ 10^{-6}] \quad (5.3)$$

where α is the acceleration of the ground, meaning that the effective strain can be obtained by multiplying the vulnerability index value with the maximum of acceleration of the ground (α) in Gal (=cm/s2), which is a very reliable indicator of the possibility and the ease of deformation of the measured sites, and which helps to determine the weakest points of the soil. The maximum accelerations were taken from the paraseismic code of construction in Morocco (RPS, 2011). It was created by the ministry of National Planning of Urbanism, Housing and City Policy in 2000 and revised in 2011. The attributed accelerations of each station were chosen depending to the zone they belong to it. We notice that the seismic zones acceleration

in the RPS 2011 is divided into 5 zones, 0, 1, 2, 3 and 4 according to the seismicity level of each region. The attributed accelerations to these zones are respectively 4, 7, 10, 14 and 18 g% (RPS, 2011). Our stations were located in 3 different seismic zones, where eight stations were situated in the highest seismicity level (zone 4), six of them were situated in zone 3 and one was situated in zone 2 (**Figure 5-5_page 83**). The methods described above are applied to the ambient seismic noise signal of the 15 sites chosen for this study, and the results obtained are presented in **Table 5-1_page 84**.

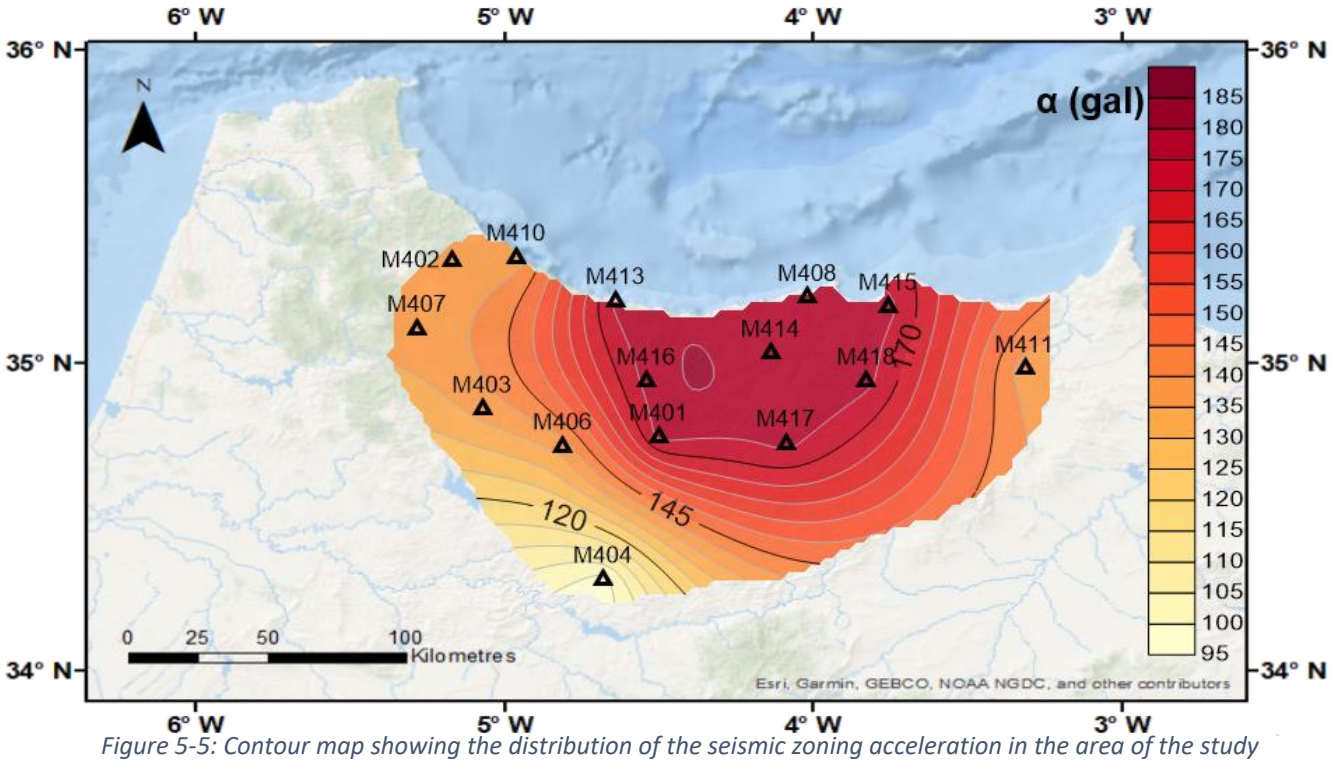

Figure 5-5: Contour map showing the distribution of the seismic zoning acceleration in the area of the study which is based on the (RPS, 2011) Moroccan paraseismic building code.

Stations	F_0 (Hz)	T (s)	A_0	Kg	α (gal)	γ	Z (m)
M401	10.26	0.10	1.78	0.31	176.40	52.92	3.08
M402	2.09	0.48	2.90	4.02	137.20	548.80	30.87
M403	7.29	0.14	1.72	0.41	137.20	54.88	5.05
M404	7.63	0.13	5.68	4.23	98.00	411.60	4.73
M406	2.98	0.34	2.65	2.36	137.20	329.28	18.44
M407	13.08	0.08	2.06	0.32	137.20	41.16	2.16
M408	3.64	0.27	1.72	0.81	176.40	141.12	13.81
M410	0.98	1.02	3.42	11.93	137.20	1632.68	92.43
M411	11.46	0.09	1.51	0.19	137.20	27.44	2.62
M413	3.18	0.31	2.47	1.91	176.40	335.16	16.84
M414	0.93	1.07	1.59	2.72	176.40	476.28	99.31
M415	11.13	0.09	1.82	0.30	176.40	52.92	2.74
M416	9.81	0.10	2.05	0.43	176.40	70.56	3.29
M417	1.40	0.71	2.52	4.53	176.40	793.80	55.04
M418	4.94	0.20	1.62	0.53	176.40	88.20	8.88

Table 5-1: The estimation of the different parameters related to the liquefaction index in all the seismic stations of the studied region such as frequency F0, period T, amplitude A0, Kg index, acceleration α, strain γ and thickness Z.

5.8 Results and discussion

The processing of computing the HVSR was based on micro-tremor measurement and was conducted under each particular station of the Topo Iberia network. The fundamental frequency and the amplification factor were estimated and plotted in contour maps (**Figure 5-6 a** and **b_page 86**), where the fundamental frequency F_o range from 0.93 to 13.07 Hz and the amplification factor A_o ranged from 1.5 to 5.68. We can conclude the existence of high and low frequencies and also a large amplification factor in the area. The vulnerability index Kg, which assesses the liquefaction potential for near groundwater in the area of the study, can be derived from the fundamental frequency and the amplification factor. The Kg index and the strain values were also displayed in a contour map (**Figure 5-7 a** and **b_page 87**), where the kg and strain values range from station to another depending on geology of the medium and the existing of the shallow aquifer of each spot. The lowest Kg values were estimated at eight different stations, where the values were less than 1. Furthermore, the uppermost computed value was found in the station M410 with a value of 11.93. The other six stations values were around 2 and 4. While for the strain, seven stations have values less than 100, where the highest value goes to the station M410 with 1632.68. Moreover, the other seven stations give a strain result wide-ranging between 100 and 800. It is also observed an increasing in thickness from east to west where it decrease sharply after the station M418, also after the station M414 the thickness values start to fluctuate until the end of the AA' cross section (**Figure 5-8 a** and **b_page 88**). Furthermore, the **Figure 5-8 a** and **c** show globally a fluctuation in values of thickness with a sudden drop at the start from north to south with a slight decrease at the south most of the BB' cross section.

a)-

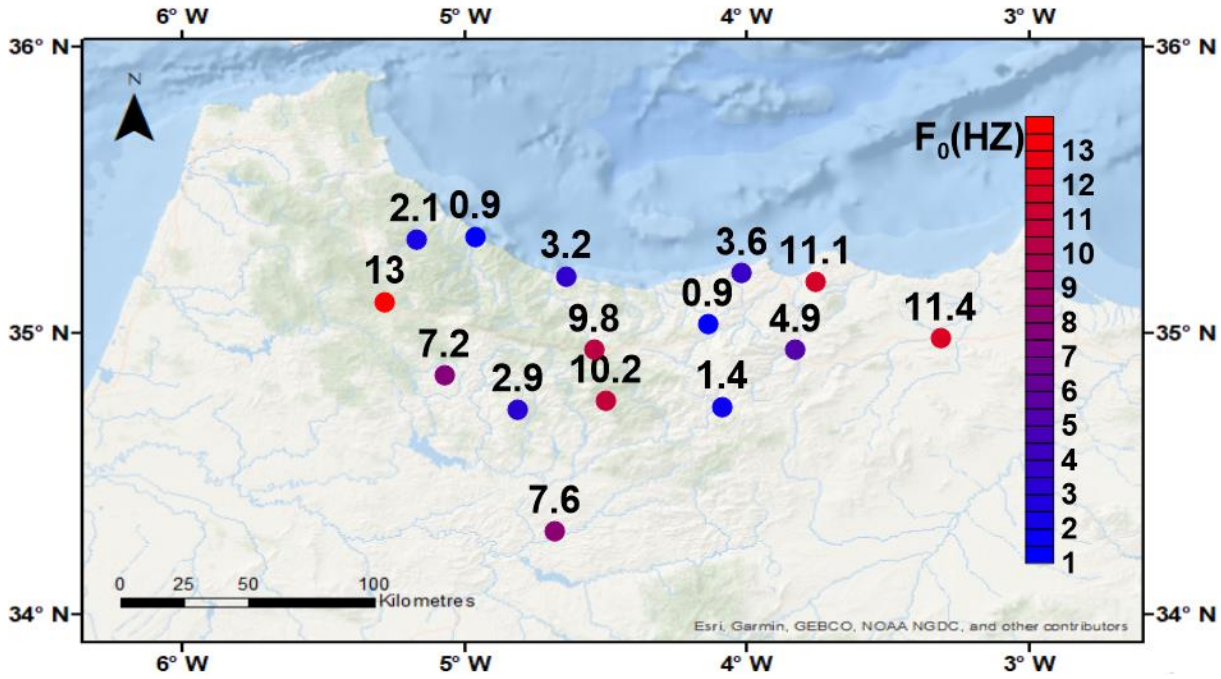

b)-

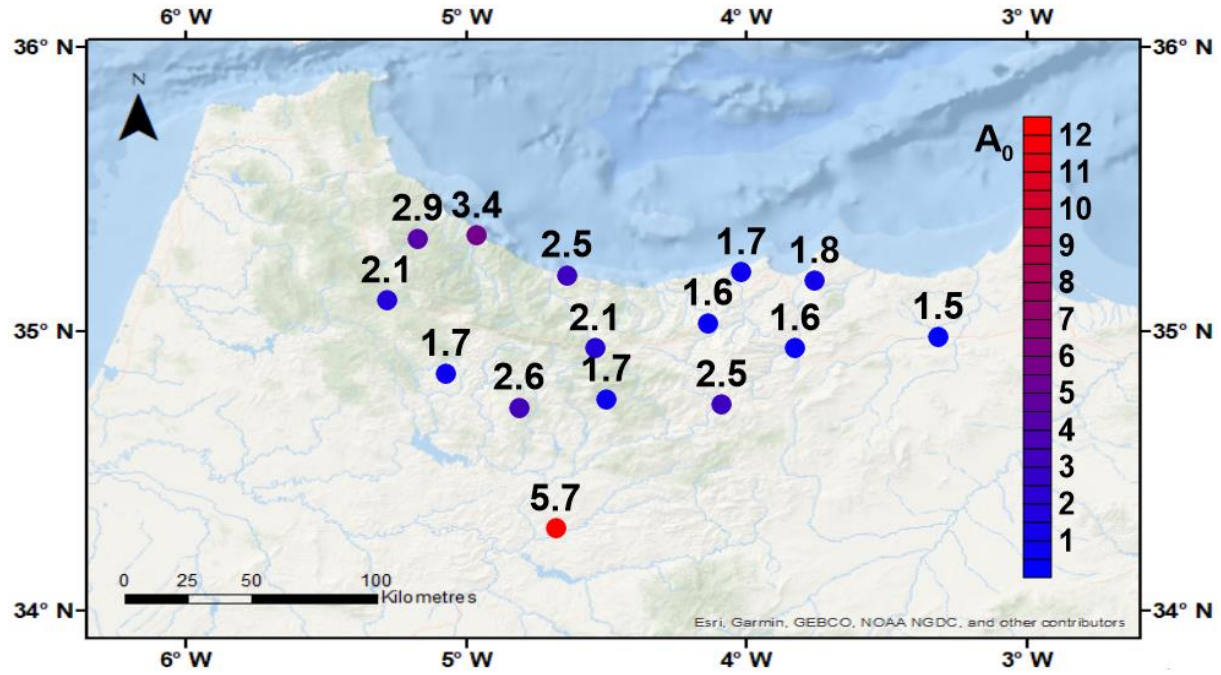

Figure 5-6: Contour maps showing the distribution of H/V parameters that define the ground characteristic in our zone of investigation such as: (a): Fundamental frequency (F0) and (b): Amplitude (A0) under each particular

a)-

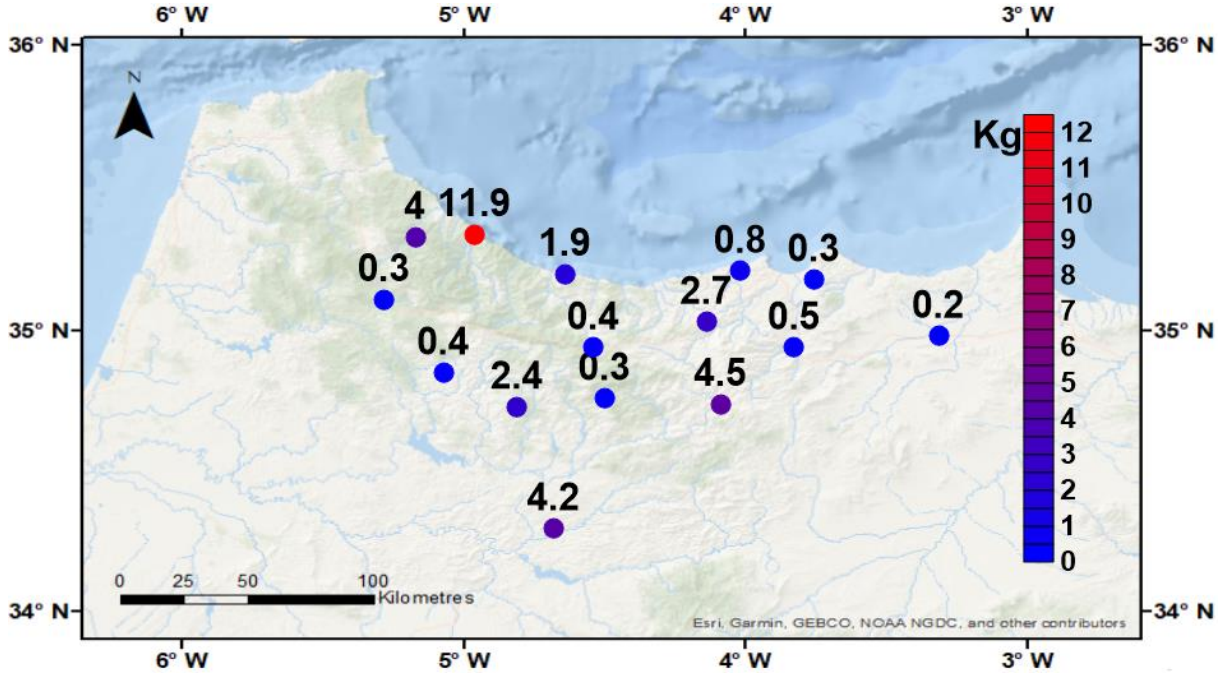

b)-

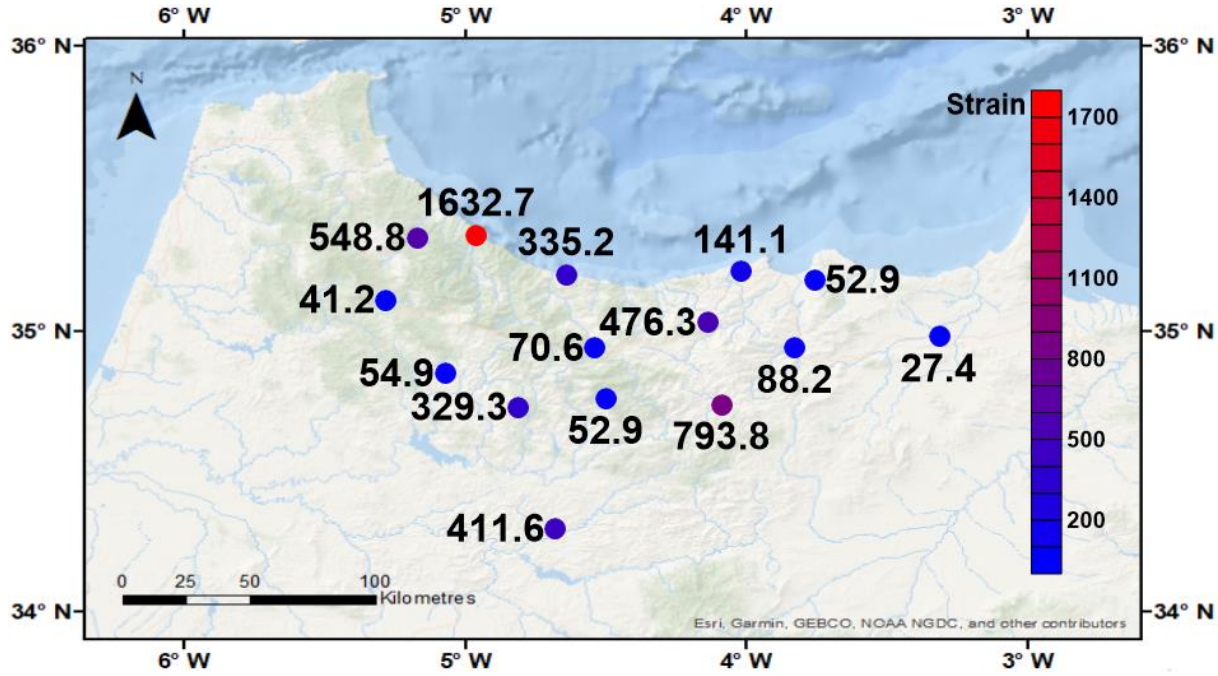

Figure 5-7: Contour maps showing the distribution of different parameters that illustrate vulnerability in the location of the study such as: (a): liquefaction index (Kg) and (b): strain (γ) under each particular station.

a)-

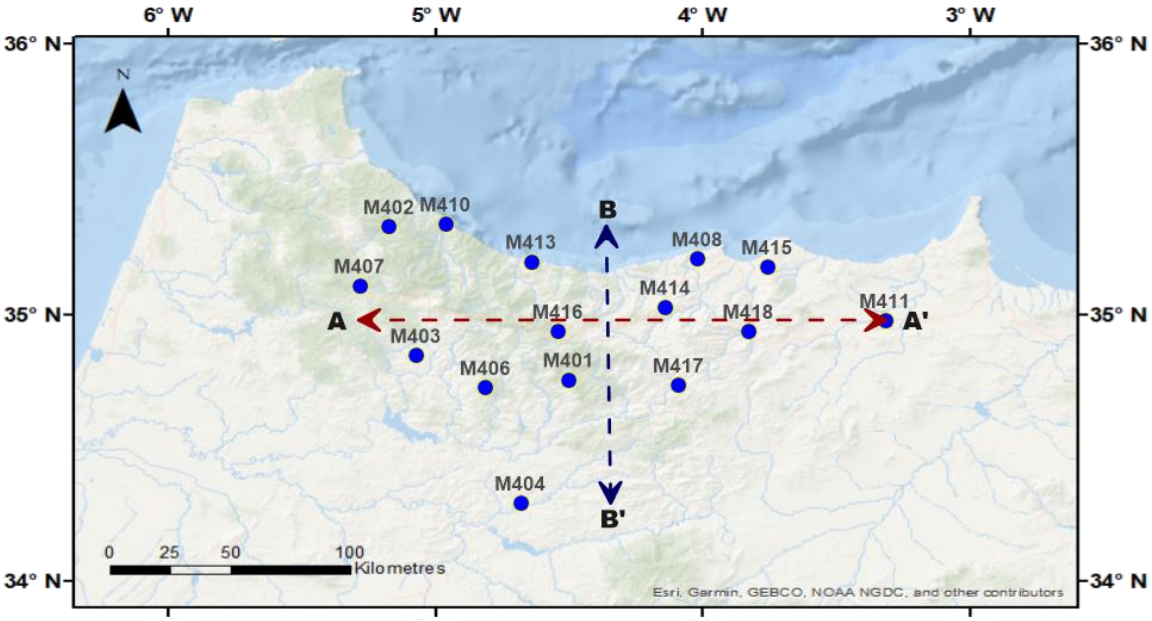

b)-

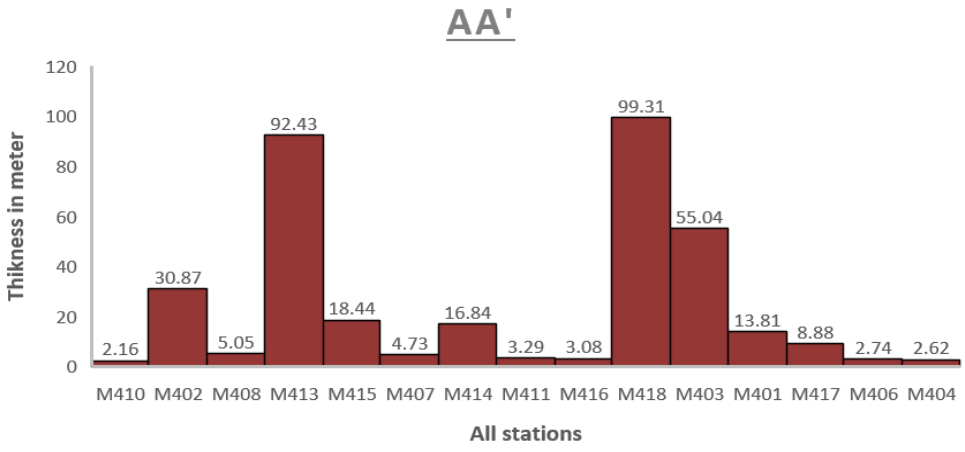

c)-

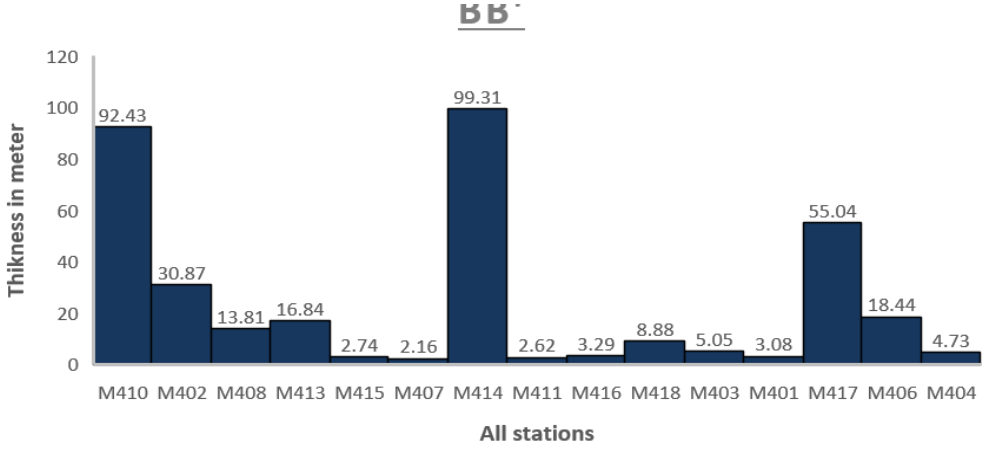

Figure 5-8: Distribution of the seismic stations in the study zone from north to south (AA') and from west to east (BB'). (a): Contour map showing the seismic station distribution where AA' and BB' are the cross sections from west to east and from north to south successively. (b): Histogram showing the variation of thickness within the AA' cross section (west to east sequentially). (c): Histogram showing the variation of thickness within the BB' cross section (north to south sequentially).

To account for these valuable results, we must discuss the HVSR and Kg values in the heed of geological setting and the existing aquifer nappes in the region. To do so, each particular station needs to be discussed distinctly.

Although the Rif area is well known by high precipitations and rain fall during the rainy season (Salhi et al., 2019), the region does not contain any huge or even moderate aquifer nappes (ABHL, 2014) (see **Figure 5-2_page 77**). Hence, most of the calculated liquefaction probabilities show very low values. The groundwater flow path is headed south from high altitude levels in the Rif area, as a consequence, all the precipitation in the region travel to south to form aquifer nappes in the low altitude regions (south Rif and pre-Rif) instead of being recharged in the Rif area (Sabri et al., 2019). Hence, the ground water flow path is correlated with the absence of ground water in the studied region.

The geological spreading of the fifteen stations was divided into several geological zones on which we will proceed to discuss. The stations M401, M403, M406, M407, M415, M416 and M418 were deployed on the Intrarif zone, which is also called the Tanger and Ketama unit (Chalouan et al., 2008). All the seven stations that are spread in the same geological unit came out with approximately the same results in frequency range, strain and Kg index. The geological layers under these stations are characterized by high frequency values, a low strain index and poor values of liquefaction parameter with a slight deviation in Kg for the station M406 when comparing it to the other seven stations. Numerically the fundamental frequency F0 is spanning between 2.98 Hz and 13.07 Hz (see **6-1**) and the strain values were less than 100 beside M406. While for the liquefaction parameter, the Kg index were less than one (Kg<1) for all stations but M406, and gave a 2.35 value as a result (see Table 5-1_ page 85). All the computed Kg values are very low to arise any liquefaction potential under those stations. The low Kg index can be explained by the absence of any form of an aquifer nappe in 2014 where the seven stations were situated (see **Figure 5-1_page 74** and **Figure 5-2_page 77**).

The stations M402, M408 and M410 are established in the dorsal Calcaire zone (**Fig 4-1_page 56**). The fundamental frequency of both stations, M402 and M408 are less than 4 Hz, the strain was 548.8 and 141.12 and the Kg index was about 4.02 and 0.81 respectively. In contrast the station M410 shows a low fundamental frequency (F0 < 1), a high strain value of about 1632.68 and a high Kg index value around 12. The M410 Kg index value is the highest between all the computed values (see **Table 5-1_page 85**) and it can be explained by the existence of Bou-Ahmed aquifer under the M410 station in the year of 2014 (ABHL, 2014) (see **Figure 5-2_page 77**).

The stations M404 and M417 belong to the Prerif and Mesorif respectively while both stations M414 and M413 belong to the flysh domaine. The fundamental frequency of these stations is particular to each specific medium, where M404 fundamental frequency value was near to the average frequency of the intrarif deployed stations. While the fundamental frequency of the stations M414, M413 and M417 were not too distant from the average frequency (2.23 Hz) outcomes of the Alboran domain deployed stations. Furthermore, the strain values of the four stations were high where all values were greater than 300. Also, the stations didn't show any significant potential of liquefaction where the kg index was low than 5 ($kg<5$) for all of them. Consequently, we can link the poor liquefaction potential to the absence of any surface ground water under or near to these four stations.

The station M411 belongs to the Neogene sediment (SUTER, 1980) where the fundamental frequency was high with a value of 11.45 Hz and the strain was low with a value of 27.44. The computed Kg index value under the M411 station was less than one. Furthermore, this station is not situated on any of the underground nappes of the Melouia Bassin. For that we can infer that there is no probability of existing underground water under this particular station. Hence, when comparing the low probability of liquefaction "Kg" and the absence of any aquifer nappe under the station, we can corroborate that both assumptions are correlated and lead us to the same conclusion of no liquefaction risk near around and under the M411 station.

All the stations except M410 are situated in terraces, hills and mountains and belong to Pre-Pleistocene. On this base, we can compare our results with Iwasaki (Iwasaki et al., 1982) and Youd and Perkins (Youd and Perkins, 1978) classified tables of susceptibility of sedimentary deposits to liquefaction on the base of topography and geology. The classification of Iwasaki and Youd and Perkins clearly correlate with our results. Hence, the liquefaction potential under most of the stations is not likely to happen. On the other hand, the station M410 is situated in a post-nappes series (PIQUE et al., 1994) which comprise recent Quaternary deposits (Pleistocene-Holocene) (Chalouan et al., 2008) with modern Alluvium (SUTER, 1980). The Youd and Perkins classification state that the Quaternary near to a river channel can contain either very high, high or low liquefaction probability (Youd and Perkins, 1978). Moreover, by virtue to Iwasaki classification of "sedimentary deposits susceptibility to liquefaction", the liquefaction occurrence near to the station M410 is possible especially that it is surrounded by natural levee (Iwasaki et al., 1982). Thus, liquefaction potential occurrence could be generated under and around the surroundings of M410 station.

5.9 Conclusion

In the present study, micro-tremor measurements were performed under 15 stations during 2014. We elicited whole-yearly noise samples of 2014 and then we applied the HVSR technique to compute the mean of fundamental frequency and amplitude. We also computed the frequency and amplitude standard deviation to ensure a high-standard, low-bias trade-off results. Afterwards, using Nakamura's method, we inferred the Kg index to evaluate the liquefaction potential under each particular station. The liquefaction parameter was compared to the hydrological, geological and even to topographic settings, where the most part of the stations show relatively a low Kg index, which displays a good conformity with regard to the region and it characteristics (hydrology and geology). Additionally, the results of the Kg index that show a low occurrence of liquefaction can be as well correlated to Iwasaki et al and Youd and Perkins classification tables (Iwasaki et al., 1982; Youd and Perkins, 1978). The HVSR technique is a useful tool when comparing it with the geological and the hydrological results in the near surface and it could be also cost-effective and efficient to identify most susceptible sites to strong ground shaking from inbounding earthquakes. In addition, it can be stated that micro-tremor measurement can be a suitable method together with other conventional methods to explore liquefaction occurrence.

Due to the reduced number of stations implemented in the region comparing to the surface of the study, the estimation is not enough to build-up a risk map of liquefaction. However, this findings work is useful for: evaluating the region approximate to the stations that could be affected by the probability of hazards and for disaster prevention planning. In structural and geotechnical engineering, the liquefaction index is one of many parameters that influences the seismic response of buildings by the soil-structure interaction (SSI) (Çelebi et al., 2012), therefore, it is required to take it into account when designing new constructions and rehabilitating existing infrastructures. The present investigation can be a handy tool for civil engineering and research as elementary information for regional studies. Geotechnical studies should definitely be accomplished in areas of high or moderate risk for the existing structures in order to examine and mitigate liquefaction hazards prior to near and far future development.

To sum up, the areas underneath most of the stations has been classified as not likely in terms of liquefaction hazard in an event of future earthquake. The study results should serve as a handbook where to focus the liquefaction potential investigations. Moreover, it is a perspective of future research to validate and refine it with more information.

General conclusion

Ever since the Rif area has known from decades a large number of earthquakes, our interest become highly responsive. In this purpose, we have chosen to investigate the variety of tectonic movements by using the attenuation scattering of coda waves and its dependency with the frequency. The illustrated case in this work implies 70 seismic events focusing on the Rif Mountains with recorded seismic data during all 2014 period. These recordings have been used with a magnitude (Ml) less than 5. In this work we utilized 15 broadband stations deployed in a surface area defined by longitudes 34°N to 35.50°N and latitude 5.3°W and 3.20°W. The quality factor is inversely proportional to the seismic attenuation which is defined by the backscattering model model (Aki and Chouet, 1975). The quality factor estimated values were computed at different central band frequencies that start from 1.5 till 18Hz for five lapse time windows 20, 30, 40, 50 and 60 s. For 20s window lapse time, the quality factor average for the whole study area gives estimation of about 83,55 ± 10,84 at 1.5 Hz and 491,66 ± 150,07 at 18Hz, as well as the estimation for 60s window lapse time is about 157,49 ± 15,61 at 1.5 Hz and 1787,65 ± 807,88 at 18Hz central band frequencies. We found that the quality factor rise when both frequency and lapse time window increase; which reveals a clear dependency between the quality factor and frequency and reflects heterogeneities within the underlying crust and the complexity of geological/geophysical pattern in this zone. In addition to that, evaluating the liquefaction potential is one of the most useful investigations for risk mitigation and seismic hazard zonation and assessment. The parameter of the seismic vulnerability can be quantified and expressed by Kg index which is derived from the well-known ambient noise Horizontal-to-Vertical Spectral Ratio (HVSR) method of Nakamura. The HVSR method was conducted on the whole micro-tremor data of 2014. By extracting the fundamental frequency F0 and the amplification factor A_o from the micro-tremor data, the Kg index was calculated and the liquefaction potential was evaluated. The lowest estimated Kg value was about of 0.19 [34.97°N - 3.32°W] while the highest value reached 11.93 [35.33°N - 4.96°W] which refers to the station situated near the Bou-Ahmed river branch north Morocco. Accordingly, the low Kg values exhibit a dominance in the Rif area, which can be related to minor water content, thus unsaturated ground granules.

To the best of our knowledge, and for the first time in Morocco, we propose a careful study of the attenuation of coda waves and the liquefaction potential in the region of Rif. We proved, as all the earlier research like to describe, the complexity of the geological bedrock in this area

which comprise the internal zone, the Flysch nappes and the external zone. Therefore, this study is a new contribution in the seismological field, in Morocco.

We have seen in this thesis, the usefulness of such parameters in tracking zones with high risks especially with a dense network. It would be interesting to proceed in other studies to make a micro-zonation with the same parameters and why not to split up the attenuation into the scattering and absorption parameters. These attenuation derivatives will profound the investigation survey, will give more detailed information to obtain greater interpretations and will push toward a high degree of comprehension.

REFERENCES

- *Abd el-aal, A. el-aziz K., 2018. New relationship between fundamental site frequency and thickness of soft sediments from seismic ambient noise. J Seismol 22, 1315–1323. https://doi.org/10.1007/s10950-018-9753-x*
- *ABHL, 2014. L'ETAT DE LA QUALITE DES EUAX DE LA ZONE D'ACTION DE L'AGENCE DU BASSIN HYDRAULIQUE DU LOUKKOS. Agence de Bassin Hydraulic Loukkos (ABHL).*
- *Ait Brahim, L., 1991. Tectoniques cassantes et états des contraintes récents au Nord du Maroc.. Ph.D.*
- *Aki, K., 1969. Analysis of the seismic coda of local earthquakes as scattered waves. Journal of Geophysical Research (1896-1977) 74, 615–631. https://doi.org/10.1029/JB074i002p00615*
- *Aki, K., 1969. Analysis of the seismic coda of local earthquakes as scattered waves. J. Geophys. Res. 1896-1977 74, 615–631. https://doi.org/10.1029/JB074i002p00615*
- *Aki, K., 1980. Attenuation of shear-waves in the lithosphere for frequencies from 0.05 to 25 Hz. Physics of the Earth and Planetary Interiors 21, 50–60. https://doi.org/10.1016/0031-9201(80)90019-9*
- *Aki, K., 1980. Attenuation of shear-waves in the lithosphere for frequencies from 0.05 to 25 Hz. Phys. Earth Planet. Inter. 21, 50–60. https://doi.org/10.1016/0031-9201(80)90019-9*
- *Aki, K., Chouet, B., 1975. Origin of coda waves: Source, attenuation, and scattering effects. J. Geophys. Res. 80, 3322–3342. https://doi.org/10.1029/JB080i023p03322*
- *Aki, K., Chouet, B., 1975. Origin of coda waves: Source, attenuation, and scattering effects. J. Geophys. Res. 80, 3322–3342. https://doi.org/10.1029/JB080i023p03322*
- *Aki, K., Tsujiura, M., 1959. Correlation study of near earthquake waves. Bull. Earthquake.*
- *Aki, K., Tsujiura, M., Hori, M., Goto, K., 1958. Spectral Study of Near Earthquake Waves (1). 東京大學地震研究所彙報 Bull. Earthq. Res. Inst. Univ. Tokyo 36, 71–98.*
- *Akinci, A., Taktak, A., Ergintav, S., 1994. Attenuation of coda waves in Western Anatolia. Physics of The Earth and Planetary Interiors - PHYS EARTH PLANET INTERIORS 87, 155–165. https://doi.org/10.1016/0031-9201(94)90028-0*
- *Akkaya, İ., 2020. Availability of seismic vulnerability index (Kg) in the assessment of building damage in Van, Eastern Turkey. Earthq. Eng. Eng. Vib. 19, 189–204. https://doi.org/10.1007/s11803-020-0556-z*
- *Andrade, J.E., Ramos, A.M., Lizcano, A., 2013. Criterion for flow liquefaction instability. Acta Geotech. 8, 525–535. https://doi.org/10.1007/s11440-013-0223-x*
- *Andrieux, J.A., 1971. La Structure du Rif central : Etude des relations entre le tectonique de compression et les nappes de glissement dans un tronçon de la chaîne alpine. [s.n.]. [S.l.].*
- *Andrus, R.D., Stokoe, K.H., 1999. Liquefaction Resistance Based on Shear Wave Velocity (No. Report No:-0022 ,Technical Report NCEER-97).*
- *Arab, O., Azguet, R., Ouchen, I., El Fellah, Y., Harnafi, M., Sebbani, J., Villaseñor, A., 2020. Attenuation of seismic coda waves in the Rif area, northern Morocco. Journal of African Earth Sciences 165, 103815. https://doi.org/10.1016/j.jafrearsci.2020.103815*
- *Atkinson, G.M., 2004. Empirical Attenuation of Ground-Motion Spectral Amplitudes in Southeastern Canada and the Northeastern United States. https://doi.org/10.1785/0120030175*

- *Azguet, R., Bouskri, G., Timoulali, Y., Harnafi, M., Fellah, Y.EL., 2019. Attenuation of coda waves in the SW of High-Atlas area, Morocco. Geodesy and Geodynamics 10, 297–306. https://doi.org/10.1016/j.geog.2019.05.001*
- *Bard, P.-Y., 1999. Microtremor measurements: A tool for site effect estimation? The effects of surface geology on seismic motion 3, 1251–1279.*
- *Bargach, K., Ruano, P., Chabli, A., Galindo-Zaldívar, J., Chalouan, A., Jabaloy, A., Akil, M., Ahmamou, M., Sanzde Galdeano, C., Benmakhlouf, M., 2004. Recent Tectonic Deformations and Stresses in the Frontal Part of the Rif Cordillera and the Saïss Basin (Fes and Rabat Regions, Morocco). Pure Appl. Geophys. 161, 521–540. https://doi.org/10.1007/s00024-003-2461-6*
- *Benmakhlouf, M., Galindo-Zaldívar, J., Chalouan, A., Sanz de Galdeano, C., Ahmamou, M., López-Garrido, A.C., 2012. Inversion of transfer faults: The Jebha–Chrafate fault (Rif, Morocco). J. Afr. Earth Sci. 73–74, 33–43. https://doi.org/10.1016/j.jafrearsci.2012.07.003*
- *Berger, J., Davis, P., Ekström, G., 2004. Ambient Earth noise: A survey of the Global Seismographic Network. J. Geophys. Res. Solid Earth 109. https://doi.org/10.1029/2004JB003408*
- *Bird, P., 2003. An updated digital model of plate boundaries. Geochem. Geophys. Geosystems 4. https://doi.org/10.1029/2001GC000252*
- *Bora, N., Biswas, R., Dobrynina, A.A., 2018. Regional variation of coda Q in Kopili fault zone of northeast India and its implications. Tectonophysics 722, 235–248. https://doi.org/10.1016/j.tecto.2017.11.008*
- *Borja, R.I., 2006. Condition for liquefaction instability in fluid-saturated granular soils. Acta Geotech. 1, 211. https://doi.org/10.1007/s11440-006-0017-5*
- *Boulanouar, A., El Moudnib, L., Padhy, S., Harnafi, M., Villasenor, A., Gallart, J., Pazos, A., RAHMOUNI, A., Boukalouch, M., Sebbani, J., 2017. Estimation of Coda Wave Attenuation in Northern Morocco. Pure and Applied Geophysics 175. https://doi.org/10.1007/s00024-017-1726-4*
- *Boulanouar, A., Moudnib, L.E., Ford, S.R., Harnafi, M., Villasenor, A., Gallart, J., Rahmouni, A., Boukalouch, M., Sebbani, J., 2016. Coda wave attenuation tomography in Northern Morocco 6.*
- *Bour, M., Fouissac, D., Dominique, P., Martin, C., 1998. On the use of microtremor recordings in seismic microzonation. Soil Dynamics and Earthquake Engineering 17, 465–474. https://doi.org/10.1016/S0267-7261(98)00014-1*
- *Brahim, L.A., Chotin, P., 1984. Mise en evidence d'un changement de direction de compression dans l'avant-pays rifain (Maroc) au cours du Tertiaire et du Quaternaire.*
- *BRIAN J. MITCHELL, 1981. REGIONAL VARIATION AND FREQUENCY DEPENDENCE OF Qz IN THE CRUST OF THE UNITED STATES [WWW Document]. REGIONAL VARIATION AND FREQUENCY DEPENDENCE OF Qz IN THE CRUST OF THE UNITED STATES. URL http://citeseerx.ist.psu.edu/viewdoc/download?doi=10.1.1.859.6702&rep=rep1&type=pdf (accessed 10.18.19).*
- *Byrne, P.M., Park, S.-S., Beaty, M., Sharp, M., Gonzalez, L., Abdoun, T., 2004. Numerical modeling of liquefaction and comparison with centrifuge tests. Can. Geotech. J. 41, 193–211. https://doi.org/10.1139/t03-088*

- *Byrne, P.M., Park, S.-S., Beaty, M., Sharp, M., Gonzalez, L., Abdoun, T., 2004. Numerical modeling of liquefaction and comparison with centrifuge tests. Can. Geotech. J. 41, 193–211. https://doi.org/10.1139/t03-088*
- *Castellano, M., Del Pezzo, E., De Natale, G., Zollo, A., 1984. Seismic coda Q and turbidity coefficient at the Phlegraean Fields volcanic area: Preliminary results. Bull. Volcanol. 47, 219–224. https://doi.org/10.1007/BF01961551*
- *CATNAT, 2021, 2021. Bilan statistique des catastrophes naturelles survenues dans le Monde entre 2001-2020 [WWW Document]. URL https://www.catnat.net/donneesstats/dernieres-actualites/21507-bilan-statistique-des-catastrophes-naturelles-survenues-dans-le-monde-entre-2001-2020 (accessed 12.5.21).*
- *Çelebi, E., Göktepe, F., Karahan, N., 2012. Non-linear finite element analysis for prediction of seismic response of buildings considering soil-structure interaction. Nat. Hazards Earth Syst. Sci. 12, 3495–3505. https://doi.org/10.5194/nhess-12-3495-2012*
- *Chalouan, A., Galindo-Zaldívar, J., Akil, M., Marín, C., Chabli, A., Ruano, P., Bargach, K., Galdeano, C.S. de, Benmakhlouf, M., Ahmamou, M., Gourari, L., 2006. Tectonic wedge escape in the southwestern front of the Rif Cordillera (Morocco). Geol. Soc. Lond. Spec. Publ. 262, 101–118. https://doi.org/10.1144/GSL.SP.2006.262.01.06*
- *Chalouan, A., Michard, A., el Kadiri, K., Negro, F., Frizon de Lamotte, D., Soto, J., Saddiqi, O., 2008. Chalouan et al The Rif Belt.*
- *Chalouan, A., Michard, A., el Kadiri, K., Negro, F., Frizon de Lamotte, D., Soto, J., Saddiqi, O., 2008. Chalouan et al The Rif Belt.*
- *Chalouan, A., Michard, A., Feinberg, H., Montigny, R., Saddiqi, O., 2001. The Rif mountain building (Morocco): A new tectonic scenario. Bulletin de la Societe Geologique de France 172, 603–616. https://doi.org/10.2113/172.5.603*
- *Champagnac, J.-D., Yuan, D.-Y., Ge, W.-P., Molnar, P., Zheng, W.-J., 2010. Slip rate at the north-eastern front of the Qilian Shan, China. Terra Nova 22, 180–187. https://doi.org/10.1111/j.1365-3121.2010.00932.x*
- *Chéry, J., Carretier, S., Ritz, J.-F., 2001. Postseismic stress transfer explains time clustering of large earthquakes in Mongolia. Earth Planet. Sci. Lett. 194, 277–286. https://doi.org/10.1016/S0012-821X(01)00552-0*
- *Chiaro, G., Koseki, J., Sato, T., 2012. Effects of initial static shear on liquefaction and large deformation properties of loose saturated Toyoura sand in undrained cyclic torsional shear tests. Soils and Foundations 52, 498–510. https://doi.org/10.1016/j.sandf.2012.05.008*
- *Choobbasti, A.J., Naghizadehrokni, M., Rezaei, S., 2015. Liquefaction assessment by microtremor measurements in Babol city, in: Fifth International Conference on Geotechnique, Construction Materials and Environment,. Osaka, Japan.*
- *d'Acremont, E., Gutscher, M.-A., Rabaute, A., Mercier de Lépinay, B., Lafosse, M., Poort, J., Ammar, A., Tahayt, A., Le Roy, P., Smit, J., Do Couto, D., Cancouët, R., Prunier, C., Ercilla, G., Gorini, C., 2014. High-resolution imagery of active faulting offshore Al Hoceima, Northern Morocco. Tectonophysics 632, 160–166. https://doi.org/10.1016/j.tecto.2014.06.008*
- *Dainty, A.M., Toksöz, M.N., 1981. Seismic codas on the Earth and the Moon: a comparison. Phys. Earth Planet. Inter. 26, 250–260. https://doi.org/10.1016/0031-9201(81)90029-7*

- *de Capoa, P., Di Staso, A., Perrone, V., Zaghloul, M.N., 2007. The age of the foredeep sedimentation in the Betic–Rifian Mauretanian Units: A major constraint for the reconstruction of the tectonic evolution of the Gibraltar Arc. Comptes Rendus Geoscience 339, 161–170. https://doi.org/10.1016/j.crte.2007.01.003*
- *Del Pezzo, E., Patanè, D., 1992. Coda Q Dependence on Time, Frequency and Coda Duration Interval at Mt. Etna, Sicily. pp. 109–119. https://doi.org/10.1007/978-3-642-77008-1_9*
- *Del Pezzo, E., Zollo, A., 1984. Attenuation of coda waves and turbidity coefficient in central Italy.*
- *DUGGEN, S., HOERNLE, K., VAN DEN BOGAARD, P., GARBE-SCHÖNBERG, D., 2005. Post-Collisional Transition from Subduction- to Intraplate-type Magmatism in the Westernmost Mediterranean: Evidence for Continental-Edge Delamination of Subcontinental Lithosphere. J. Petrol. 46, 1155–1201. https://doi.org/10.1093/petrology/egi013*
- *El Fellah, Y., 2015. Etude du bruit sismique au Maroc septentrional : quantification de la densité de puissance spectrale, tomographie et distribution des vitesses des ondes de surface.*
- *El Fellah, Y., Bouskri, G., Harnafi, M., El-Aziz Khairy Abd El-Aal, A., Timoulali, Y., Ouchen, I., Azguet, R., 2019. Tracking regional heterogeneities through seismic ambient noise constrains: What Rayleigh wave tomography can tell about deep structures in northern Morocco. Journal of African Earth Sciences 160, 103615. https://doi.org/10.1016/j.jafrearsci.2019.103615*
- *El Fellah, Y., Bouskri, G., Harnafi, M., El-Aziz Khairy Abd El-Aal, A., Timoulali, Y., Ouchen, I., Azguet, R., 2019. Tracking regional heterogeneities through seismic ambient noise constrains: What Rayleigh wave tomography can tell about deep structures in northern Morocco. Journal of African Earth Sciences 160, 103615. https://doi.org/10.1016/j.jafrearsci.2019.103615*
- *El Fellah, Y., El-Aal, A.E.-A.K.A., Harnafi, M., Villaseñor, A., 2017. New comprehensive standard seismic noise models and 3D seismic noise variation for Morocco territory, North Africa, obtained using seismic broadband stations. Exploration Geophysics 48, 272–283. https://doi.org/10.1071/EG15053*
- *Elgamal, A., Yang, Z., Parra, E., 2002. Computational modeling of cyclic mobility and post-liquefaction site response. Soil Dynamics and Earthquake Engineering 22, 259–271. https://doi.org/10.1016/S0267-7261(02)00022-2*
- *Faccenna, C., Piromallo, C., Crespo-Blanc, A., Jolivet, L., Rossetti, F., 2004. Lateral slab deformation and the origin of the western Mediterranean arcs. Tectonics 23. https://doi.org/10.1029/2002TC001488*
- *Fadil, A., Vernant, P., McClusky, S., Reilinger, R., Gomez, F., Ben Sari, D., Mourabit, T., Feigl, K., Barazangi, M., 2006. Active tectonics of the western Mediterranean: Geodetic evidence for rollback of a delaminated subcontinental lithospheric slab beneath the Rif Mountains, Morocco. Geology 34, 529–532. https://doi.org/10.1130/G22291.1*
- *Fergany, E.A., Bonnefoy-Claudet, S., 2009. Microtremor Measurements in the Nile Delta Basin, Egypt: Response of the Topmost Sedimentary Layer. Seismological Research Letters 80, 591–598. https://doi.org/10.1785/gssrl.80.4.591*
- *Frizon de Lamotte, D., Andrieux, J., Guezou, J.C., 1991. Cinematique des chevauchements neogenes dans l'Arc betico-rifain; discussion sur les modeles geodynamiques. Bull. Société Géologique Fr. 162, 611–626. https://doi.org/10.2113/gssgfbull.162.4.611*

- *Galindo-Zaldívar, J., Chalouan, A., Azzouz, O., Sanz de Galdeano, C., Anahnah, F., Ameza, L., Ruano, P., Pedrera, A., Ruiz-Constán, A., Marín-Lechado, C., Benmakhlouf, M., López-Garrido, A.C., Ahmamou, M., Saji, R., Roldán-García, F.J., Akil, M., Chabli, A., 2009. Are the seismological and geological observations of the Al Hoceima (Morocco, Rif) 2004 earthquake (M=6.3) contradictory? Tectonophysics, The geology of vertical movements of the lithosphere 475, 59–67. https://doi.org/10.1016/j.tecto.2008.11.018*
- *Gao, L.S., 1984. Coda wave analysis for distinguishing attenuation due to isotropic scattering from attenuation due to absorption. Pure Appl. Geophys. 122, 1–9. https://doi.org/10.1007/BF00879645*
- *Giampiccolo, E., Tusa, G., Langer, H., Gresta, S., 2002. Attenuation in Southeastern Sicily (Italy) by applying different coda methods. Journal of Seismology 6, 487–501. https://doi.org/10.1023/A:1021150819311*
- *Gil, A., Gallart, J., Diaz, J., Carbonell, R., Torne, M., Levander, A., Harnafi, M., 2014. Crustal structure beneath the Rif Cordillera, North Morocco, from the RIFSIS wide-angle reflection seismic experiment. Geochem. Geophys. Geosyst. 15, 4712–4733. https://doi.org/10.1002/2014GC005485*
- *Gil, A., Gallart, J., Diaz, J., Carbonell, R., Torne, M., Levander, A., Harnafi, M., 2014. Crustal structure beneath the Rif Cordillera, North Morocco, from the RIFSIS wide-angle reflection seismic experiment. Geochem. Geophys. Geosyst. 15, 4712–4733. https://doi.org/10.1002/2014GC005485*
- *Gosar, A., 2007. Microtremor HVSR study for assessing site effects in the Bovec basin (NW Slovenia) related to 1998 Mw5.6 and 2004 Mw5.2 earthquakes. Engineering Geology 91, 178–193. https://doi.org/10.1016/j.enggeo.2007.01.008*
- *Gupta, S.C., Singh, V.N., Kumar, A., 1995. Attenuation of coda waves in the Garhwal Himalaya, India. Physics of the Earth and Planetary Interiors 87, 247–253. https://doi.org/10.1016/0031-9201(94)02968-H*
- *Gupta, S.C., Teotia, S.S., Rai, S.S., Gautam, N., 1998. Coda Q Estimates in the Koyna Region, India. Pure appl. geophys. 153, 713–731. https://doi.org/10.1007/s000240050216*
- *Gutscher, M.-A., 2004. What Caused the Great Lisbon Earthquake? Science 305, 1247–1248. https://doi.org/10.1126/science.1101351*
- *Gutscher, M.-A., Dominguez, S., Westbrook, G.K., Le Roy, P., Rosas, F., Duarte, J.C., Terrinha, P., Miranda, J.M., Graindorge, D., Gailler, A., Sallares, V., Bartolome, R., 2012. The Gibraltar subduction: A decade of new geophysical data. Tectonophysics 574–575, 72–91. https://doi.org/10.1016/j.tecto.2012.08.038*
- *Gutscher, M.-A., Malod, J., Rehault, J.-P., Contrucci, I., Klingelhoefer, F., Mendes-Victor, L., Spakman, W., 2002. Evidence for active subduction beneath Gibraltar. Geology 30, 1071–1074. https://doi.org/10.1130/0091-7613(2002)030<1071:EFASBG>2.0.CO;2*
- *Hanka, 2000. URL https://geofon.gfz-potsdam.de/geofon/manual/welcome.html (accessed 12.5.21).*
- *Harris, R.A., 1998. Forecasts of the 1989 Loma Prieta, California, earthquake. Bulletin of the Seismological Society of America 88, 898–916.*
- *Hasegawa, H.S., 1985. Attenuation of Lg waves in the Canadian Shield. Bulletin of the Seismological Society of America 75, 1569–1582.*
- *Havskov, J., Malone, S., McClurg, D., Crosson, R., 1989. Coda Q for the state of Washington. Bulletin of the Seismological Society of America 79, 1024–1038.*

- *Hellweg, M., Spudich, P., Fletcher, J.B., Baker, L.M., 1995. Stability of coda Q in the region of Parkfield, California: View from the U.S. Geological Survey Parkfield Dense Seismograph Array. Journal of Geophysical Research: Solid Earth 100, 2089–2102. https://doi.org/10.1029/94JB02888*
- *Herraiz, M., Espinosa, A.F., 1987. Coda waves: A review. Pure Appl. Geophys. 125, 499–577. https://doi.org/10.1007/BF00879572*
- *Herrmann, R.B., 1980. Q estimates using the coda of local earthquake. Bull. Seismol. Soc. Am. 70, 447–468. https://doi.org/10.1785/BSSA0700020447*
- *Hird, C.C., Hassona, F.A.K., 1990. Some factors affecting the liquefaction and flow of saturated sands in laboratory tests. Engineering Geology 28, 149–170. https://doi.org/10.1016/0013-7952(90)90039-4*
- *Hunt, R.E., 1986. Geotechnical Engineering Analysis and Evaluation. New York, NY: McGraw-Hill.*
- *Idriss, I.M., Boulanger, R.W., 2006. Semi-empirical procedures for evaluating liquefaction potential during earthquakes. Soil Dynamics and Earthquake Engineering, 11th International Conference on Soil Dynamics and Earthquake Engineering (ICSDEE): Part II 26, 115–130. https://doi.org/10.1016/j.soildyn.2004.11.023*
- *Ishihara, K., 1978. Introduction to Dynamic Soil Mechanism.*
- *Iwasaki, T., Tokida, K., Tatsuoka, F., Watanabe, S., Yasuda, S., Sato, H., 1982. Microzonation for soil liquefaction potential using simplified methods. In: Proceedings of the 3rd International Conference on Microzonation 13919–1330.*
- *James, M., 2009. The use of waste rock inclusions to control the effects of liquefaction in tailings impoundments (phd). École Polytechnique de Montréal.*
- *Jin and Aki, 1988. Spatial and Temporal Variations of Extreme Climate Events in Xinjiang, China during 1961-2010 [WWW Document]. URL https://www.scirp.org/journal/paperinformation.aspx?paperid=69846 (accessed 11.6.19).*
- *Jolivet, L., Augier, R., Faccenna, C., Negro, F., Rimmele, G., Agard, P., Robin, C., Rossetti, F., Crespo-Blanc, A., 2008. Subduction, convergence and the mode of backarc extension in the Mediterranean region. Bull. Société Géologique Fr. 179, 525–550. https://doi.org/10.2113/gssgfbull.179.6.525*
- *Juang, C.H., Ching, J., Luo, Z., Ku, C.-S., 2012. New models for probability of liquefaction using standard penetration tests based on an updated database of case histories. Engineering Geology 133–134, 85–93. https://doi.org/10.1016/j.enggeo.2012.02.015*
- *Juang, C.H., Li David Kun, Fang Sunny Ye, Liu Zhuzhao, Khor Eng Hui, 2008. Simplified Procedure for Developing Joint Distribution of amax and Mw for Probabilistic Liquefaction Hazard Analysis. Journal of Geotechnical and Geoenvironmental Engineering 134, 1050–1058. https://doi.org/10.1061/(ASCE)1090-0241(2008)134:8(1050)*
- *Juang, C.H., Yuan, H., Lee, D.-H., Lin, P.S., 2003. Simplified cone penetration test-based method for evaluating liquefaction resistance of soils. Journal of Geotechnical and Geoenvironmental Engineering 129, 66–80. https://doi.org/10.1061/(ASCE)1090-0241(2003)129:1(66)*
- *Juang, H., Yuan, H., Lee, D.-H., Ku, C.-S., 2002. Assessing CPT-based methods for liquefaction evaluation with emphasis on the cases from the Chi-Chi, Taiwan, earthquake. Soil Dynamics and Earthquake Engineering 22, 241–258. https://doi.org/10.1016/S0267-7261(02)00013-1*

- *Kadiri, K.E., Galdeano, C.S. de, Pedrera, A., Chalouan, A., Galindo-Zaldívar, J., Julià, R., Akil, M., Hlila, R., Ahmamou, M., 2010. Eustatic and tectonic controls on Quaternary Ras Leona marine terraces (Strait of Gibraltar, northern Morocco). Quat. Res. 74, 277–288. https://doi.org/10.1016/j.yqres.2010.06.008*
- *Kanai, K., Tanaka, T., 1961. On Microtremors VIII. Bulletin of Earthquakes Research Institute, 39, 97-114.*
- *Kayabasi, A., Gokceoglu, C., 2018. Deformation Modulus of Rock Masses: An Assessment of the Existing Empirical Equations. Geotech Geol Eng 36, 2683–2699. https://doi.org/10.1007/s10706-018-0491-1*
- *Khalqillah, A., Muksin, U., Musfirah, Ningsih, W.A., Irwandi, 2019. SVIM: A Program for Seismic Vulnerability Index Determination and HVSR Data Processing. IOP Conf. Ser.: Earth Environ. Sci. 273, 012016. https://doi.org/10.1088/1755-1315/273/1/012016*
- *Klitgord, K.D., Schouten, H., 1986. Plate kinematics of the central Atlantic. https://doi.org/10.1130/DNAG-GNA-M.351*
- *Knopoff, L., Hudson, J.A., 1964. Scattering of Elastic Waves by Small Inhomogeneities. The Journal of the Acoustical Society of America 36, 338–343. https://doi.org/10.1121/1.1918957*
- *Kopnichev, Y.F., 1975. A model qf generation of the tail of the seismogram (English Trans.). Dokl. Akad. Nauk SSSR 222, 13-15.*
- *Koulali, A., Ouazar, D., Tahayt, A., King, R.W., Vernant, P., Reilinger, R.E., McClusky, S., Mourabit, T., Davila, J.M., Amraoui, N., 2011. New GPS constraints on active deformation along the Africa–Iberia plate boundary. Earth Planet. Sci. Lett. 308, 211–217. https://doi.org/10.1016/j.epsl.2011.05.048*
- *kramer, S.L., 1996. Geotechnical Earthquake Engineering.*
- *Kumar, C.H.P., Sarma, C.S.P., Shekar, M., Chadha, R.K., 2007. Attenuation studies based on local earthquake Coda waves in the southern Indian peninsular shield. Nat Hazards 40, 527–536. https://doi.org/10.1007/s11069-006-9017-x*
- *Leon, E., Gassman, S.L., Talwani, P., 2006. Accounting for Soil Aging When Assessing Liquefaction Potential. J. Geotech. Geoenvironmental Eng. 132, 363–377. https://doi.org/10.1061/(ASCE)1090-0241(2006)132:3(363)*
- *Lermo, J., Chávez-García, F.J., 1993. Site effect evaluation using spectral ratios with only one station. Bulletin of the Seismological Society of America 83, 1574–1594.*
- *Lermo, J., Chávez-García, F.J., 1994. Are microtremors useful in site response evaluation? Bulletin of the Seismological Society of America 84, 1350–1364.*
- *Lonergan, L., White, N., 1997. Origin of the Betic-Rif mountain belt. Tectonics 16, 504–522. https://doi.org/10.1029/96TC03937*
- *Luján, M., Crespo-Blanc, A., Balanyá, J.C., 2006. The Flysch Trough thrust imbricate (Betic Cordillera): A key element of the Gibraltar Arc orogenic wedge. Tectonics 25. https://doi.org/10.1029/2005TC001910*
- *Macmurdo, J., 1824. XXI. Papers relating to the earthquake which occurred in India in 1819. Philos. Mag. 63, 105–119. https://doi.org/10.1080/14786442408644477*
- *Mancilla, F. de L., Stich, D., Morales, J., Julià, J., Diaz, J., Pazos, A., Córdoba, D., Pulgar, J.A., Ibarra, P., Harnafi, M., Gonzalez-Lodeiro, F., 2012. Crustal thickness variations in northern Morocco. Journal of Geophysical Research: Solid Earth 117. https://doi.org/10.1029/2011JB008608*

- *Meghraoui, M., Morel, J.-L., Andrieux, J., Dahmani, M., 1996. Tectonique plio-quaternaire de la chaine tello-rifaine et de la mer d'Alboran; une zone complexe de convergence continent-continent. Bull. Société Géologique Fr. 167, 141–157.*
- *Moratti, G., Piccardi, L., Vannucci, G., Belardinelli, M.E., Dahmani, M., Bendkik, A., Chenakeb, M., 2003. The 1755 "Meknes" earthquake (Morocco): field data and geodynamic implications. J. Geodyn., Active Faults: Analysis, Processes and Monitoring 36, 305–322. https://doi.org/10.1016/S0264-3707(03)00052-8*
- *Morel, J.-L., 1987. Évolution récente de l'orogène rifain et de son avant-pays depuis la fin de la mise en place des nappes (Rif, Maroc) (These de doctorat). Paris 11.*
- *Morel, J.L., 1992. Carte des mouvements récents du Rif. Notes et Mém. Serv. géol. Maroc, n° 365.*
- *Morel, J.L., Meghraoui, M., 1996. Goringe-Alboran-Tell tectonic zone: A transpression system along the Africa-Eurasia plate boundary. Geology 24, 755–758. https://doi.org/10.1130/0091-7613(1996)024<0755:GATTZA>2.3.CO;2*
- *Morley, C.K., 1987. Origin of a major cross-element zone: Moroccan Rif. Geology 15, 761–764. https://doi.org/10.1130/0091-7613(1987)15<761:OOAMCZ>2.0.CO;2*
- *Morley, C.K., 1987. Origin of a major cross-element zone: Moroccan Rif. Geology 15, 761–764. https://doi.org/10.1130/0091-7613(1987)15<761:OOAMCZ>2.0.CO;2*
- *Morley, C.K., 1992. Notes on Neogene basin history of the Western Alboran Sea and its implications for the tectonic evolution of the Rif-Betic orogenic belt. J. Afr. Earth Sci. Middle East 14, 57–65. https://doi.org/10.1016/0899-5362(92)90055-H*
- *Mukhopadhyay, S., Sharma, J., 2010. Attenuation characteristics of Garwhal–Kumaun Himalayas from analysis of coda of local earthquakes. J Seismol 14, 693–713. https://doi.org/10.1007/s10950-010-9192-9*
- *Nakamura, Y., 1989. A METHOD FOR DYNAMIC CHARACTERISTICS ESTIMATION OF SUBSURFACE USING MICROTREMOR ON THE GROUND SURFACE. Railway Technical Research Institute, Quarterly Reports 30.*
- *Nakamura, Y., 1996. Real-time information systems for hazard mitigation [WWW Document]. URL https://www.iitk.ac.in/nicee/wcee/article/11_2134.PDF (accessed 3.30.20).*
- *Nakamura, Y., 1997. SEISMIC VULNERABILITY INDICES FOR GROUND AND STRUCTURES USING MICROTREMOR 7.*
- *Nakamura, Y., 2000. Clear identification of fundamental idea of Nakamura's technique and its applications. Proc. XII World Conf. Earthquake Engineering 2656.*
- *Nakamura, Y., 2008. ON THE H/V SPECTRUM.*
- *Negro, F., Sigoyer, J. de, Goffé, B., Saddiqi, O., Villa, I.M., 2008. Tectonic evolution of the Betic–Rif arc: New constraints from 40Ar/39Ar dating on white micas in the Temsamane units (External Rif, northern Morocco). https://doi.org/10.1016/j.lithos.2008.06.011*
- *Ouchen, I., Fellah, Y.E., Aal, A.E.-A.K.A.E.-, Harnafi, M., 2018. Soil amplification factors at the seismographic network stations sites in morocco from seismic ambient noise. International Journal of Engineering & Technology 7, 4304–4310. https://doi.org/10.14419/ijet.v7i4.20216*
- *PIQUE, A., SOULAIMANI, A., LAVILLE, E., AMRHAR, M., BOUABDELLI, M., HOEPFFNER, C., CHALOUAN, A., 1994. Géologie du Maroc ; les domaines régionaux et leur évolution structurale, Pumag. ed.*

- *Platt, J.P., Behr, W.M., Johanesen, K., Williams, J.R., 2013. The Betic-Rif Arc and Its Orogenic Hinterland: A Review. Annual Review of Earth and Planetary Sciences 41, 313–357. https://doi.org/10.1146/annurev-earth-050212-123951*
- *Poncelet, N., 2012. Élaboration et implémentation d'un protocole de laboratoire pour l'étude du potentiel de liquéfaction de résidus miniers (masters). École Polytechnique de Montréal.*
- *Popescu, R., Prevost, J.H., 1993. Centrifuge validation of a numerical model for dynamic soil liquefaction. Soil Dynamics and Earthquake Engineering 12, 73–90. https://doi.org/10.1016/0267-7261(93)90047-U*
- *Poujol, A., 2014. Analyse des déformations actuelles dans le Rif (Maroc) : approche morphotectonique (phdthesis). Université Montpellier II - Sciences et Techniques du Languedoc.*
- *Poulos, S.J., Castro Gonzalo, France John W., 1985. Liquefaction Evaluation Procedure. Journal of Geotechnical Engineering 111, 772–792. https://doi.org/10.1061/(ASCE)0733-9410(1985)111:6(772)*
- *Pujades, L.G., Canas, J.A., Egozcue, J.J., Puigví, M.A., Gallart, J., Lana, X., Pous, J., Casas, A., 1990. Coda-Q Distribution In the Iberian Peninsula. Geophys J Int 100, 285–301. https://doi.org/10.1111/j.1365-246X.1990.tb02486.x*
- *Pulli, J.J., 1984. Attenuation of coda waves in New England. Bulletin of the Seismological Society of America 74, 1149–1166.*
- *Rahimi, H., Hamzehloo, H., 2008. Lapse time and frequency-dependent attenuation of coda waves in the Zagros continental collision zone in Southwestern Iran. J. Geophys. Eng. 5, 173–185. https://doi.org/10.1088/1742-2132/5/2/004*
- *Rautian, T.G., Khalturin, V.I., 1978. The use of the coda for determination of the earthquake source spectrum.*
- *Rezaei, S., Choobbasti, A.J., 2014. Liquefaction assessment using microtremor measurement, conventional method and artificial neural network (Case study: Babol, Iran). Front. Struct. Civ. Eng. 8, 292–307. https://doi.org/10.1007/s11709-014-0256-8*
- *Ritz, J.F., Brown, E.T., Bourlès, D.L., Philip, H., Schlupp, A., Raisbeck, G.M., Yiou, F., Enkhtuvshin, B., 1995. Slip rates along active faults estimated with cosmic-ray–exposure dates: Application to the Bogd fault, Gobi-Altaï, Mongolia. Geology 23, 1019–1022. https://doi.org/10.1130/0091-7613(1995)023<1019:SRAAFE>2.3.CO;2*
- *Rizza, M., Ritz, J.-F., Braucher, R., Vassallo, R., Prentice, C., Mahan, S., McGill, S., Chauvet, A., Marco, S., Todbileg, M., Demberel, S., Bourlès, D., 2011. Slip rate and slip magnitudes of past earthquakes along the Bogd left-lateral strike-slip fault (Mongolia). Geophys. J. Int. 186, 897–927. https://doi.org/10.1111/j.1365-246X.2011.05075.x*
- *Robertson, P.K., Wride, C. (Fear), 1998. Evaluating cyclic liquefaction potential using the cone penetration test. Can. Geotech. J. 35, 442–459. https://doi.org/10.1139/t98-017*
- *Roecker, S., Tucker, B., King, J., Hatzfeld, D., 1982. Estimates of Q in Central Asia as a function of frequency and depth using the coda of locally recorded earthquakes. Bulletin of the Seismological Society of America 72.*
- *Romagny, A., Ph. Münch, Cornée, J.-J., Corsini, M., Azdimousa, A., Melinte-Dobrinescu, M.C., Drinia, H., Bonno, M., Arnaud, N., Monié, P., Quillévéré, F., Ben Moussa, A., 2014. Late Miocene to present-day exhumation and uplift of the Internal Zone of the Rif chain: Insights from low temperature thermochronometry and basin*

analysis. J. Geodyn., SI : Geodynamic evolution of the Alboran domain 77, 39–55. https://doi.org/10.1016/j.jog.2014.01.006

- *Rovelli, A., 1983. Time-frequency analysis of seismic excitation and estimates of attenuation parameters for the Friuli (Italy) local earthquakes. Phys. Earth Planet. Inter. 33, 94–110. https://doi.org/10.1016/0031-9201(83)90143-7*
- *RPS, 2011. LE REGLEMENT DE CONSTRUCTION PARASISMIQUE RPS 2000-Version 2011.*
- *Sabri, K., Marrero-Diaz, R., Ntarmouchant, A., Bento dos Santos, T., Ribeiro, M.L., Solá, A.R., Smaili, H., Benslimane, A., Chibout, M., Pérez, N.M., Padrón, E., Melián, G.V., Asensio-Ramos, M., Carreira, P.M., Jesus, A.P., 2019. Geology and hydrogeochemistry of the thermo-mineral waters of the South Rif Thrust (Northern Morocco). Geothermics 78, 28–49. https://doi.org/10.1016/j.geothermics.2018.11.005*
- *Saita, J., Nakamura, Y., Sato, T., 2012. Liquefaction caused by the 2011 off the Pacific Coast of Tohoku Earthquake and the Result of the Prior Microtremor Measurement 7.*
- *Salhi, A., Martin-Vide, J., Benhamrouche, A., Benabdelouahab, S., Himi, M., Benabdelouahab, T., Casas Ponsati, A., 2019. Rainfall distribution and trends of the daily precipitation concentration index in northern Morocco: a need for an adaptive environmental policy. SN Appl. Sci. 1, 277. https://doi.org/10.1007/s42452-019-0290-1*
- *Satake, K., Abe, K., 1983. A fault model for the Niigata, Japan, earthquake of June 16, 1964. J,Phys,Earth 31, 217–223. https://doi.org/10.4294/jpe1952.31.217*
- *Sato, H., Fehler, M.C., 1998. Seismic wave propagation and scattering in the heterogeneous Earth. AIP Series in Modern Acoustics and Signal Processing.*
- *SCHEIMER, J., Landers, T., E., 197AD. Short period coda of a local event at LASA, Seismic Discrimination. Semiannual Tech.*
- *Sedaghati, F., Pezeshk, S., 2016. Estimation of the Coda-Wave Attenuation and Geometrical Spreading in the New Madrid Seismic Zone. Bulletin of the Seismological Society of America 106, 1482–1498. https://doi.org/10.1785/0120150346*
- *Seed, H.B., 1979. Soil Liquefaction and Cyclic Mobility Evaluation for Level Ground during Earthquakes. J. Geotech. Eng. Div. 105, 201–255. https://doi.org/10.1061/AJGEB6.0000768*
- *Seed, H.B., Idriss, I.M., 1970. A Simplified Procedure for Evaluating Soil Liquefaction Potential (Report NO. ERRC 70-9). Berkeley, CA: Earthquake Engineering Research Institute.*
- *Seed, H.B., Idriss, I.M., 1971. SIMPLIFIED PROCEDURE FOR EVALUATING SOIL LIQUEFACTION POTENTIAL. Journal of Soil Mechanics & Foundations Div.*
- *Seed, H.B., Idriss, I.M., 1982. Ground motions and soil liquefaction during earthquakes.*
- *Singh, S., Herrmann, R.B., 1983. Regionalization of crustal coda Q in the continental United States. Journal of Geophysical Research: Solid Earth 88, 527–538. https://doi.org/10.1029/JB088iB01p00527*
- *Sivathayalan, S., Ha, D., 2011. Effect of static shear stress on the cyclic resistance of sands in simple shear loading. Can. Geotech. J. 48, 1471–1484. https://doi.org/10.1139/t11-056*
- *Sonmez, B., Ulusay, R., Sonmez, H., 2008. A study on the identification of liquefaction-induced failures on ground surface based on the data from the 1999 Kocaeli and Chi-Chi earthquakes. Engineering Geology 97, 112–125. https://doi.org/10.1016/j.enggeo.2007.12.008*

- *Spakman, W., Wortel, R., 2004. A Tomographic View on Western Mediterranean Geodynamics, in: Cavazza, W., Roure, F., Spakman, W., Stampfli, G.M., Ziegler, P.A. (Eds.), The TRANSMED Atlas. The Mediterranean Region from Crust to Mantle: Geological and Geophysical Framework of the Mediterranean and the Surrounding Areas. Springer, Berlin, Heidelberg, pp. 31–52. https://doi.org/10.1007/978-3-642-18919-7_2*
- *Stein, S., Wysession, M., 2003. STEIN, S. WYSESSION, M. 2003. An Introduction to Seismology, Earthquakes, and Earth Structure. xi + 498 pp. Oxford: Blackwell Science. Price 34.95, US $79.95 (paperback). ISBN 0 865 42078 5. Blackwell Publishing 140, 733–734. https://doi.org/10.1017/S0016756803318837*
- *Sunaryo, 2017. Study of seismic vulnerability index (Kg) from dominant frequency (f0) and amplification factor (A0) by means of microzonation data: Case study on Batubesi dam of Nuha, East Luwu, South Sulawesi, Indonesia, in: 2017 International Seminar on Sensors, Instrumentation, Measurement and Metrology (ISSIMM). Presented at the 2017 International Seminar on Sensors, Instrumentation, Measurement and Metrology (ISSIMM), pp. 78–81. https://doi.org/10.1109/ISSIMM.2017.8124266*
- *SUTER, G., 1980. Carte structurale de la chaîne rifaine à 1/500000. Notes Mémoires du Serv. Géologique du Maroc 245a et b, 1–60.*
- *Tahayt, A., 2008. Apport des mesures de la géodésie spatiale dans l'étude des déformations tectoniques actuelles dans la Méditerranée occidentale (phd). Université de Toulouse, Université Toulouse III - Paul Sabatier.*
- *Tejera De Leon, J., 1997. Signification de la limite Jebha-Arbaoua (Maroc nord-occidental): une rampe latérale au-dessus dúne discontinuité crustale héritée de la période de "rifting." J. Afr. Earth Sci. 24, 455–472. https://doi.org/10.1016/S0899-5362(97)00075-4*
- *Teves-Costa, P., Matias, L., Bard, P.Y., 1996. Seismic behaviour estimation of thin alluvium layers using microtremor recordings. Soil Dynamics and Earthquake Engineering 15, 201–209. https://doi.org/10.1016/0267-7261(95)00038-0*
- *Torne, M., Fernàndez, M., Comas, M.C., Soto, J.I., 2000. Lithospheric Structure Beneath the Alboran Basin: Results from 3D Gravity Modeling and Tectonic Relevance. J. Geophys. Res. 105, 3209–3228. https://doi.org/10.1029/1999JB900281*
- *Torne, M., Fernàndez, M., Comas, M.C., Soto, J.I., 2000. Lithospheric Structure Beneath the Alboran Basin: Results from 3D Gravity Modeling and Tectonic Relevance. J. Geophys. Res. 105, 3209–3228. https://doi.org/10.1029/1999JB900281*
- *Troncosso, J.H., 1986. Critical state of tailings silty sands for earthquake loading, Soil Dynamics and Earthquake Engineering, 5(4), pp. 286-252.*
- *Tuttle, M.P., Schweig, E.S., Sims, J.D., Lafferty, R.H., Wolf, L.W., Haynes, M.L., 2002. The Earthquake Potential of the New Madrid Seismic Zone. Bull. Seismol. Soc. Am. 92, 2080–2089. https://doi.org/10.1785/0120010227*
- *Vaid, Y.P., Fisher, J.M., Kuerbis, R.H., Negussey, D., 1990. Particle Gradation and Liquefaction. J. Geotech. Eng. 116, 698–703. https://doi.org/10.1061/(ASCE)0733-9410(1990)116:4(698)*
- *Vaid, Y.P., Stedman, J.D., Sivathayalan, S., 2001. Confining stress and static shear effects in cyclic liquefaction. Can. Geotech. J. 38, 580–591. https://doi.org/10.1139/t00-120*
- *van der Woerd, J., Dorbath, C., Ousadou, F., Dorbath, L., Delouis, B., Jacques, E., Tapponnier, P., Hahou, Y., Menzhi, M., Frogneux, M., Haessler, H., 2014. The Al Hoceima Mw 6.4 earthquake of 24 February 2004 and its*

aftershocks sequence. J. Geodyn., SI : Geodynamic evolution of the Alboran domain 77, 89–109. https://doi.org/10.1016/j.jog.2013.12.004

- *Vergés, J., Fernàndez, M., 2012. Tethys–Atlantic interaction along the Iberia–Africa plate boundary: The Betic–Rif orogenic system. Tectonophysics, Orogenic processes and structural heritage in Alpine-type mountain belts 579, 144–172. https://doi.org/10.1016/j.tecto.2012.08.032*
- *Vernant, P., Fadil, A., Mourabit, T., Ouazar, D., Koulali, A., Davila, J.M., Garate, J., McClusky, S., Reilinger, R., 2010. Geodetic constraints on active tectonics of the Western Mediterranean: Implications for the kinematics and dynamics of the Nubia-Eurasia plate boundary zone. J. Geodyn., WEGENER 2008 - Proceedings of the 14th General Assembly of Wegener 49, 123–129. https://doi.org/10.1016/j.jog.2009.10.007*
- *Wang, W., 1979. Some findings in soil liquefaction. Report Water Conservancy and Hydro- Electric Power Scientific Research Institute, Pékin, Chine. pp. 1-17.*
- *Wathelet, M., Chatelain, J.-L., Cornou, C., Giulio, G.D., Guillier, B., Ohrnberger, M., Savvaidis, A., 2020. Geopsy: A User-Friendly Open-Source Tool Set for Ambient Vibration Processing. Seismological Research Letters 91, 1878–1889. https://doi.org/10.1785/0220190360*
- *Widmer-Schnidrig, R., 2003. What Can Superconducting Gravimeters Contribute to Normal-Mode Seismology? Bull. Seismol. Soc. Am. 93, 1370–1380. https://doi.org/10.1785/0120020149*
- *Wielandt, E., 2002. International Geophysics, Seismometry Ch 18. International Handbook of Earthquake and Engineering Seismology.*
- *Woodgold, C.R.D., 1994. Coda Q in the Charlevoix, Quebec, region: Lapse-time dependence and spatial and temporal comparisons. Bulletin of the Seismological Society of America 84, 1123–1131.*
- *Xia, H., Hu, T., 1991. Effects of Saturation and Back Pressure on Sand Liquefaction. J. Geotech. Eng. 117, 1347–1362. https://doi.org/10.1061/(ASCE)0733-9410(1991)117:9(1347)*
- *Yang J., Sze H. Y., 2011. Cyclic Strength of Sand under Sustained Shear Stress. Journal of Geotechnical and Geoenvironmental Engineering 137, 1275–1285. https://doi.org/10.1061/(ASCE)GT.1943-5606.0000541*
- *Yang, J., Savidis, S., Roemer, M., 2004. Evaluating Liquefaction Strength of Partially Saturated Sand. J. Geotech. Geoenvironmental Eng. 130, 975–979. https://doi.org/10.1061/(ASCE)1090-0241(2004)130:9(975)*
- *Ye, B., Ye, G., Zhang, F., Yashima, A., 2007. Experiment and Numerical Simulation of Repeated Liquefaction-Consolidation of Sand. Soils and Foundations 47, 547–558. https://doi.org/10.3208/sandf.47.547*
- *Youd, T.L., 2014. GROUND FAILURE INVESTIGATIONS FOLLOWING THE 1964 ALASKA EARTHQUAKE 11.*
- *Youd, T.L., Idriss, I.M., 2001. Liquefaction Resistance of Soils: Summary Report from the 1996 NCEER and 1998 NCEER/NSF Workshops on Evaluation of Liquefaction Resistance of Soils. J. Geotech. Geoenvironmental Eng. 127, 297–313. https://doi.org/10.1061/(ASCE)1090-0241(2001)127:4(297)*
- *Youd, T.L., Perkins, D.M., 1978. Mapping Liquefaction-Induced Ground Failure Potential. Journal of the Geotechnical Engineering Division 104, 433–446.*
- *Yuan, H., Hui Yang, S., Andrus, R.D., Hsein Juang, C., 2004. Liquefaction-induced ground failure: a study of the Chi-Chi earthquake cases. Engineering Geology, Reconnaissance of the Chi-Chi Earthquakes, Taiwan 71, 141–155. https://doi.org/10.1016/S0013-7952(03)00130-3*

- *Zakir, A., Chalouan, A., Feinberg, H., 2004. Tectono-sedimentary evolution of a fore-chain domain : example of the Habt and Sidi Mrayt basins, northwestern external Moroccan Rif ; stratigraphic precisions and tectonic modelling. Bull. Société Géologique Fr. 175, 383–397. https://doi.org/10.2113/175.4.383*
- *Zhang, J.-M., Wang, G., 2012. Large post-liquefaction deformation of sand, part I: physical mechanism, constitutive description and numerical algorithm. Acta Geotech. 7, 69–113. https://doi.org/10.1007/s11440-011-0150-7*

Appendix

4-1: The estimation of quality factor values at five lapse time windows for fifteen stations and for the whole zone.

Stations	M401	M402	M403	M404	M406	M407	M408	M410	M411	M413	M414	M415	M416	M417	M418	whole zone
fc(Hz) / tL=20s	**Qc ± SD**															
1.5	81.2 ± 10	76.8 ± 16.9	79.2 ± 11.5	76.6 ± 5.6	73.6 ± 11.6	78.5 ± 25	66.7 ± 15.6	95.9 ± 34.9	103.2 ± 16.6	81.5 ± 28.4	94.6 ± 18.9	100.7 ± 24.6	83.2 ± 7.1	76.7 ± 12.6	82.6 ± 22.2	83.39 ± 10.46
3	118 ± 15.9	137 ± 21.2	119.1 ± 19	143.1 ± 58.9	118.7 ± 23.5	147.1 ± 47.4	105.4 ± 13.2	132.1 ± 39.5	184.5 ± 61.9	148.5 ± 46.3	98.6 ± 21.9	149.8 ± 26	94.8 ± 9.2	98.3 ± 9.6	124.7 ± 30.3	127.97 ± 24.5
6	158.8 ± 24	176.1 ± 44.2	191.2 ± 21.3	276.2 ± 59	183.4 ± 26.5	220.7 ± 58.5	157 ± 21.7	183.5 ± 24.9	274.3 ± 80.6	237.8 ± 101.5	161.4 ± 40.7	205.4 ± 32.2	162 ± 35	138.5 ± 14.1	215.9 ± 64	196.14 ± 42.01
9	209.5 ± 25.4	233.6 ± 65.4	253.8 ± 17.7	326.9 ± 35.6	223.6 ± 32.5	302.7 ± 127.6	221.4 ± 23.2	265.2 ± 35.5	399 ± 102.9	267.3 ± 59.6	225.1 ± 44.4	268.6 ± 37.7	230.7 ± 26.9	219.5 ± 25.8	278 ± 89	261.65 ± 50.64
12	242.9 ± 24.6	288.9 ± 90.1	299.3 ± 35.5	382.7 ± 35.6	264.3 ± 38.7	415.3 ± 165.8	280.6 ± 39.4	336.5 ± 41	540.6 ± 161.8	327.7 ± 80.6	291.7 ± 88.4	357.9 ± 81.2	285.2 ± 35.1	267.9 ± 23.4	351.3 ± 121.7	328.87 ± 75.57
18	303.7 ± 27.1	450.3 ± 147.8	431.2 ± 103.7	708.6 ± 302.4	428.7 ± 132.7	549.6 ± 246.9	402 ± 42.8	517.4 ± 122.6	871.7 ± 355.7	457.1 ± 117	438 ± 197.1	617 ± 160.8	351 ± 44.3	328.2 ± 25	520.4 ± 231.4	491.66 ± 150.07
tL=30s																
1.5	101.1 ± 24.6	128.4 ± 21.1	101.8 ± 19.8	77.2 ± 3.7	103.8 ± 19.4	104.6 ± 14.9	108.4 ± 17	133.4 ± 33.5	122.8 ± 19.9	103 ± 12.7	115.3 ± 17.5	109.6 ± 17.9	91.1 ± 12.4	93.2 ± 14.8	117 ± 32.6	107.38 ± 14.65
3	134.8 ± 9.4	150 ± 9.6	133 ± 10.7	161.7 ± 16.8	134.2 ± 19.2	160.8 ± 27.2	142.4 ± 52.4	162.7 ± 5.7	193.1 ± 21.6	160.5 ± 32	120.1 ± 21.1	157.6 ± 11.5	118 ± 6.3	114.7 ± 6.2	138.8 ± 25.6	145.5 ± 21.14
6	181.2 ± 22.3	186.8 ± 15.2	218.3 ± 21.4	307.5 ± 43.6	205.4 ± 30.3	238.5 ± 38.5	210.9 ± 47.5	242.2 ± 81.1	346.4 ± 83.4	252.4 ± 70.5	201.5 ± 36.7	235 ± 26.5	178 ± 25	166.1 ± 9.6	233.1 ± 47.5	226.89 ± 48.64
9	233.7 ± 14.5	260 ± 37.7	281.7 ± 32.5	381.6 ± 48.3	256.6 ± 39.5	367 ± 129.4	273.1 ± 45.5	356.7 ± 119.9	440.3 ± 98.2	305.3 ± 69.9	273.1 ± 55.1	316.4 ± 31.9	247.9 ± 24.3	237.8 ± 11.3	320.4 ± 64.9	303.45 ± 60.26
12	275.3 ± 18.5	376.1 ± 69.5	338.3 ± 48.7	472.7 ± 57.9	326 ± 58	469.4 ± 134.1	346 ± 66.4	502.3 ± 258.8	587.2 ± 143.9	409 ± 141.9	359.2 ± 94.9	410.3 ± 53.6	305.5 ± 42.3	283.3 ± 19.1	435 ± 106.6	393.04 ± 88.17
18	361.3 ± 33.9	781.5 ± 226.5	515.4 ± 172.8	1052.4 ± 483.2	657.5 ± 268.5	770.4 ± 196.5	616.7 ± 315.5	580.4 ± 135.9	961.6 ± 411.8	713.1 ± 376.7	694.5 ± 410.1	771.8 ± 197.9	407.6 ± 79.2	376.4 ± 30.6	729.1 ± 197	665.98 ± 199.13
tL=40s																
1.5	111.6 ± 18.1	160.8 ± 16.6	128.7 ± 15.6	104.4 ± 3.6	118.6 ± 18.6	137.2 ± 15.1	131.5 ± 6.7	136.4 ± 27.9	128.3 ± 14.4	127.8 ± 18.7	127.4 ± 12.5	115.4 ± 15.3	121.7 ± 14.9	124 ± 15.1	153.7 ± 39.2	128.51 ± 14.72
3	151.9 ± 10.2	171.9 ± 12.8	159.1 ± 11.4	188.8 ± 8.7	150.7 ± 9.9	187.6 ± 18.3	150.5 ± 21.8	168.4 ± 25.5	198.7 ± 21.9	177 ± 29.9	139.5 ± 16.6	160.6 ± 13.2	137.8 ± 9.9	134.2 ± 10.6	157.4 ± 28.8	162.27 ± 19.52
6	210.1 ± 19.2	218.4 ± 21.5	257.6 ± 26.5	310.8 ± 25.8	232.7 ± 19.3	285.6 ± 62.1	242.5 ± 29.7	253.5 ± 42.5	394.3 ± 178.3	280.6 ± 53.3	244.4 ± 37.2	252.7 ± 38	212.6 ± 29.7	199.2 ± 9.7	271.8 ± 54.3	257.79 ± 48.79
9	264 ± 15.2	331.9 ± 44.2	339.1 ± 52	437.6 ± 16.3	298.5 ± 27.5	483.2 ± 257.4	319.9 ± 50.4	388.9 ± 90.1	519.7 ± 220.3	474.8 ± 260.7	353.1 ± 80.8	354.2 ± 70.7	286.5 ± 32.2	275.4 ± 22.1	404.8 ± 99.4	368.78 ± 80.2
12	317.4 ± 21.3	510 ± 95.2	422.2 ± 80.7	617.9 ± 82.7	418.9 ± 78.5	492.7 ± 96	404.5 ± 77	566.4 ± 196.3	630.5 ± 159.7	805.4 ± 708.5	491.5 ± 162.6	479.7 ± 144.2	354.2 ± 56.3	337.5 ± 34.4	584.1 ± 171.5	495.53 ± 130.6
18	444.2 ± 60.1	1191.5 ± 368.2	696 ± 258	1339.4 ± 169.8	1107.5 ± 664.5	1107.5 ± 664.5	648.6 ± 263.5	1651.2 ± 1398	1070.4 ± 328.9	1135 ± 838.9	812.5 ± 327	1197.2 ± 905.4	507.4 ± 140.1	475.2 ± 67.1	1518.2 ± 1023	993.44 ± 378.63
tL=50s																
1.5	129.9 ± 23.5	167.6 ± 28.2	137.8 ± 17.9	124.6 ± 10.4	129.6 ± 11.5	141.1 ± 18	146.2 ± 5.3	157.1 ± 29.2	157.9 ± 25.8	145.3 ± 32.1	142.2 ± 10.5	140.7 ± 19.1	133.4 ± 9.5	133 ± 13.4	165.9 ± 19.1	143.49 ± 13.32
3	172.4 ± 11	177.9 ± 14.9	164 ± 8.4	191.8 ± 18.4	172.1 ± 15.9	200.3 ± 18.4	164.3 ± 13.6	181.8 ± 30.3	201.5 ± 46.4	194.9 ± 40.7	162.6 ± 13.1	193.9 ± 26.8	159.8 ± 10.8	151.3 ± 7.3	185.5 ± 25.9	178.29 ± 15.98
6	229.6 ± 14.9	249.7 ± 22.3	288.8 ± 39.5	360.1 ± 41.4	259.8 ± 24.4	294.7 ± 23	275.6 ± 46	286.7 ± 27.7	462.9 ± 355.8	309.4 ± 47.8	297.3 ± 54.4	291.3 ± 71.1	262.7 ± 68.8	239.2 ± 27.2	322.4 ± 56.1	295.35 ± 57.08
9	290.8 ± 11	406 ± 63.4	417.4 ± 105.7	559.1 ± 123.9	360.9 ± 64.7	488.3 ± 122.3	366.4 ± 90.2	436.3 ± 63.4	658 ± 625.8	555.3 ± 227.1	487.4 ± 185	448.4 ± 179.8	352.5 ± 93.1	342 ± 68.8	526.9 ± 177.1	446.38 ± 99.81
12	358.3 ± 23.6	713.4 ± 171.9	551.5 ± 173.7	757.2 ± 155	559.5 ± 177	744.3 ± 291.4	466.2 ± 127.4	649.9 ± 140.8	663.3 ± 162.9	972 ± 680	767.9 ± 419.1	681.6 ± 432.5	443.6 ± 135.6	433.6 ± 91.9	795.2 ± 286.9	637.18 ± 166.46
18	542.5 ± 75	1904.6 ± 750.1	1030.9 ± 575.8	2093.8 ± 634.8	1459.3 ± 727.2	1702.7 ± 226.4	658 ± 98.4	1683.9 ± 724.3	1362 ± 709.4	1483.2 ± 679.2	1627.5 ± 1395	1437.4 ± 960.9	694 ± 349	642.5 ± 158	1978.9 ± 1099	1353.41 ± 518.94
tL=60s																
1.5	133.2 ± 15.4	170.9 ± 17.9	153.2 ± 18	162.1 ± 17.8	136.7 ± 14.1	160.2 ± 15.5	163.7 ± 7.9	173.3 ± 30.2	176.5 ± 28.2	167.9 ± 28.3	151.9 ± 9.5	169.7 ± 18.1	137.1 ± 23.2	133.3 ± 10.4	172.5 ± 25.7	157.49 ± 15.61
3	182.4 ± 11.8	183 ± 17.5	170.2 ± 5.4	199.2 ± 8.1	176.5 ± 25.3	210.4 ± 9.7	181.1 ± 12.6	186 ± 15.3	228.1 ± 29.5	212.4 ± 32.8	183.3 ± 20.2	203.8 ± 17.8	172.4 ± 12.1	168.4 ± 9.7	212.4 ± 36.9	191.3 ± 18.35
6	247.1 ± 14.8	279.6 ± 38.2	300.9 ± 37.3	423.8 ± 78.4	291.9 ± 53.4	297.9 ± 15.6	285.5 ± 31.4	324.8 ± 19.8	559.6 ± 514.9	365.6 ± 67.3	372.4 ± 117.7	310.3 ± 80	295.2 ± 90.3	284.2 ± 58.9	381.9 ± 76.8	334.73 ± 78.09
9	325.1 ± 16	517 ± 125.5	449.1 ± 99.2	752.5 ± 278.7	467.9 ± 176	499.2 ± 150.5	390 ± 74.9	534.5 ± 78.2	786.3 ± 734.4	708.7 ± 290.2	684.1 ± 351.1	506.6 ± 197.8	423.1 ± 136	432.5 ± 128.8	655.6 ± 244	542.16 ± 141.18
12	416.8 ± 34.6	1035.6 ± 410.6	579.9 ± 154.6	1095.4 ± 368.1	839.2 ± 522.6	799.8 ± 319.4	539.4 ± 150	834.9 ± 173.8	1478.4 ± 1952	1345 ± 1074.9	1207.8 ± 873.8	931.8 ± 528.7	558.4 ± 223.9	564.8 ± 166.7	1011.9 ± 322.8	882.6 ± 316.89
18	689 ± 120.3	2906.2 ± 585.5	1079.4 ± 429	3447.8 ± 930.2	1567.3 ± 391.5	1660.4 ± 690.5	1184 ± 745.4	2770.7 ± 1504	2136.8 ± 890.8	1750.5 ± 998.1	1796.6 ± 5926	1440.1 ± 890.3	946.5 ± 523.2	874.9 ± 271	2264.7 ± 777.1	1787.65 ± 807.88

Table 4-2: The estimation of the average of quality factor at 1 Hz and n values for five lapse time.

Stations	M401	M402	M403	M404	M406	M407	M408	M410	M411	M413	M414	M415	M416	M417	M418	Average
tL	**Qo ± ΔQo**															
60(s)	130.67 ± 22.13	143.4 ± 65.97	128.55 ± 25.15	156.79 ± 64.66	129.86 ± 44.01	127.29 ± 38.09	117.09 ± 26.72	146.68 ± 63.16	171.17 ± 49.2	156.89 ± 49.63	141.38 ± 49.03	131.54 ± 33.63	95.53 ± 11.64	98.34 ± 11.22	171.9 ± 61.37	136.47 ± 17.72
50(s)	111.01 ± 10.08	107.53 ± 37.36	105.5 ± 16.67	95.7 ± 24.26	79.68 ± 21.25	108.03 ± 26.13	91.53 ± 8.74	94.06 ± 26.96	99.49 ± 12.62	126.28 ± 34.6	98.46 ± 24.4	113.14 ± 26.54	79.43 ± 9	78.19 ± 9.11	125.1 ± 35.71	100.88 ± 12.06
40(s)	86.75 ± 4.27	71.69 ± 22.14	78.87 ± 9.23	71.17 ± 9.35	58.56 ± 15.55	86.61 ± 13.7	73.42 ± 9.96	85.71 ± 26.48	83.04 ± 5.66	86.36 ± 14.68	62.82 ± 10.81	69.59 ± 15.39	62.72 ± 9.08	57.14 ± 11.05	95.56 ± 28.48	75.33 ± 10.07
30(s)	73.72 ± 3.28	52.48 ± 14.91	58.89 ± 5.37	45.39 ± 5.93	44.67 ± 10.01	52.61 ± 7.81	60.34 ± 8.76	57.34 ± 12.6	75.16 ± 5.36	60.17 ± 7.41	46.76 ± 11.16	50.65 ± 9.8	49.32 ± 6.17	45.83 ± 7.97	57.3 ± 9.2	55.38 ± 7.37
20(s)	55.56 ± 4.01	37.31 ± 9.06	46.66 ± 4.46	34.31 ± 8.06	34.74 ± 7.66	37.33 ± 8.05	37.39 ± 4.56	38.34 ± 10.79	60.61 ± 6.37	48.57 ± 7.83	35.72 ± 9.61	31.7 ± 13.54	40.46 ± 6.4	32.7 ± 7.83	44.2 ± 5.33	41.04 ± 6.72
	n ± Δn															
60(s)	0.45 ± 0.01	0.76 ± 0.23	0.59 ± 0.27	0.79 ± 0.25	0.66 ± 0.15	0.73 ± 0.21	0.64 ± 0.16	0.73 ± 0.07	0.74 ± 0.18	0.7 ± 0.17	0.72 ± 0.22	0.69 ± 0.17	0.71 ± 0.14	0.68 ± 0.12	0.66 ± 0.18	0.68 ± 0.06
50(s)	0.47 ± 0.08	0.77 ± 0.22	0.66 ± 0.27	0.87 ± 0.17	0.83 ± 0.34	0.77 ± 0.32	0.66 ± 0.2	0.82 ± 0.39	0.84 ± 0.52	0.71 ± 0.22	0.8 ± 0.18	0.7 ± 0.24	0.72 ± 0.19	0.7 ± 0.22	0.74 ± 0.18	0.74 ± 0.07
40(s)	0.53 ± 0.07	0.87 ± 0.43	0.71 ± 0.03	0.9 ± 0.15	0.9 ± 0.28	0.78 ± 0.34	0.73 ± 0.06	0.82 ± 0.23	0.86 ± 0.23	0.82 ± 0.25	0.86 ± 0.05	0.85 ± 0.14	0.75 ± 0.07	0.78 ± 0.05	0.77 ± 0.37	0.8 ± 0.07
30(s)	0.54 ± 0.1	0.9 ± 0.23	0.75 ± 0.14	1.05 ± 0.38	0.93 ± 0.4	0.94 ± 0.2	0.77 ± 0.28	0.91 ± 0.22	0.86 ± 0.2	0.83 ± 0.29	0.93 ± 0.29	0.94 ± 0.31	0.77 ± 0.04	0.79 ± 0.09	0.87 ± 0.13	0.85 ± 0.09
20(s)	0.62 ± 0.07	0.93 ± 0.09	0.8 ± 0.1	1.12 ± 0.26	0.94 ± 0.25	1.03 ± 0.09	0.85 ± 0.02	0.99 ± 0.08	0.91 ± 0.17	0.84 ± 0.02	0.94 ± 0.04	1.17 ± 0.17	0.82 ± 0.05	0.91 ± 0.22	0.89 ± 0.08	0.92 ± 0.09

Table 4-3: Location and characteristics of all temporary stations used in this study.

Station	Network	Station location	N° of Component	Sensor type	Latitude (°N)	Longitude (°W)	Altitude (m)
M401	Topo-Iberia	Taghazout	3	Trillium 120	34.75	4.5	1264.3
M402	Topo-Iberia	Talambote	3	Trillium 120	35.33	5.17	259.6
M403	Topo-Iberia	Bni Ahmed	3	Trillium 120	34.84	5.07	597.6
M404	Topo-Iberia	Tissa	3	Trillium 120	34.29	4.68	332.7
M406	Topo-Iberia	Douar Mchaa	3	Trillium 120	34.73	4.81	1112.3
M407	Topo-Iberia	Derdara	3	Trillium 120	35.10	5.28	476.0
M408	Topo-Iberia	Tafensa	3	Trillium 120	35.20	4.02	341.9
M410	Topo-Iberia	Stehate	3	Trillium 120	35.34	4.96	83.8
M411	Topo-Iberia	Driouch	3	Trillium 120	34.97	3.33	343.8
M413	Topo-Iberia	Jebha	3	Trillium 120	35.19	4.65	241.7
M414	Topo-Iberia	Bni Hadifa	3	Trillium 120	35.02	4.14	916.2
M415	Topo-Iberia	Trougout	3	Trillium 120	35.17	3.76	150.0
M416	Topo-Iberia	Issaken	3	Trillium 120	34.93	4.54	1635.5
M417	Topo-Iberia	Boured	3	Trillium 120	34.74	4.09	880.2
M418	Topo-Iberia	Arbaa Taourirt	3	Trillium 120	34.93	3.83	428.4

Table 4-4: List of earthquakes used for estimation of coda Q.

Origine time			Latitude (°N)	Longitude (°W)	magnitude (ML)	depth (km)
Date	Hr.Min	Sec				
01/06/2014	23:15	42.4	35.143	4.217	1.9	
01/09/2014	02:17	45.1	34.848	3.166	2.7	
02/02/2014	03:40	22.3	34.928	4.189	2.1	
02/05/2014	21:52	55.9	35.359	4.661	2.9	30.5
02/06/2014	22:27	39.2	34.436	3.162	3	21.4
02/08/2014	19:11	0.9	35.113	4.101	1.8	15.9
03/03/2014	02:55	25.3	34.523	5.094	3	
03/03/2014	03:49	29.8	34.63	5.177	3.8	
03/05/2014	01:00	13.2	33.464	4.951	3	
03/06/2014	09:43	50.8	35.08	3.862	2.4	
04/08/2014	06:50	20.5	34.886	4.578	2.1	0.1
04/10/2014	02:12	58.9	35.128	4.433	2.4	
04/10/2014	21:18	53.1	34.889	4.436	2	10.6
05/06/2014	13:39	11.4	35.113	4.758	1.9	7.2
06/06/2014	23:39	46.2	35.048	4.3	1.7	0.1
07/04/2014	13:31	26.8	35.636	3.662	2.4	30.6
09/04/2014	05:47	9.4	35.591	3.807	2.4	
09/08/2014	10:30	38.8	35.233	4.225		
09/08/2014	15:45	51.9	35.332	4.19	3.6	
09/08/2014	19:17	32.8	35.202	4.19		0.1
09/09/2014	17:55	49.6	38.289	6.278	3.1	70
09/10/2014	02:44	1.6	35	4.498	2.7	
09/10/2014	16:55	0.8	34.995	4.495	3.1	
09/10/2014	17:45	27.2	35.101	4.142	1.9	
09/10/2014	20:21	14.1	34.978	4.521	3.2	
09/10/2014	20:26	15.9	35.01	4.502	2.6	0.1
09/10/2014	21:01	54.2	35.001	4.501	3.2	0.1
10/08/2014	03:47	38	35.154	4.168	1.4	
10/08/2014	08:48	16.7	35.135	4.162	1.4	0.1
10/08/2014	11:38	53.3	35.146	4.164	1.8	
10/10/2014	05:53	30.3	34.99	4.495	2.8	
10/10/2014	14:32	6.5	35.009	4.507	2.2	
10/10/2014	16:31	51.8	35.024	4.51	2.4	
10/10/2014	18:01	42.1	35.01	4.503	2.3	

11/03/2014	12:27	11.1	34.352	5.051	4.6	19.3
11/08/2014	10:33	13.4	35.139	4.187	2.1	
11/10/2014	09:27	38.7	35.007	4.502	2.6	0.1
11/10/2014	17:14	1.1	34.916	4.436	2.1	5.8
11/10/2014	20:42	19.3	34.894	4.424	1.8	7.1
11/10/2014	21:35	24.9	34.944	4.433	2.4	
12/10/2014	18:57	58.5	35.011	4.506	2.2	
13/05/2014	02:55	18.4	34.791	3.791	3	9.1
13/06/2014	22:10	31	35.109	3.938	1.2	7.4
13/08/2014	15:48	1.9	34.608	3.032	3.2	
14/03/2014	21:50	53.6	33.775	3.664	4.6	15
14/05/2014	13:51	52.6	33.479	4.998	3	15
14/10/2014	08:14	11.6	35.112	3.851	2.4	15
15/08/2014	10:36	55.1	35.156	4.1	1.9	16.7
16/04/2014	12:02	22.2	35.109	3.871	4	7.8
17/04/2014	13:47	26.5	35.795	2.909	2.3	15
17/04/2014	17:13	52.7	33.536	4.85	3	0.3
17/06/2014	17:24	19.9	35.169	3.947	2.5	14.5
19/03/2014	20:41	34.4	35.201	4.137	1.7	0.1
19/04/2014	00:57	22.6	33.455	5.051	3	
19/08/2014	22:17	17.5	35.169	3.61	2.7	15
20/08/2014	02:02	58.3	34.038	5.988	3	15
21/01/2014	04:57	32.8	34.691	5.556	2.1	
24/03/2014	12:33	37.9	35.362	4.66	3.1	25.8
25/05/2014	04:51	30	35.116	4.095	1.8	10.7
25/05/2014	14:53	6.3	35.106	4.345	2.6	11.5
26/02/2014	02:29	30.5	35.184	4.757	2.1	18.8
28/05/2014	02:33	54.2	35.728	3.343	2.2	47.8
28/06/2014	06:27	35.5	35.562	2.838	1.9	
29/07/2014	20:10	52.1	34.927	4.22	1.8	
29/07/2014	22:53	42.3	35.014	4.259	4	
29/08/2014	10:28	24.9	35.205	4.231	2.4	15
31/07/2014	17:14	34.4	35.176	3.855	3.7	
31/07/2014	19:53	49.4	35.421	4.686	4	34.5
31/07/2014	20:12	18.5	34.81	0.118	3.2	0.6
31/08/2014	05:46	43.2	34.747	3.161	2.6	

Earthquake localisation by Seisan software using Hypocenter program (HYP).

- How to create an S-file.

We first need to merge the data of all the stations. To do so, we should access to WOR directory and put the data in a directory named “Test”. Then we go to the terminal, and enter to the “Test” directory where we put the data as shown in the screen shot below. By that time we execute the commands below hereunder:

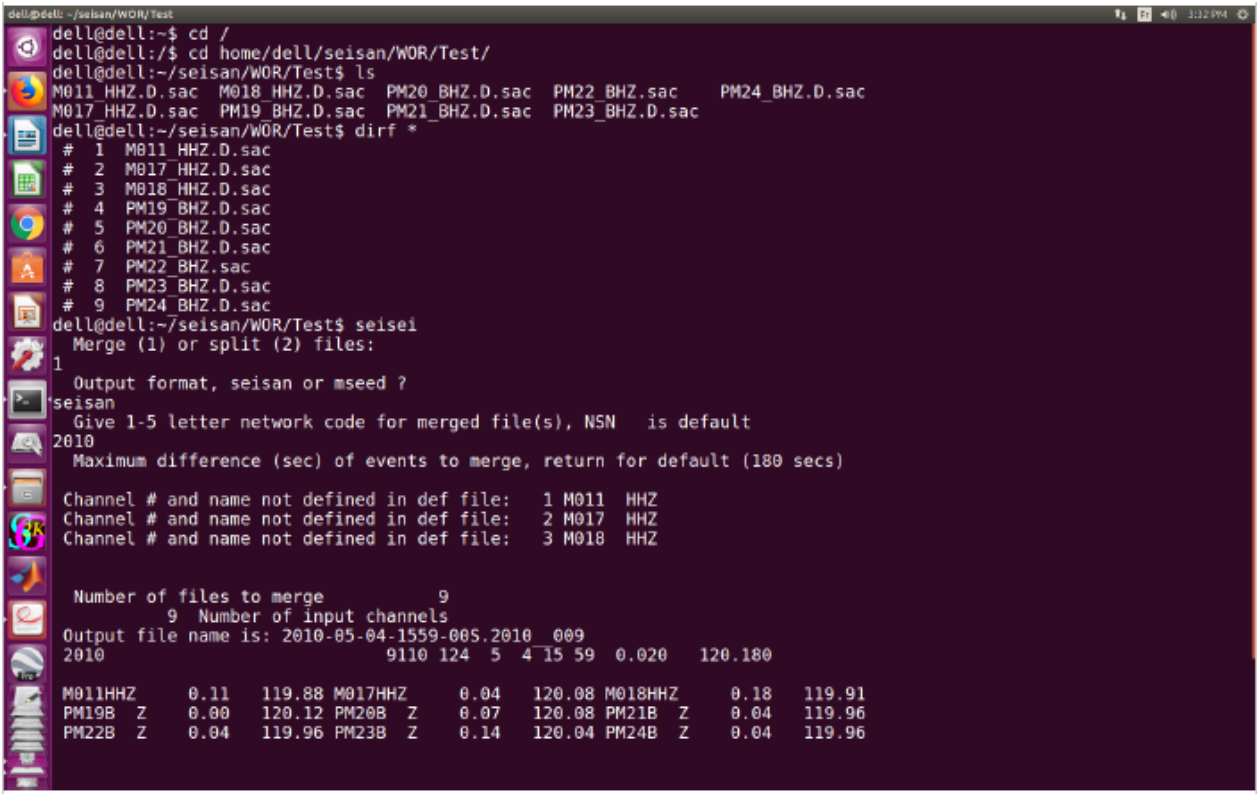

Figure 6-1: Terminal screen steps of creating S-file

Commands:

1.“dirf *” :(to group the data in a list)
2. “seisei” :(to merge the data)
3. “1” :(to merge files)
4. “seisan”.
5. “2010” In my case. The name of the network code.
6. click enter if we want default (180 secs), if not write your number of seconds for example “300”. an

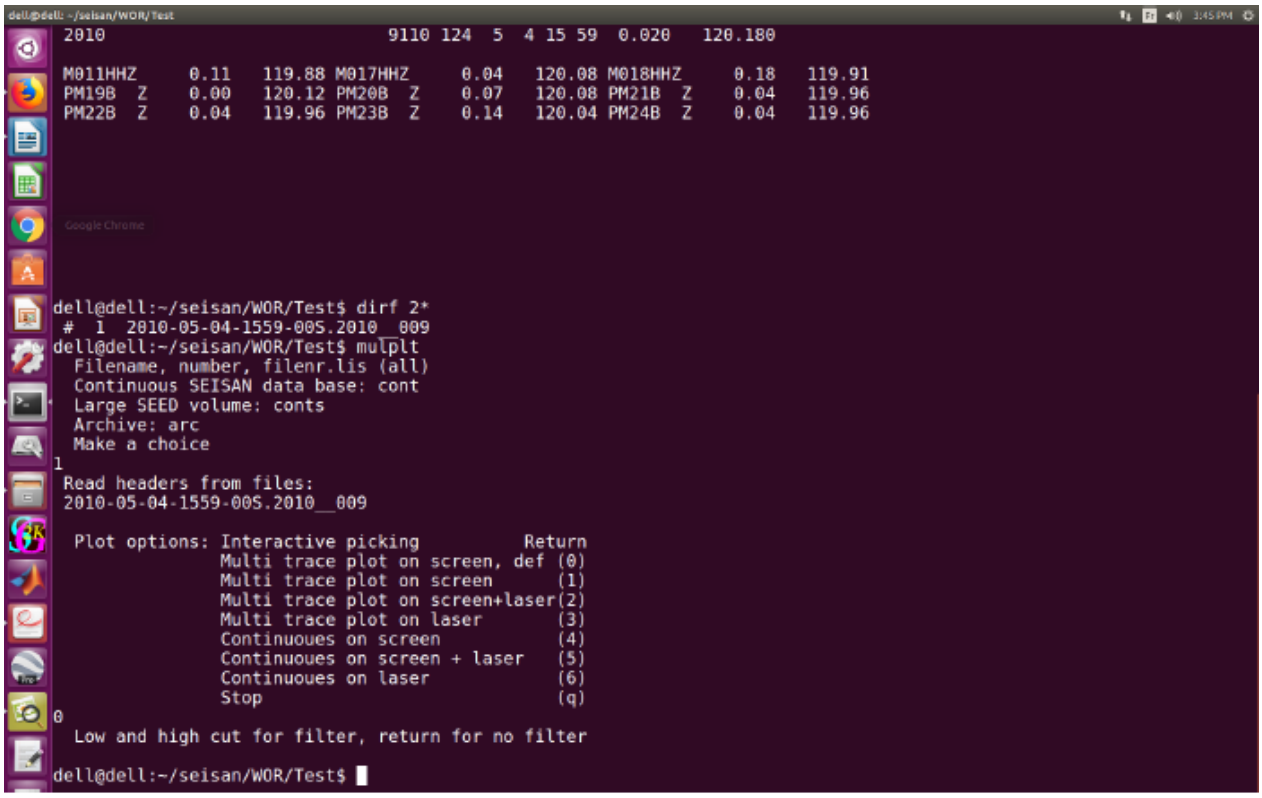

Figure 6-2: Terminal screen steps of creating an S-file (follow-up)

Commands:

7. “dirf 2* :
8. “mulplt” : (to plot the S-file)
9. “1” :(to make the choice)
10. “0” for default.
11. click enter for no filter.

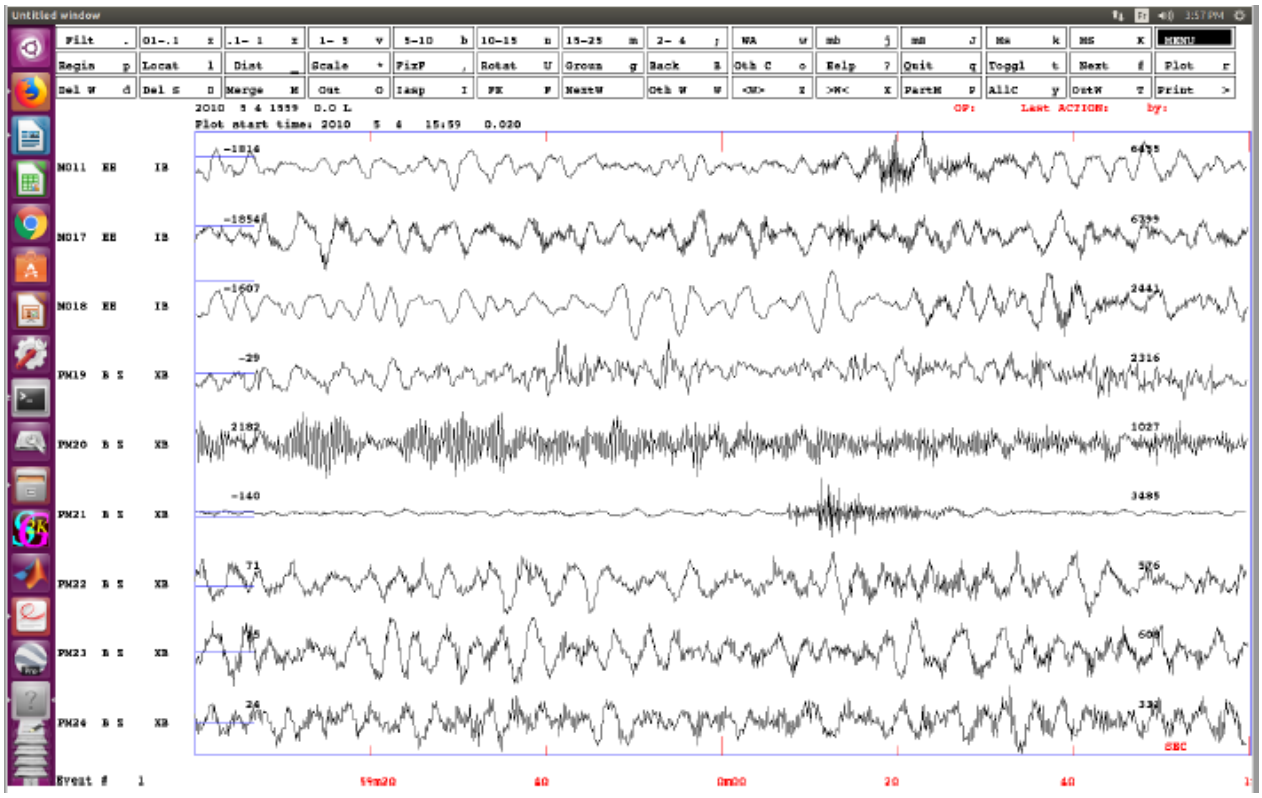

Figure 6-3: Graphic aspect of SEISAN software showing different events composing the S-file

Commands:

12. Tape P. to register the S-file to enter to it by eev.

Commands:

13. “L”. L for local R for regional and D for distant event. In our case it’s a local event.
14. “2010” for the operator code.
15. “„” to put the S-file in the local directory “Test”.
16. “Y”.
17. “eev”.

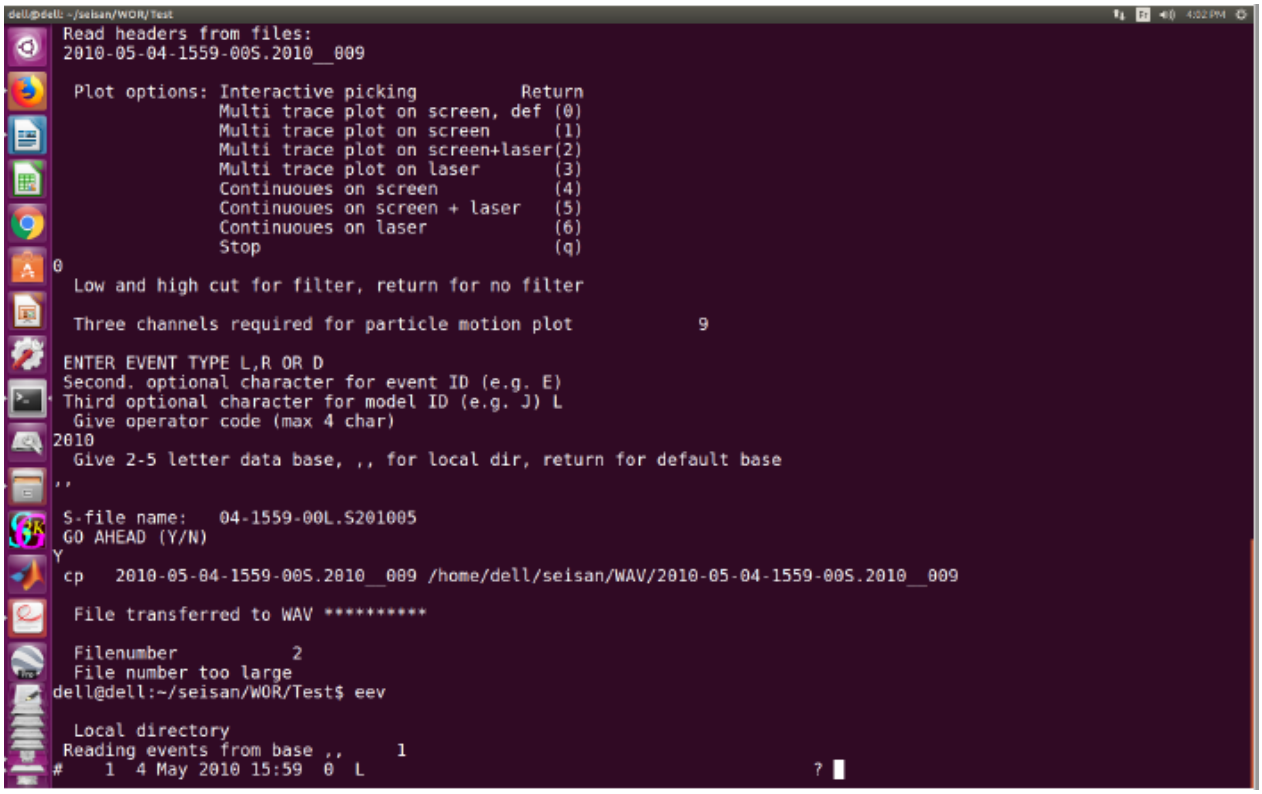

Figure 6-4: Terminal screen steps of creating an S-file (follow-up)

Then here we are. Each time we want to have access to the "Test" directory in seisan. We type eev command ➡ plot by typing po.

2. Localisation.

Localisation in seisan is made by the program hypo, and it is executed in two steps; the first is to prepare an input file named "STATION0.HYP" as shown bellow. (Refer to hypocent.pdf which is given in INF directory in SEISAN to mount the input file). We note that the coordinate of stations need to be in degrees and minutes (example):

Name of the station	Latitude in degree	Latitude in minutes	Direction	Longitude in degree	Longitude in minutes	Direction	Elevation in meter
M018	33	37.22	N	04	26.54	W	1090

```
RESET TEST(34)=1.5
RESET TEST(35)=2.5
RESET TEST(36)=0.0
RESET TEST(41)=20000.0
RESET TEST(43)=5.0
RESET TEST(51)=3.6
RESET TEST(50)=1.0
RESET TEST(56)= 1.0
RESET TEST(58)= 99990.0
RESET TEST(40)=0.0
RESET TEST(60)=0.0
RESET TEST(71)=1.0
RESET TEST(75)=1.0
RESET TEST(76)=0.910
RESET TEST(77)=0.00087
RESET TEST(78)=-1.67
RESET TEST(79)=1.0
RESET TEST(80)=3.0
RESET TEST(81)=1.0
RESET TEST(82)=1.0
RESET TEST(83)=1.0
RESET TEST(88)=1.0
RESET TEST(85)=0.1
RESET TEST(91)=0.1


  M0183337.22N  426.54W1090
  M0193156.15N  427.22W1095
  M2013316.24N  610.00W 863
  M2023255.19N  530.49W1443
  M2033209.01N  537.51W2219
  M2043051.52N  902.49W 953
  M2053222.36N  619.08W 608
  M2063248.04N  634.41W 748
  M2073111.15N  803.44W1059




  6.2      0.0
  6.6     12.0
  7.1     23.0       B
  8.05    31.0       N
  8.25    50.0
  8.5     80.0

15.0 1100.2200. 1.74
TES
```

Figure 6-5: Input file that classify the parameters used to compute the location of a given earthquake

The step after is picking P waves on at least 3 stations. If require more accuracy pick on S waves.

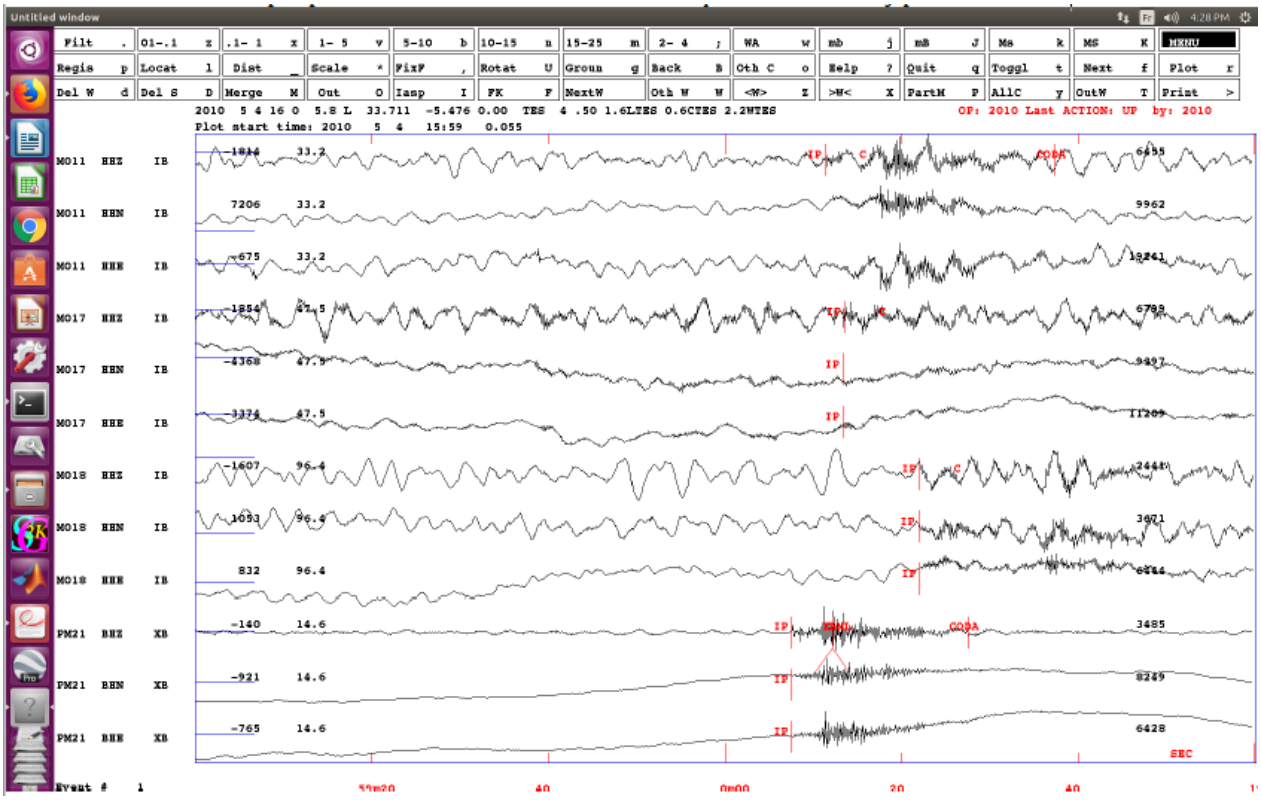

Figure 6-6: Graphic aspect of SEISAN software showing P waves picking on horizontal and vertical component of each event.

Tipe l (L, not one) to localise the event.

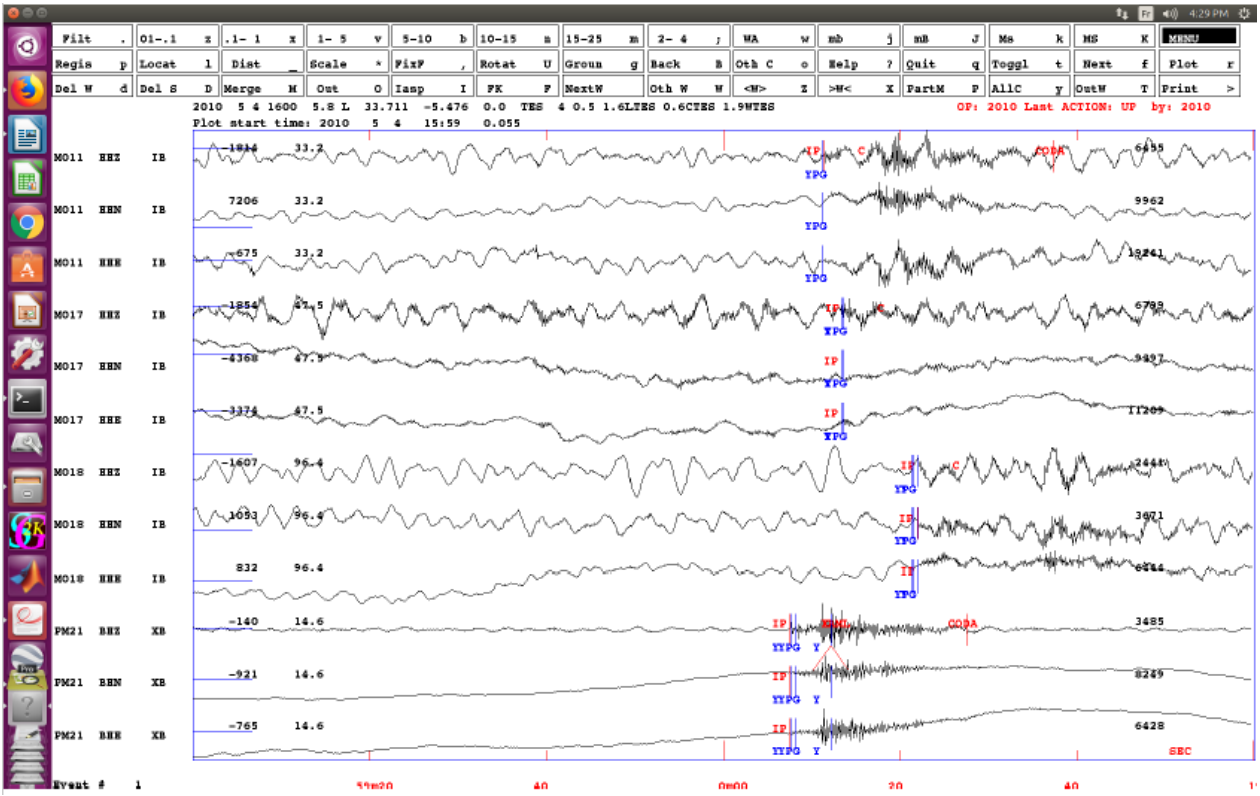

Figure 6-7: Graphic aspect of SEISAN software showing the difference between the picked and computed travel time of each event.

Then you have an output file called gmap.cur.kml.

Figure 6-8: Google Earth map showing the position of the event and the stations used to localize the earthquake.

The output file could be plotted in different programs as Epimap or Google Earth etc.

Abstract

The aim of this work is to estimate the attenuation of seismic coda waves and the liquefaction potential in the region of Rif northern Morocco. The investigation using the attenuation of coda wave's technic has been accomplished relying on the back-scattering model. The quality factor of Coda Qc was computed under 5 lapse time windows 20, 30, 40, 50 and 60s at different central band frequencies from 1.5 to 18HZ. Moreover, the assumption of the dependency principle between the quality factor and the frequency and the lapse time windows has been proven. This statement lead the facts to substantiate the presence of heterogeneities under the crust and to reveal the intricacy of the geological/geophysical pattern. The quantification of the Qc has come to put the region of the Rif in a tectonic active region. On the other hand the estimation of the liquefaction potential was evaluated using the so-called HVSR Nakamura method `Horizontal-To-Vertical Spectral Ratio`. The purpose of the liquefaction inquest is to be capable to evaluate the seismic vulnerability in the Rif area by adding parameters other than the quality factor. In addition, the estimation of the liquefaction potential can lean on the value of the vulnerability index, the geological setting and the existence of aquifer nappes. The Kg index has shown a low content of liquefaction in the Rif. All this outcomes refers to unsaturated ground granules due to a minor content. Therefore, the Rif area is not high risky toward the liquefaction.

Key words (7): Attenuation; Coda wave; Quality factor; Liquefaction; Micro-tremor measurement; Seismic vulnerability; Rif region.

Résumé

Le but de ce travail est d'estimer l'atténuation des ondes sismiques de la coda, et l'estimation du potentiel de liquéfaction dans la région du Rif nor du Maroc. L'investigation utilisant la technique d'atténuation des ondes coda a été réalisé en se basant sur le modèle de rétrodiffusion. Le facteur de qualité de Coda Qc a été calculé dans 5 fenêtres de temps 20, 30, 40, 50 et 60s à différentes fréquences de la bande centrale de 1.5 à 18HZ. De plus, l'hypothèse du principe de dépendance entre le facteur de qualité et la fréquence et les fenêtres de temps a été prouvée. Cette affirmation a conduit les faits à étayer la présence d'hétérogénéités sous la croûte et à révéler la complexité du modèle géologique/géophysique. La quantification du Qc est venue placer la région du Rif dans une région tectonique active. D'autre part, l'estimation du potentiel de liquéfaction a été évaluée en utilisant la méthode dite HVSR de Nakamura `Horizontal-To-Vertical Spectral Ratio`. Le but de l'estimation du potentiel de liquéfaction est d'être capable d'évaluer la vulnérabilité sismique dans la région du Rif en ajoutant des paramètres autres que le facteur de qualité. En outre, l'estimation du potentiel de liquéfaction peut s'appuyer sur la valeur de l'indice Kg, le contexte géologique et l'existence de nappes aquifères. L'indice de vulnérabilité a montré une faible teneur de liquéfaction dans le Rif. Tous ces résultats se réfèrent à des granules de sol non saturés en raison d'un contenu mineur. Par conséquent, la région du Rif ne présente pas de risque élevé de liquéfaction.

Mot clés (7) : Atténuation; l'onde de Coda; Facteur de qualité; Liquéfaction; Mesure de bruit de fond; Vulnérabilité sismique; Région du Rif.